IONIZING ELECTRON INCIDENTS AS AN EFFICIENT WAY TO REDUCE VISCOSITY OF HEAVY PETROLEUM FLUIDS

A Thesis

by

MASOUD ALFI

Submitted to the Office of Graduate Studies of
Texas A&M University
in partial fulfillment of the requirements for the degree of

MASTER OF SCIENCE

August 2012

Major Subject: Petroleum Engineering

IONIZING ELECTRON INCIDENTS AS AN EFFICIENT WAY TO REDUCE VISCOSITY OF HEAVY PETROLEUM FLUIDS

A Thesis

by

MASOUD ALFI

Submitted to the Office of Graduate Studies of
Texas A&M University
in partial fulfillment of the requirements for the degree of

MASTER OF SCIENCE

Approved by:

Chair of Committee,	Maria A. Barrufet
Committee Members,	Rosana G. Moreira
	W. John Lee
Head of Department,	A. Daniel Hill

August 2012

Major Subject: Petroleum Engineering

ABSTRACT

Ionizing Electron Incidents as an Efficient Way to Reduce Viscosity of Heavy Petroleum Fluids. (August 2012)

Masoud Alfi, B.S., Amirkabir University of Technology (Tehran Polytechnic)

Chair of Advisory Committee: Dr. Maria A. Barrufet

The dependence on oil and the fact that petroleum conventional reservoirs are becoming depleted direct attentions toward unconventional—and harder to access—reservoirs. Among those, heavy and extremely heavy oil reservoirs and tar sands form a considerable portion of all petroleum resources. Conventional thermal and thermocatalytic refining methods are not affordable choices in some cases, as they demand a considerable energy investment. On the other hand, electron irradiation, as a novel technology, provides more promising results in heavy oil upgrading.

Electron irradiation, as a method of delivering energy to a target molecule, ensures that most of the energy is absorbed by the molecule electronic structure. This leads to a very efficient generation of reactive species, which are capable of initiating chemical reactions. In contrast, when using thermal energy, only a small portion of the energy goes into the electronic structure of the molecule; therefore, bond rupture will result only at high energy levels.

The effect of electron irradiation on different heavy petroleum fluids is investigated in this study. Radiation–induced physical and chemical changes of the fluids have been evaluated using different analytical instruments. The results show that high energy electron particles intensify the cracking of heavy hydrocarbons into lighter species. Moreover, irradiation is seen to limit any post–treatment reactions, providing products of higher stability. Depending on the characteristics of the radiolyzed fluid, irradiation may change the distribution pattern of the products, or

the radiolysis process may follow the same mechanism that thermal cracking does. In addition to that, we have studied the effectiveness of different influencing variables such as reaction temperature, absorbed dose values, and additives on radiolytic reactions. More specifically, the following subjects are addressed in this study:

- Radiation–induced chain reactions of heavy petroleum fluids
- Complex hydrocarbon cracking mechanism
- High and low temperature radiolysis
- Synergetic effects of different chemical additives in radiolysis reactions
- Time stability of radiation products

DEDICATION

to my family:

your love and support will always be remembered, fondly in good times, and as encouragement in bad.

ACKNOWLEDGMENTS

First and foremost, I would like to thank my advisor, Dr. Maria A. Barrufet for her valuable guidance and advice. This thesis would not have been possible without her tremendous contribution. She never accepted less than my best effort. Additionally, I would like to show my gratitude to Dr. Rosana G. Moreira, who encouraged and challenged me throughout my academic program and provided me with the authority to use the electron accelerator facility. I am also grateful for Dr. W. John Lee for serving in my committee and for providing his valuable time.

I am indebted to many of my colleagues, especially Mr. Peter Slater and Ms. Erin Amundsen from ConocoPhillips, Bartlesville technology center, for their great help in analyzing heavy oil samples. I would also like to extend my heartfelt thanks to my good friend, Paulo Da Silva who has made available his support to this project in a number of ways.

Finally, an honorable mention goes to my parents, my brother Mehrdad, my lovely sister Mahshid, and especially, my uncle Abbas, whose encouragement and patient love enabled me to complete this project. Words alone cannot express what I owe them for their understanding and support.

NOMENCLATURE

D	Absorbed dose
ϵ	Energy imparted
$(R_{in,out})_{u,c}$	Radiant energy of charged or uncharged particles
m	Mass
t	Time
$\dot{D}$	Absorbed dose ratio
h	Planck constant ($6.62606957 \times 10^{-34}$ J.s)
ν	Frequency
Q_{min}	minimum energy loss in a single collision (eV)
Q_{max}	maximum energy loss in a single collision (eV)
Q_{avg}	average energy loss in a single collision (eV)
$W(Q)$	Probability density ($\frac{1}{\mathrm{eV}}$)
μ	Macroscopic cross section ($\frac{1}{\mathrm{m}}$), viscosity of the fluids (cp)
k_0	$8.99 \times 10^9 (\frac{\mathrm{Nm^2}}{\mathrm{C^2}})$
e	Magnitude of electron charge (1.6022×10^{-19}C)
n	Number of electrons per unit volume in the medium
c	Speed of light in vacuum ($2.9979 \times 10^8 \frac{\mathrm{m}}{\mathrm{s}}$)
β	$\frac{V}{c}$ = Speed of the particle relative to light
I	Mean excitation energy of the medium (MeV), current (A)
τ	Kinetic energy of the electrons relative to the electron rest energy
E, T	Energy of charged particle (MeV)
Z	Atomic number
R_{CSDA}	Continuous Slowing Down Approximation range ($\frac{\mathrm{gr}}{\mathrm{cm^2}}$)
ρ	Density ($\frac{\mathrm{gr}}{\mathrm{cm^3}}$)
N	Number of secondary electrons generated in ionization chamber
A	Cross section (cm^2)

Φ	Fluence ($\frac{1}{\mathrm{cm}^2}$)
$\dot{\Phi}$	Fluence rate ($\frac{1}{\mathrm{cm}^2\mathrm{s}}$)
W	Energy required to generate a pair of ions in the ionization chamber (MeV)
$\dot{E_{abs}}$	Total energy absorption in the gas chamber (MeV)
T_b	Boiling point temperature at atmospheric pressure (°C)

GLOSSARY

AR	Atmospheric residuum
DAO	Deasphalted oil
FID	Flame ionization detector
GC	Gas chromatography
GC–MSD	Gas chromatograph–mass selective detector
LET	linear energy transfer
RTC	Radiation thermal cracking
RGA	Refinery gas analyzer
RVR	Relative viscosity reduction
SIMDIS	Simulated distillation
TC	Thermal cracking
TCD	Thermal conductivity detector
VDG	Van de Graaff

TABLE OF CONTENTS

Page

Page

Page

LIST OF TABLES

LIST OF FIGURES

FIGURE Page

FIGURE Page

FIGURE Page

1. INTRODUCTION

During the last six decades, the indispensable role of petroleum in development and industry has drastically increased its consumption. High demand of petroleum products and inability of conventional reservoirs to fulfill the growing inquiries brought the attention to, rather harder to extract and process, unconventional reserves. Although these resources offer a long–life production and a good upside potential to boost recoveries through new technologies, transformation of such unfamiliar resources into reserves has posed awkward challenges to the industry. Complicated reservoir rock characteristics; upgrading, processing, and refining capacities; and environmental concerns are among the current challenges. The question is whether the industry can increase the production of unconventional resources to a level that compensates the declined production of depleting conventional reservoirs.

Among unconventional resources, bitumen and extra–heavy oil reservoirs form considerable portion of the reserves. Natural bitumen and extra–heavy crudes are closely related types of petroleum and differ only by the degree they are degraded. These alterations, mainly caused by bacterial attack, result in the loss of lighter components and consequently a higher concentration of asphaltene and other non-hydrocarbon components. Although bitumen and heavy oil are encountered worldwide, 85% of the bitumen reserves are located in Alberta, Canada, and 90% of the extra–heavy oil reserves are located in the eastern Venezuela basin [1, 2]. Difficulties arise while dealing with such a heavy hydrocarbon fluid from the time it is extracted, using heavy oil recovery methods, through the time it is transported to the refinery units and finally when it is upgraded into more utilizable hydrocarbons [3].

This thesis follows the style of the *Journal of Fuel Processing Technology*.

Upgrading is defined as a process where heavy complex hydrocarbon molecules break into lighter, and more utilizable species. The minimum objective of the upgrading is to reduce the viscosity without adding costly solvents, whereas the full upgrading approach is to process the oil to obtain higher quality products. Among the upgrading methods, thermal cracking, catalytic cracking, and hydroprocessing are the most important. Although effective in throughput, these processes are not technically efficient, as they require a substantial energy investment and, in some cases, expensive chemical catalysts. In addition, unavoidable environmental pollution problems, such as sulfur dioxide emission, are the by–effects of such processes [4].

While high energy demand of conventional thermal and thermocatalytic process casts doubts on the application of such methods, ionizing incidents, as an emerging upgrading technology, have been observed to be a promising and efficient way of providing higher selectivity, quality, and quantity of the treated feed [5]. Noting that no previous work has evaluated the physical changes of radiolyzed hydrocarbons, thermal and radiation thermal cracking of heavy asphaltic and deasphalted fluids were compared to find the changes, induced by electron irradiation. In this study, high energy electron particles, generated using a Van de Graaff accelerator from biological and agricultural engineering department at Texas A&M University, were used as ionizing agents. The yields were analyzed in terms of their viscosity and density as well as their boiling point distribution. To provide more information about the process and analyze its industrial applicability, the viscosity of the products were monitored till 120 days after the tests. Additionally, light hydrocarbon analyses helped us to better understand the radiolytic behavior of the fluids.

Different aspects of hydrocarbon radiolysis and its application in petroleum processing technologies are discussed comprehensively in section 2. Section 3 provides a brief theory about ionizing incidents and their characteristics. Knowing the behavior of charged particles and their interaction with the media can help to better understand the energy deposition phenomena. Section 4 describes the experimen-

tal procedure and material. It covers all the details about the reaction setup, as well as the petroleum fluids and analytical tools. Section 5 presents the results of different radiolysis experiments. This part covers the radiation induced cracking of two different hydrocarbon fluids and the impact of different influencing factors, such as reaction temperature and the amount of absorbed energy, on the radiation throughput. Finally, the last section summarizes the study with conclusions and recommendations for future work.

2. LITERATURE REVIEW

The current section provides precious information about different aspects of hydrocarbon irradiation and can be used as a comprehensive reference for any related study. Integrating the various studies on different aspects of radiolytic reactions of hydrocarbon components, the probable advantages and disadvantages of using ionizing incidents in hydrocarbon processing technologies, as well as effective parameters and potential applications can be generalized to an extended scope.

2.1 Irradiation of Different Hydrocarbon Components

Irradiation of different hydrocarbon groups, including heavy petroleum fluids, coal, model hydrocarbons, distillation cuts, light hydrocarbons, gaseous hydrocarbons, lubricants, polymers, and aromatics is reviewed in this section to provide detailed information on radiation induced behavior of each specie and the consequent changes.

2.1.1 Heavy petroleum fluids

The term "hydrocarbon enhancement electron beam technology (HEET)" was first used by Mirkin et al. [6] to generalize new approaches to radiation processing of petroleum products. Investigating different natural and artificial heavy oil samples, they showed that for all HEET cases, the output of light products is 20 to 25% higher than those of thermocatalytic processes. Note that, despite the complicated nature of the present–day crude upgrading technologies, HEET refinery systems use simple regulation of parameters of radiation thermal processing in a limited range of technologically justified values. Moreover, this technology provides the opportunity to use byproducts of radiation processing as chemical agents, leading to an efficient control of radiolysis reactions. The capital cost of a HEET–based pilot was reported

to be considerably less than that of a thermocatalytic one with the same processing capacity. Fig. 2.1 provides a schematic design of a HEET reactor that is comprised of a preprocessing unit, a metering system, and a reaction chamber to expose the samples to high energy electrons.

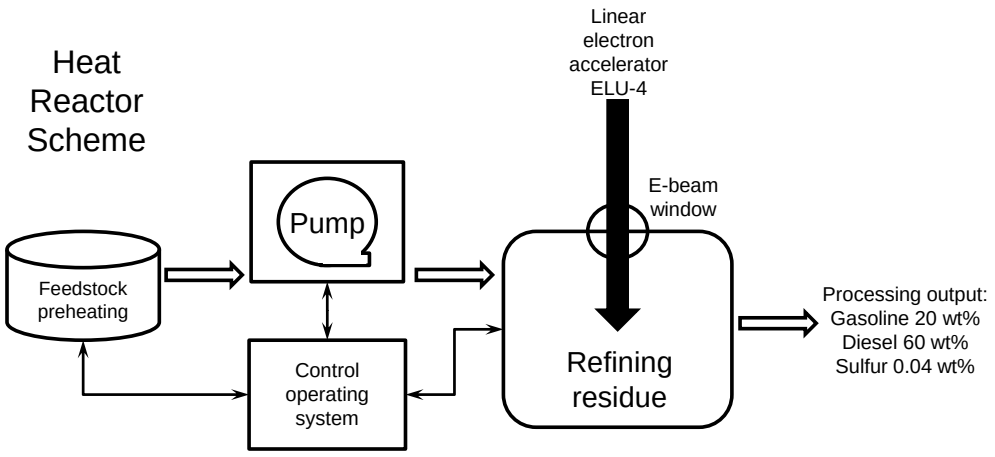

Fig. 2.1.: Layout of HEET facility (reproduced after Mirkin et al. [6])

The reactor can be used in three potential situations:

- As a visbreaking assembly to make viscous samples transportable
- As a new generation of HEET–based refineries
- As additional units in traditional refining systems

Irradiation of highly viscous oil with high content of sulfur, heavy paraffins, and heavy residue material shows that induced chemical reactions for model hydrocarbons with very simple structures vary from those of very complex mixtures, where the presence of different hydrocarbon species results in strong synergetic effects [7].

Zaykina et al. used different temperature and dose rate values to control the hydrocarbon content of the final yield. The results show that the radiation thermal method intensifies cracking rate when compared to thermal cracking. Decreasing the delivered dose rate and temperature results in lower probability of disintegration of large radicals. In fact, experimental conditions strongly affect the distribution of different species and lead to different ratios of polymerization and isomerization.

Studies on radiolysis of two different petroleum fluids from Kazakhstan fields demonstrate that various hydrocarbon species behave differently while being exposed to ionizing irradiation [8]. Irradiation of the first sample (Karazhanbas oil, that is characterized by high contents of heavy aromatics) showed polymerization reactions along with intermolecular isomerization as a consequence of radiation–induced reactions in complex hydrocarbon mixtures. On the other hand, the latter oil sample (Kumkol field oil with low amount of aromatic compounds and high content of paraffinic components) did not exhibit that degree of isomerization but a heightened rate of radiation destruction and low concentration of isoalkanes. The results illustrate the considerable role of synergetic effects on radiolytic reaction rates and yield. Improved isomerization along with sulfur content reduction was also observed as a result of high–dose–rate radiolysis of bitumen and gas mixtures [9].

Skripchenko et al. [10] showed that gamma irradiation of heavy hydrocarbons leads to a destructive process, changing solubility and yield of light fractions in experiments. They observed that irradiated petroleum products represent more chemical activity while being kept in contact with atmospheric oxygen. This was demonstrated by an increase in the intensity of the absorption bands of groups containing oxygen in their IR spectra. According to the authors, irradiated samples are vulnerable to any changes—even while getting exposed to distillation heat—due to their active characteristic. However, in this study, we prove that irradiated samples are fully stable. In fact, the life of active species is too short that they disappear right after the experiments.

One of the most interesting applications of ionizing incidents refers to interpretation of the chemical changes that occur for the samples while getting exposed to gamma ray in order to simulate carbonization of sedimentary organic matter in the presence of heat, which may be affected by irradiation as well [11]. The results show that radiolyzed bitumen contains less volatile components than the original case and consequently has more residue. In fact, radiolysis causes the emission of gases and consequent crosslinkings. Evolved gases are comprised mainly of H_2, CH_4, CO_2, and CO. It is predictable to obtain higher coke residue for radiolyzed samples; that is attributed to the loss of volatile fragments during radiolysis and also to crosslinking reactions, occurring inside the samples. Crosslinking of the resin molecules can be the reason for higher asphaltene content of radiolyzed samples.

Zaykin et al. [12] studied the synergetic effects of ionized ozone–containing air and ionizing irradiation on the hydrocarbon content of heavy petroleum fluids. Note that ozonides and sulfoxides have the ability to initiate radical chain reactions to amplify thermal destruction of hydrocarbon molecules. Two different scenarios were applied upon petroleum samples of high viscosity and sulfur content:

1. Preliminary bubbling by ionized air at room temperature followed by radiation thermal cracking at higher temperatures

2. Simultaneous bubbling and irradiation at temperatures of 20°C to 40°C

The first scenario decreased the amount of irradiated dose that is necessary for maximum yield of liquid samples along with a 40°C decrease in cracking onset temperature. Additionally, a 10% increment was observed in the gasoline concentration, which comes with some alterations in the hydrocarbon content of the gasoline fraction in the liquid yield of RTC. The results demonstrated an increase in total yield of liquid fractions with boiling point less than 350°C compared to the case of thermal cracking coupled with preliminary, conventional ozonolysis. Although radiation was observed to raise gasoline content of the experiment's liquid yield, the amount of liq-

uid yield was reduced by the cracking reactions. The second scenario demonstrated synergetic effects of cold irradiation and ozonolysis on oil samples and their dependence on characteristics of irradiated samples. For a model sample with aromatic content of around 30%, considerable increase in the yield of light compounds and pronounced alteration of heavy residues was reported.

Heavy petroleum fractions, as emission band carriers, appear to be proper candidates to study radiolysis processes occurring in astronomical objects [13]. Radiation–induced reactions of distillate aromatic extract (DAE) with aromaticity of 45% show that irradiation increases the hexane insoluble fraction of DAE—usually defined as kerogen—eight times due to crosslinking reactions. Gas chromatography analysis shows that gases such as H_2, CH_4, and CO evolve during irradiation. In general, hydrogen will be forming the most abundant gaseous products, liberated as a consequence of hydrogen abstraction reactions and carbon–carbon bond formation. Thus, as a result of hydrogen extraction, formation of heavier hydrocarbons is predictable.

Yang et al. [14] provided a laboratory scale investigation on high temperature electron beam irradiation as an economically favorable method to upgrade heavy petroleum products. Their study covers experiments on hexadecane, naphtha and asphaltene. According to the authors, C–H bond cleavage occurred during radiation thermal cracking of C_{16} samples. Despite the thermal cracking cases, H_2 exists in gas samples of the radiation experiment and more olefin content is detectable as a consequent of irradiation. Isoparaffin content was reported to increase for irradiated samples, which is an indication of isomerization (isoparaffins are valuable hydrocarbons since they increase the octane rating of hydrocarbons resulting in quality fuels). The authors have introduced the idea of partial upgrading to overcome heavy oil transportation problems. They also presented a new design for heavy oil upgrading in pipelines. In this plan, electrons will affect the fluid inside the pipeline while the fluid is flowing. Applying the suggested setup can improve the process throughput by continuously exposing samples to ionizing particles. In another study, the same

authors coupled heat transfer and the radiation Monte Carlo simulation to model the electron beam upgrading process of multiphase and singlephase C_{16} radiolysis. The work is known as a pioneer in this field as no previous effort had been done to simulate electron beam processing of petroleum products [15].

As stated also in a number of other works, radiation thermal cracking of components with high concentrations of heavy paraffins and low aromatic content differs from that of samples with considerable amounts of heavy aromatics rings [16]. Zaykin et al. [16] studied radiation thermal cracking of fluids with a high concentration of C_{15}–C_{22} hydrocarbons and low amounts of polycyclic aromatics and pitch (the sample is known as a low–viscosity, low–sulfur fluid). The results showed low levels of isomerization and high polymerization rates along with low yield of light fractions at low dose values. The molecular weight of the gasoline fraction was observed to increase after irradiation, which indicates increased destruction of paraffins in the middle of molecules as dose rate increased. It raises the probability of alkyl radical recombination with subsequent formation of paraffin molecules lighter than the molecules destroyed but heavier than gasoline molecules. Note that the increase in the number of C–C bonds in a molecule causes excitation energy redistribution over the larger number of carbon bonds, diminishing the efficiency of C–C bond cleavage [17].

Although application of ionizing incidents in the petroleum industry has had a rapid growth during the recent decades, none of the works investigated the rheological property changes that are brought about because of radiation induced reactions. Alfi et al. [18, 19] showed that electron–induced thermal cracking of deasphalted and highly asphaltic petroleum fluids results in samples with lower viscosities than the thermal cracking cases. On top of that, irradiated samples exhibited time–stable characteristics. This technology can be applied either in oil well head locations or petroleum refineries.

2.1.2 Coal

Application of gamma irradiation on hydrogenation products of coal samples and distillation analysis of treated and untreated samples indicate that the yield of light fraction (boiling at temperatures up to 300°C) falls as a consequence of irradiation, which can be attributed to variability of the products of coal hydrogenation [10]. Such changes mean that the polycondensation occurs and molecular weight of the exposed samples increases. Irradiation of coal–oil mixtures revealed that the yield of oil and benzene soluble substances rises while the amount of oxygen molecules in the hydrocarbon structure decreases after radiolysis. Gamma ray is also capable of activating coal samples substantially [20].

Irradiation appears to be a promising method to replace conventional chemical and mechanical pretreatments for hydrogenation of coal samples into low–molecular–weight soluble species [21, 22]. It provides considerable changes in the composition of dry brown coal, such as, partial decarboxylation of carbonic acid derivatives or breaking of alkyl $–CH_2–$, especially $–CH_3$ chains (the evolution of gases was observed during irradiation as a result of these reactions). Note that the yield of volatiles was reported to increase with further increases in the irradiated dose. Considering the relation between irradiation dose and conversion of coal in hydrogenation, one can see that conversion attains a maximum and then decreases with further increase of the exposed dose. This study showed that addition of organic solvents such as tetralin and ethanol substantially improves reactivity of the coal samples. Comparison of these cases with the different conventional pretreatment methods such as methylation in $(CH_3)_2SO_4$, reduction with $LiAlH_4$, and HCl treatment showed that the highest reactivity was achieved for irradiation in the presence of ethanol. Different analyses reveal that degradation and crosslinking constitute the majority of radiation–induced reactions where degradation prevails over the other pretreatment scenarios. After the most readily degradable components have been decomposed, polymerization becomes effective, resulting in crosslinked matter with low reaction potential. Although some

of the reported results of coal irradiation appear to be contradictory, the problem arises from the circumstances under which radiolysis reactions have been performed. Not all the authors have mentioned the detailed conditions of the irradiation process, which may be the reason for some of the conflicts as this study shows that conditions such as temperature, dose rate, absorbed dose, etc. have significant effect on the process output.

In efforts to obtain useful information about coal structure and examine the possibility that coals matured under the action of irradiation in earth's crust, gamma irradiation of coal samples and investigation of decomposition gases have shown that the amount of decomposed gases has no predictable relation with irradiation time (which is in fact, an index representing amount of absorbed dose), indicating the possibility that secondary reactions occur, as shown in Equation 2.1 [23].

$$\text{Coal} \overset{\gamma-Irr}{\rightsquigarrow} \text{Primary Products} \overset{\gamma-Irr}{\rightsquigarrow} \text{Secondary Products} \tag{2.1}$$

These secondary reactions have been also mentioned by Mitsui and Shimizu [24]. The G–value of hydrogen (G–value is defined as the number of molecules undergoing degradation for absorbed energy of 100 eV) shows small increases with irradiation time that are probably due to the secondary decomposition. The fact that hydrogen constitutes more than 90% of radiation–induced evolved gases with less than 1% of hydrocarbon gases while coal–mine gas contains over 95% methane with traces of hydrogen suggests that coalification did not proceed under the influence of irradiation. Another study by Mitsui et al. [25] shows that degradation and polymerization take place simultaneously.

Cataldo et al. [11] demonstrated that the basic structure of the coal would survive intact with no substantial changes for radiolysis with absorbed dose values around 1 MGy. According to them, irradiation is responsible for emission of H_2, CH_4, and CO/CO_2 with formation of tight crosslinks in radiolyzed coal samples; that emission results in higher amounts of coke residue for radiation–treated coal samples.

Comparing radiation thermal cracking of coal, coal–tetralin, and coal–asphalt samples in the presence of hydrogen at temperature of 400°C with thermal cracking cases, Mitsui and Shimizu [24] concluded that gamma irradiation accelerates decomposition of heavy hydrocarbons in coal but does not affect lighter species much. Irradiation of the mixtures of coal and tetralin expedited decomposition of heavy contents from the early times of irradiation. Moreover, changes in the amount of evolved gas and oil products in radiation thermal cracking of coal and asphalt mixtures confirms accelerated decomposition of both coal and asphalt samples. Corresponding analyses of gas products introduce methane and carbon monoxide as the dominant components of the liberated gases. The formation of gaseous hydrocarbons was intensified as an outcome of irradiation, whereas the formation of carbon monoxide and carbon dioxide exhibited independent trends to irradiation. Kinetic studies of H_2, CO, and CH_4 in thermoradiation decomposition of oil–bituminous rock demonstrated great dependence of gas yield on radiation temperature [26].

Haenel et al. [27] investigated the reactions that take place during coal degradation under ionizing irradiation by the use of model hydrocarbons in different solvents and provided details of all possible reactions and consequent yields, considering radical anions as the species generated during radiation–induced reactions of polar solvents (the medium volatile bituminous coal was used to evaluate degradation of coal structures). However, with respect to the degradation of the macromolecular coal, irradiation turned out to be less efficient than conventional reductive methods.

2.1.3 Model hydrocarbons

Wu et al. [28,29] investigated thermal cracking (TC) and radiation thermal cracking (RTC) of hexadecane in liquid and gas phases and compared the results to better understand the processes. In general, they believed that liquid–phase cracking is subject to a single step mechanism while gas–phase cracking is subject to a double or multiple step decomposition model [30]. Gas–phase C_{16} irradiation shows only nor-

mal alkanes and 1–alkenes as the dominant products of radiation thermal cracking without any products resulting from addition reactions. The concentration of gas (C_1 to C_4) and light (C_5 to C_{15}) products shows nearly independent trends for irradiation time at experimental temperature of 330°C. Higher temperatures lead to an increased yield of gas products and a decreased yield of light fraction. Because of low reactant concentrations in gas–phase irradiation, parent radicals undergo unimolecular β scission and no addition products will be formed. On the other hand, scission products together with addition products were observed for liquid–phase radiation. When alkene molecules were added to the parent radicals at higher concentrations of alkenes (achieved at longer irradiation times), longer residence time increased addition products, resulting in lower amounts of light (C_5 to C_{15}) fractions for liquid–phase radiation thermal cracking than gas–phase radiolysis. Increasing temperature, however, prevents addition reactions and increases content of other products. Considering the kinetics of the radiolysis reactions, for both liquid– and gas–phase radiation, k_{RTC} values increase with temperature and dose rate. The ratio of k_{RTC}/k_{TC} is large at lower temperatures and decreases as the temperature increases but increases with dose rate. The ratio of H_2 yield is reported to be higher for the radiation case than for the case of thermal cracking (H_2 yield increases with temperature and irradiation dose). C–H bond dissociation and direct molecular H_2 formation have been recognized as the processes leading to hydrogen formation in hexadecane radiolysis. Note that the product pattern with or without radiation is expected to be the same, but phase dependent. Kinetic approaches toward chain reactions in the radiolysis of n–C_{16}, the activation energies, and different parameters related to the reactions such as C–C dissociation, H abstraction, β scission and addition reaction were discussed by the same authors [30]. The rate of n–C_{16} decomposition was observed to strongly depend on chain termination reaction pathway.

To get more information on the chemistry of the processes taking place in the presence of ionizing energy, Tyshchenko [31] investigated three different hydrocar-

bon model systems comprised of different mixtures to evaluate four types of reactions named as: isomerization of alkanes, cyclization of alkanes, dehydrogenation of cycloalkanes into aromatics and condensation of aromatics. Increasing the irradiation dose from 5×10^5 rad to 1×10^7 rad resulted in significant enhanced condensation of aromatic compounds along with intensified dehydrogenation of cycloalkanes into aromatic hydrocarbons. The models also showed isomerization of the alkanes at low doses. Note that synergetic effects of individual components in hydrocarbon mixtures sometimes play an important role as it may cause ionization or excitation transfer among species [32].

According to Topchiev et al. [33], C–C bond rupture plays a vital role in formation of different saturated and unsaturated hydrocarbons during gamma–radiolysis of medium and heavy petroleum products. While conducting irradiation at room temperature, hydrogen gas was reported to dominate the other species. The composition of methane and hydrogen in evolved gas depends on the relative content of CH_3 groups in the molecules. Higher CH_3 ratios result in higher methane and lower hydrogen concentration. Alkyl radical recombination suppressed considerably when the experimental temperature was lowered to the range of 0°C to –196°C. This response can be accounted for by the fact that radicals, formed as a result of H detachment, will recombine with hydrogen atoms again due to handicapped diffusion at low temperatures. Very low temperatures also help us to prove the presence of free radicals in the radiolyzed samples through the low–temperature free–radical stabilization phenomenon. In fact, at –196°C, it is possible to stabilize almost 50% of the radicals formed at room temperature during irradiation of heptane, octane, cyclohexane and cetane.

C–H bond rupture, as a major effect of n–hexadecane irradiation, results in dimerization reactions through crosslinking of parent radicals [34]. Conducting the experiments in liquid and solid phase hexadecane, Salovey et al. evaluated the effect of physical state on radiation–induced reactions. Vibrationally excited molecules,

formed as a result of irradiation, will undergo five different reactions depending on conditions (Equations 2.2a, 2.2b, 2.2c, 2.2d and 2.2e).

$$\text{n-}C_{16}H_{34}{}^{*} \rightarrow \text{primary } C_{16}H_{33}{}^{\cdot} + H^{\cdot} \tag{2.2a}$$

$$\text{n-}C_{16}H_{34}{}^{*} \rightarrow \text{secondary } C_{16}H_{33}{}^{\cdot} + H^{\cdot} \tag{2.2b}$$

$$\text{n-}C_{16}H_{34}{}^{*} \rightarrow C_{16}H_{32} + H_2 \tag{2.2c}$$

$$\text{n-}C_{16}H_{34}{}^{*} \rightarrow C_i{}^{\cdot} + C_j{}^{\cdot} \tag{2.2d}$$

$$\text{n-}C_{16}H_{34}{}^{*} + M \rightarrow \text{n-}C_{16}H_{34} + M \tag{2.2e}$$

Consequently, observed products were categorized into three different groups based upon gas chromatography data:

- Components elute before hexadecane, that are scission products from further reaction of alkyl radicals. The yield of this group in liquid irradiation is twice that of solid hexadecane irradiation, which is attributed to the cage recombination of chain fragments in crystalline solids, resulting in suppression of main chain scission.

- Components eluting between hexadecane and octacosane (C_{28}), that are from combination of radicals generated by scission with hexadecyl radicals. Solid hexadecane reproduces a smaller amount of these components because of the suppression discussed before.

- Components eluting between octacosane and dotriacontane (C_{32}) that are treated as dimerization products that result from the combination of hexadecyl radicals. The yield of dimers has boon observed to be the same for solid– and liquid– phase irradiation. In spite of C–C bonds, C–H rupture and yield of dotriacontane from the combination of hexadecyl radicals is little affected by change of state.

The physical state of radiolyzed components was observed to greatly affect the product pattern after irradiation. The amount of evolved hydrocarbons (C_1–C_4) is twice and evolved hydrogen is 30% more for liquid hexadecane irradiation than the solid phase. The distribution of isomeric dimers suggested that the main sites of crosslinking are nonterminal, which occur at a random manner. Note that primary C–H bond rupture is half as possible as the secondary one. Moreover, CH_3–CH_2 rupture is one–fifth as probable as CH_2–CH_2 rupture, but all the internal C–C bonds have a similar chance of rupture [35].

The effect of dose rate on radiation thermal cracking of n–hexadecane suggests that increasing P (dose rate) decreases the yield of RTC products slightly (the effect of dose rate is not very significant and barely exceeds 5–6%) [36]. However, the effect of dose on the yield of RTC products showed that the overall conversion increases linearly with absorbed dose, and the yield of lighter hydrocarbons (C_5–C_{10}) will exceed that of heavier species (C_{11}–C_{15}). The effect of absorbed dose in radiolysis of *n*–hexadecane was also discussed by Soebianto et al. [37]. There, gas products were mainly formed of H_2, and liquid products contained crosslinking and scission yields in addition to unsaturated species. As irradiation dose increased, consumption of n–hexadecane and scission products increased linearly. However, hexadecene concentration increased at lower doses and leveled off for higher doses, which is an indication of secondary reactions (formation of hexadecene is attributed to liberation of H_2 and also to disproportionation of the parent radicals with scission radicals or the parents themselves). Higher doses also decreased the weight percent of dimers in oligomers and increased that of heavier oligomers, meaning that formed dimers are consumed to form heavier oligomers.

Falconer and Salovey [38] evaluated the effect of different parameters on radiolysis of n–hexadecane. The differences in behavior of hydrogen G–value with irradiated dose for liquid and solid phase irradiation were interpreted as diverse hydrogen formation mechanisms for two different states. All the low–molecular–weight species

(C_1–C_{15}) formed during solid–phase irradiation and 50% of those in liquid–phase irradiation were attributed to molecular reactions. Disproportionation of free radicals is responsible for the rest of the low–molecular–weight products. For cases of intermediate products (C_{17}–C_{31}) of irradiated liquid, 80% of the yield is formed in recombination of free radicals of the main C–C bond scission with hexadecyl radicals. The rest of the intermediate products in liquid–phase irradiation and all of those in solid–phase irradiation were formed in nonradical reactions. Besides, the use of electron scavengers such as iodine and 2–methylpentene–1 was observed to reduce all product yields. According to this study, the amount of radiolysis products shows very small dependency on the temperature; and among all the products, hydrogen yield appears to be more sensitive to temperature conditions. However, this is not in full agreement with what is mentioned on the role of temperature upon radiation–induced reactions by the other studies.

Considering the effect of molecular structure on radiolysis of liquid hydrocarbons (alkanes, alkenes, and aromatics), subjects such as G–value of different species and its relation to the structure of parent molecules, C–C bond strength and corresponding radicals for different hydrocarbons, estimation of radical yields of branched alkanes, calculation of G–value for C–C bond rupture, relation between the hydrocarbon structure and hydrocarbon free–ion yields along with their electron and ion mobility, hydrogen formation mechanism, competition of C–H and C–C bond rupture and the effect of branching on C–C bond strength were comprehensively discussed by Foldiak [17].

Topchiev et al. [39] analyzed high temperature radiation–induced reactions of n–heptane. At temperatures below 300°C, the slope of C_2 to C_5 yields with temperature is small but sharply increases at higher temperatures. The changes in behavior of the products for different temperatures suggest variations of gas formation mechanisms at different temperatures. Gas formation graphs for TC and RTC experiments indicate that RTC takes place at lower temperatures than TC. As a result of irradiation, the

amount of unsaturated hydrocarbons increases in both liquid and gas yields. Detailed descriptions of the mechanism and the kinetics of radiation–induced reactions has also been discussed by a number of authors, which provides better insight toward understanding of the radiolysis process to modify the conditions for the most desired throughput [30, 40–43].

2.1.4 Distillation cuts

Radiation thermal cracking would achieve a higher degree of conversion for the yield of products than thermal cracking [44]. Zhuravlev et al. studied vacuum gas oil irradiation of Western Siberian crude (350–450° fraction) at different temperatures and dose rates. Air–vacuum distillation of treated samples showed that the yield of gasoline and diesel fraction increases during RTC (at temperature of 400°C) by a factor of two and contains a higher concentration of lighter components than the TC ones. Note that the yield of the products of condensation in RTC is significantly lower than in TC.

Radiation–induced isomerization of gasoline fraction upgrading and the effect of aromatics and ionized air application on the radiolysis process was investigated by Zaikin and Zaikina [45]. Paraffin isomerization increased while adding bitumen (with high aromatic content) to the gasoline samples. The effect of aromatics on gasoline upgrading was appeared to come to saturation after a certain concentration. High–radiation–resistant aromatic compounds have the ability to absorb the excess energy of free radicals, giving radicals enough time to stabilize their electron structure and form isomers. Moreover, ionized air bubbling was shown to be an effective means to increase light fractions of radiolysis products. Ionized air, in fact, eases detachment of alkyl substituents by degrading aromatic structures. Consequently, heavy aromatic components enrich the gasoline fraction with light aromatics and improve isomerization, resulting in better quality of the gasoline fraction. Similar

synergetic effects were also observed for the mixtures of low quality diesel and furnace fuel.

The experiments conducted by Topchiev et al. [46] showed predominant cracking of the paraffinic hydrocarbons along with accumulation of unsaturated hydrocarbons with unsaturated bonds located at lateral chain positions for case of radiolyzed gasoline samples. They conducted the experiments at 300°C to 600°C because operating at lower temperatures would not be effective for an efficient radiative thermal cracking (adequate energy is required to supply activation energy of chain propagation) and at very high temperatures, thermal cracking would dominate the whole process. At $T = 300$°C, the formation rate of higher boiling point products increased with absorbed dose. No polymers of condensed aromatic compounds was detected by spectral analyses. In addition to liquid samples, vapor–phase irradiation was conducted on gasoline and n–alkanes to evaluate the influence of effective parameters such as pressure, absorbed dose, and dose rate. Additionally, radiation–induced reactions of three different gasoline fluids were evaluated by the same authors. Two light gasoline liquids established similar trends for the products with respect to reaction temperature. As temperature increased, the yield of C_2–C_5 fraction increased but hydrogen decreased. Higher temperatures also increased the concentration of unsaturated hydrocarbons and aromatics in liquid products. Although gas products of heavier gasoline samples followed a trend similar to those of two lighter samples, the liquid product pattern deviated from that of light–gasoline liquid products. Comparing TC and RTC cases, more unsaturated species were found in latter case. In spite of the majority of the papers, the authors, however, concluded that the degree of radiation–related conversion for the gas oil is very much less than that of thermal destruction in petroleum refinery [39, 46].

Despite what Topchiev et al. stated on the effect of temperature upon unsaturated components [39, 46], irradiating three different petroleum distilled cuts at relatively lower temperatures was shown to generate less unsaturated components at

higher temperatures [47]. However, the amount of aromatic hydrocarbons, yield of light ends in fractions, density and refractive index increased.

Il'gisonis et al. [48] described the components of a large scale experimental radiation thermal cracking plant as heating system, circulation system, condensation and separation units, liquid removal section and carbon dioxide blower. Low–octane gasoline RTC and TC results revealed that radiation increases the yield of ethylene, propylene, and butylene while reducing cracking temperature by 150–200°C.

To fully understand the radiolysis process of petroleum cuts, experiments on the behavior of gas oil under action of irradiation and heating have been carried out with straight distilled kerosine gasoline fractions, characterized by high amounts of naphthenic and aromatic hydrocarbons [49]. Using the concept of G–value, three different regions are distinguishable in the graph of ln G vs. $1/T$ (Fig. **??**). Below $T = T_p$ (T_p is defined as critical temperature with an estimation of $T_p \approx 600$K), the G–value changes relatively small with temperature (pure radiolysis, region I). For temperatures greater than T_p, G–value begins to increase rapidly with temperature (radiation–thermal cracking, region II). In this region, in fact, a considerable role begins to be played by degradation processes similar to those taking place in thermal cracking. In other words, if processes of the recombination of the radicals formed under the action of radiation predominate below T_p, above that temperature the radicals begin to decompose with the rupture of C–C bonds in a rapid pace. At higher temperatures, radiation thermal cracking passes smoothly into thermal cracking where decomposition depends only on total absorbed energy (thermal cracking, region III). The yield of gas products shows a linear trend with the absorbed dose at sufficiently high total absorbed dose values.

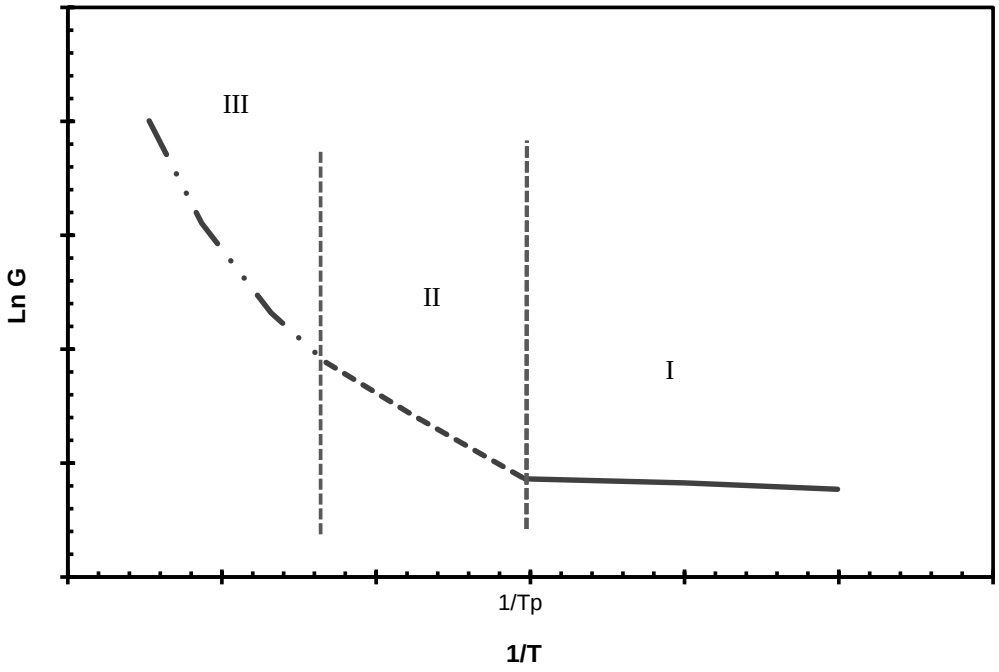

Fig. 2.2.: Variability of G–value with temperature provides three distinct regions with different reaction processes (reproduced after Brodskii et al. [49])

Carroll et al. evaluated the behavior of different hydrocarbon fuels in the presence of ionizing irradiation [50]. Although the authors did not mention anything regarding the reaction temperature, the results indicate that radiolysis took place at fairly low temperatures. The density of the fuels (as well as viscosity for high absorbed doses) increased as a result of irradiation. Moreover, distillation analysis showed an increase in the concentration of the high–boiling–point material. Irradiation was also observed to decrease hydrogen content in the samples. On the other hand, aromatic content was not reported to change considerably after radiolytic treatment.

2.1.5 Light hydrocarbons

The observed effects of gamma irradiation on thermal cracking of n– and isopentane suggest that both thermal cracking and radiation thermal cracking proceed by chain reactions which involve cracking of pentyl radicals produced as a result of either heating or irradiation [51]. As subsequent chain reactions of generated radicals are the same in cases with and without irradiation, the product pattern must be same for both the cases. Propane, ethane, methane, ethylene, butylene and hydrogen were reported as the primary products of all the experiments. Although radiation had no effect upon decomposition rate of n–pentane, for isopentane at lower temperatures or pressures, irradiation suppressed decomposition while higher temperatures and pressures led to intensified decomposition when irradiation was employed.

Foldiak and Horvath [52] evaluated radiolysis reactions in C_3 family (propane, propene, and cyclopropane) binary mixtures. According to their study, bimolecular interactions (reactions related with synergetic effects of mixture components) have considerable influence on radiolysis products (C_1 to C_6 components) when competing unimolecular reactions (the ones corresponding to each of the pure components individually) are not too fast. These results showed that the concept of protection, which is defined as interactions during radiolysis of saturated–unsaturated systems leading to shrinkage of products G–value, is not accurate in the general expression and can be extended just to a limited number of reactions. These conclusions were also further confirmed considering radiolysis yields of C_4 family (n–butane, 1–butene, cyclobutane and cyclobutene) binary mixtures [53].

2.1.6 Gaseous hydrocarbons

Generation of heavier hydrocarbons by irradiation of light gaseous propane demonstrates that polymerization can occur during ionizing irradiation [54]. Analytical experiments have shown that hexane molecules dominate the other hydrocarbon

products of propane radiolysis, which is a direct indication of dimerization reactions of propyl radicals. Additionally, the presence of water and oxygen molecules in initial components can result in formation of oxygen–containing alcohols and ethers [55]. To eliminate the participation of intermediate and final radiolysis products in radiolytic reactions with initial components, which will complicate evaluation of radiolysis process yields, and to accurately investigate the influence of radiation on well–known initial components, Ponomarev et al. [55] monitored radiolytic conversion of gaseous hydrocarbons under circulation conditions that separated condensible species from noncondensible gas reactants. In another study on radiation induced reactions of gaseous hydrocarbons (different mixtures of C_1–C_5), Ponomarev [56] showed that dimerization and trimerization reactions lead to the formation of highly branched liquid hydrocarbons with high octane numbers. As the dose rate increased, the liquid phase light component fraction and the degree of branching both increased. Note that the degree of isomerization depends on factors such as initial gas composition and irradiated dose rate. More information regarding G–values for the products of the irradiation of hydrocarbon gases along with information on reaction mechanism and kinetics is provided by Lampe [57].

Ponomarev et al. [58] studied the behavior of gas phase composition (C_1—C_5 hydrocarbons) during irradiation, along with the liquid products of radiolysis. For radiolysis of relatively light mixtures, with high methane content, irradiation resulted in an increase in molar mass. On the other hand, the molar mass of relatively heavier components, with higher concentration of C_2–C_5, gradually decreased with energy consumption, which can be attributed to the maintenance of low–molecular–weight gas components due to the physical and chemical protection of methane and ethane groups by larger homologues. The reason for this behavior is that the electronic activation potentials of methane and ethane are higher than those of heavy homologues, resulting in a probability that excess energy and charge will transfer from excited methane and ethane molecules and ions to the other alkanes. The liquid product

of gas mixture radiolysis is characterized by a high content of branched, saturated hydrocarbons, which covers molecules in the range of C_6 to C_{11}. Note that concentration of unsaturated species is insignificant in condensed liquid products. Studies by Marakov et al. [59] and Ponomarev et al. [60] provide more information about the reaction mechanism and chemistry of gas mixture radiolysis.

Crawford and O'Briant [61] investigated the effect of ionizing radiation upon methane molecules that were dissolved in reservoir fluid to see whether the recombination process of radiolytic free radicals can be so controlled that the viscosity of the heavy oil is reduced. This study differs from the rest of related works in two aspects:

- Unlike the other cases, that have all the light compounds in gaseous phase, methane radiolysis was evaluated in solution with reservoir fluid.
- Unlike the other cases, the authors aimed to evaluate applicability of ionizing particles for "in–situ upgrading" purposes.

The decomposition of methane in solution with crude oil was shown to be negligible at irradiation conditions possible for in–situ upgrading.

2.1.7 Lubricants

Studies on the effect of low temperature ionizing radiation on naphthenic hydrocarbons in lubricants have shown that naphthenic components are resistant to absorbed dose up to 1000 kGy (note that although irradiation was observed to increase the viscosity of radiolyzed samples, considering industrial limitations, samples with viscosity increases less than 25% were considered as radiation–resistant fluids) [62]. At higher absorbed doses, the change in properties of naphthenic components became more pronounced as the molecular weight increased for samples of larger cyclic structure. Distillation analysis showed that irradiation causes the naphthenic samples to distill in a wider temperature range. When the naphthenic hydrocarbons were irradiated in the absence of air, they underwent more significant changes than

the cases in contact with air. In studies of the radiation resistance of aromatic compounds in lubricants (at low temperatures), increases were observed in viscosity, molecular weight, refractive index, density and iodine number [63]. However, the viscosity increase of the aromatic hydrocarbon fractions was considerably less than that of naphthenes. Despite what was observed for naphthenic hydrocarbons, the change in viscosity properties of the aromatic compounds in lubricants became less severe as aromatic molecules got heavier. Fig. 2.3 shows viscosity changes of samples irradiated to a dose of 5×10^8 rad as a function of the content of carbon atoms in aromatic rings. The results of this study also show that formation of condensed aromatic hydrocarbons is more pronounced when samples are irradiated in contact with air.

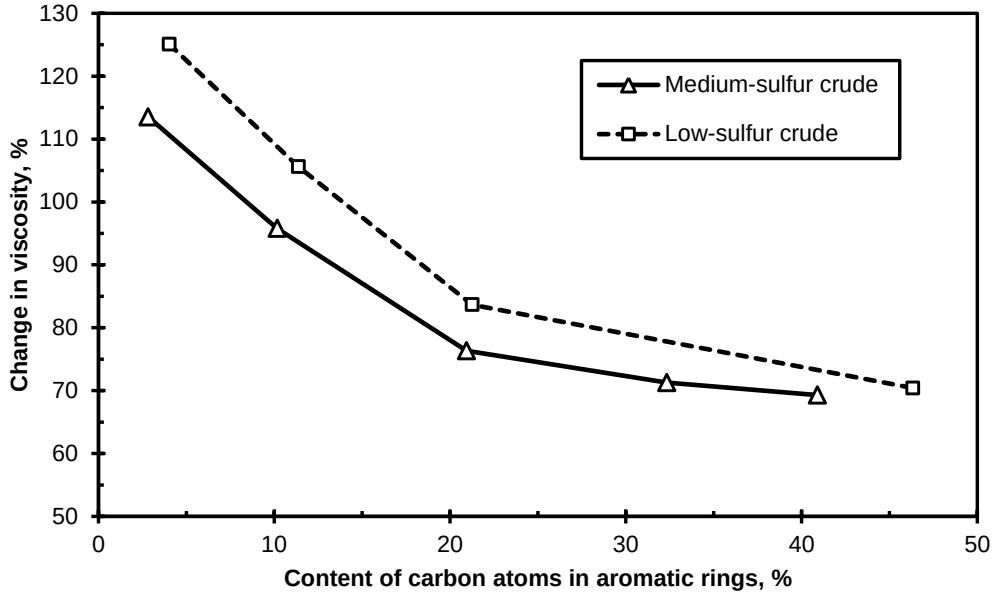

Fig. 2.3.: Fluid viscosity is greater for the cases with lower contents of carbon atoms in the aromatic ring (reproduced after Potanina et al. [63]).

Application of radiation methods to produce lubricants from heavy petroleum fluids replaces all the complex stages of lubricant production from raw petroleum fluids with a fairly simple method [64]. In contrast to the technology of fuel production, lubricant production relies on polymerization reactions which decrease mono–olefin contents, resulting in lower oxidation rates. Applying irradiation at temperatures higher than the onset of radiation thermal cracking provides a combination of high rates of destruction and olefin polymerization. In other words, the advantage of employing radiation technology in lubricant production is the ability to control non-destructive, thermally activated reactions by temperature variation, while the destruction rate is managed by variation of dose rate [64]. In addition to what is mentioned earlier, utilization of ionizing irradiation for recycling of used lubricants shows promising improvements in the contamination–removal processes [65].

2.1.8 Polymers

Chapiro [66] provided general information on various applications of ionizing incidents in the polymer industry such as radiation–induced crosslinking and curing of coatings and lacquers, radiation sterilization of plastic medical supplies, molecular weight control processes, Teflon waste handling, and so on. Transformations of radiolyzed polymers, influence of oxygen, gas formation processes, crosslinking, main chain scission and unsaturation are other polymer–related phenomena discussed by the author.

The radiation chemistry of polyethylene, polymethylene, and octacosane demonstrates crosslinking as one of the observed reactions that results in formation of heavier species [67]. Polyethylene shows the highest tendency for crosslinking reactions while the main evolved gas for all the experiments is H_2. The results also imply that C–C bond scission does not occur at random chain positions, and chain–end cleavage is preferentially more favorable.

Williams [68] performed a literature survey on different mechanisms of polymer crosslinking by ionizing incidents and named the following processes as the main mechanisms of crosslinking:

- Direct action of ions by either ion–molecule–electron or ion–molecule process

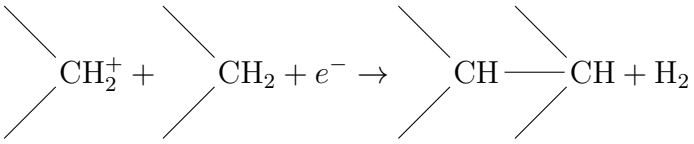

$$CH_2^+ + CH_2 + e^- \rightarrow CH{-}CH + H_2 \tag{2.3}$$

- Interaction of free radicals of low mobility

- Decay of unsaturation initially present or formed during radiolysis

The effect of nitrous oxide on the radiolysis of polyethylene, polypropylene and polyisobutylene at different N_2O pressures revealed complex and, in some cases, unusual behavior of nitrous oxide during irradiation [69]. Introduction of N_2O to the samples during irradiation cut down the dose required for crosslinking of polyethylene or polypropylene and kept polyisobutylene from degradation. Nitrous oxide disappeared at high rates but—despite the components such as oxygen, chlorine, and sulfur—no chemical addition proceeded as N_2O changed into N_2 and H_2O during radiation.

Mohan and Iyer [70] investigated radiation–induced polymerization of methyl methacrylate (MMA) in aliphatic hydrocarbon solvents to evaluate the extent of solvent incorporation into the polymer molecules and possible sites of entry. Note that the polymerization process can be influenced by the polar nature of the solvent, solubility of the polymer, viscosity and chain transfer. Their results suggested that the rate of MMA polymerization reduced in the presence of hydrocarbons, and a fraction of hydrocarbon solvent was chemically bonded to the polymer chains, constituting, in some cases, 12 wt% of polymer chains (incorporation of hydrocarbons increases with increasing chain length of solvent) in one of the following ways:

- Unsaturation in the hydrocarbon molecules
- Unsaturation in the polymer molecules
- Reaction of hydrocarbon radicals

The effect of atmospheric hydrogen on volatile products of radiolysis of polybutadien showed that with increasing pressure of hydrogen, G–values of methane and propane increased, while those of unsaturated hydrocarbons decreased [71]. The increase in saturated hydrocarbon evolution is due to the increase in polymer chain ends by irradiation in hydrogen, as the light hydrocarbon molecules are consequences of chain–end scission. The decrease of unsaturated species, on the other hand, correlates to hydrogen addition to the product of unsaturated hydrocarbons.

Radiating n–paraffins, as model components of polymers, Tabata [72] observed clear linear energy transfer (LET) effects (LET is a measure of energy transferred to a material as an ionizing particle travels through the medium). Note that LET effects come from different spatial distributions of active species such as free radicals or double bonds. In saturated linear hydrocarbons, no chain scission occurred for components heavier than a certain number of hydrocarbons, probably 20 carbons. More information on various aspects of polymer irradiation is provided in a number of other studies [73–78].

2.1.9 Aromatics

Due to special hyperconjugated electron structure of aromatic components, they exhibit more radiation–resistant characteristics than the other hydrocarbon species [17, 33, 63]. Alekhina et al. [79] studied radiation thermal stability of aromatics and nonaromatic groups. Their results showed that the radiation resistance of aromatic hydrocarbons depends on the number and relative position of the rings. Among all the aromatics, molecules with one and four rings and molecules with several rings linked by simple bonds showed the least radiation resistance. On the other hand,

naphthalenes along with molecules composed of three rings (such as phenanthrenes) exhibited the highest resistance to radiation degradation (Fig. 2.4). Han et al. [80] showed that decomposition of aromatic volatile organic components by electron beam irradiation (as a way to purify polluted water or gas) would be accelerated through radical chain reaction in the presence of chlorine components. Electron beam has also been reported to extensively decompose polyaromatics in sewage sludge [81].

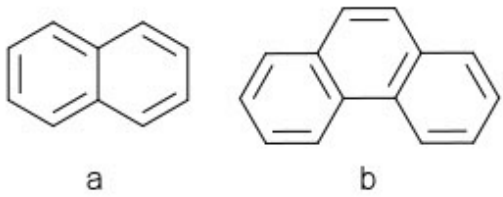

Fig. 2.4.: Atomic structure of naphthalene (a) and phenanthrene (b)

To better understand the effect of aromatics on radiolysis of n–hexadecane, Soebianto et al. studied various irradiation scenarios with different additives [37,82] (for more information see section 2.1.3). The results demonstrated the protection effect of aromatics and hydroaromatics that reduces formation of hydrogen gas, scission and crosslinking products. In the presence of aromatic compounds (with lower excitation and ionization potentials), protection occurs either through charge scavenging by the aromatics or energy transfer to the aromatics, leading to reduction of excited C_{16} molecules, and consequently, shrinkage of its decomposition products. Aromatics exhibited the same protection characteristics for n–dodecane, as a model compound for polymers [83]. Radiation protection properties of aromatics and hydroaromatics is one of the most popular subjects in hydrocarbons radiation chemistry [45,76,84,85]. Note that the hydrogen–donating properties of hydroaromatics identifies them as

radical scavengers in chemical reactions. In all cases, additives are reported to react with the main component, forming intermediate species.

2.2 Different Aspects of Irradiation

In addition to the discussed purposes, ionizing irradiation can be applied as an efficient contamination removal scenario. The current section provides more information about the other aspects of hydrocarbon radiolysis.

2.2.1 Contamination removal

Looking from various perspectives, undesirable contaminants, such as sulfur, should be removed from petroleum fractions for several reasons including reduction or elimination of sulfur caused corrosion during refining or transportation processes; increasing performance of fuels; decreasing smoke formation during the combustion process; and improving burning characteristics of fuel oils [86]. As a new technique, ionizing irradiation has offered several ways to reduce sulfur content of hydrocarbon fuels. Zaykina et al. [87] developed a two–stage radiation–based method for desulfurization of oil products. The first stage is radiation processing of oil samples and the second stage is to extract highly oxidized sulfuric compounds. In fact, as a result of radiation–induced conversion, sulfur moves into high–molecular–weight oxidized compounds in heavy fractions that can be extracted easily (the process is intensified as the amount of absorbed dose increases). Note that experimental conditions can be modified to prevent crude oil cracking and only improve desulfurization. The authors also introduced the bubbling method (using ionized air produced as a result of irradiation) as a promising way to control oxidation reduction processes of highly sulfuric petroleum fluids. The results showed that ionized ozone–containing air substantially enhances oxidation of high–sulfuric oil, improving fractionation of final

products. Some other papers also reported radiation as an efficient desulfurization scenario [9, 44].

As a way to remove environmental contamination, polycyclic aromatic hydrocarbons in sewage sludge show degradation efficiency of up to 90% when electron irradiation is employed to treat contaminated samples [80, 81]. The decomposition rate intensifies as the aromatic contaminant molecule becomes heavier (higher number of rings) or as the absorbed dose climbs. Electron beam was also demonstrated to be an effective remedy in the disinfection of wastewater and removal of organic matter [88].

The feasibility of purification of high–sulfuric combustion gases using electron particles was acknowledged by Chemielewski and Licki [89]. Parameters such as temperature, humidity, concentration of additives and irradiation dose determine the efficiency of the removal process, which may go up to 90% and 75% for SO_2 and NO_x respectively. Ionizing irradiation, in addition to regular physical, chemical, and catalytic hydroprocessing methods for petroleum demetallization, can be used as a potential way to remove the metal content of used lubricants [65, 90].

2.2.2 Energy consumption perspective

Comparison of hydrocarbon enhancement electron beam technology (HEET) with conventional thermal and thermocatalytic hydrocarbon processing methods, in terms of energy consumption in chain–cracking reactions, reveals that the total energy expended for the former case is considerably less than that of the latter one because irradiation causes chemical conversions to proceed at minimal processing temperature [91]. In fact, the energy consumption for initiating cracking in HEET is less than that of thermal processing due to direct energy transfer into feedstock molecules that results in bypassing chain initiation energy—as the most energy intensive stage in chain reactions.

2.2.3 Effect of different parameters

Lucchesi et al. [92] examined the effect of temperature and the physical phase of reactants on radiation thermal cracking of pure and mixed hydrocarbons. They observed that radiation products increase with rising temperature. On top of that, cracking yields were substantially higher in cases of vapor phase irradiation than in the liquid phase. This behavior can be explained by considering more probable radical recombinations in the solvent cage of condensed phases—known as the "cage effect" [93]. Note that the same phenomenon has been observed for liquid and solid phases [34, 38].

Based upon reaction temperature, Lucchesi et al. [94] divided radiolysis reactions into low–temperature nonchain reactions and high–temperature chain reactions. For the case of low–temperature irradiation, dehydrogenation was reported as the major reaction in low conversions. The conversion itself depended on the total absorbed energy and did not show any sensitivity to dose rate. On the other hand, high temperature radiolysis is, in fact, a chain reaction of free radicals or accelerated thermal cracking which means that irradiation will not result in any new type of reaction (typical of ions or other relatively rare species made by irradiation), other than that of intensified thermal chain reactions.

Mustafaev and Gulieva [95] developed three different temperature regions based upon radiation thermal refining of heavy petroleum fractions with boiling point temperature $T > 300°\text{C}$ and middle molecular mass $MW = 280$.

- When $20 < T < 400°\text{C}$, the process of polycondensation predominated and the number of double bonds in products decreased sharply.
- When $400 < T < 450°\text{C}$, fragmental hydrocarbon products of low boiling point formed as a result of radiation thermal induced degradation.
- When $T > 450°\text{C}$, the rate of gas production increased steeply.

Note that the temperature range provided here depends on several factors and may change from one feed type to the other. There are also other studies on synergetic effects of ionizing incidents and temperature [29,30,33,36,38,44,46,47,49,51,96]. The common point in studies related to temperature dependence of the radiolytic process is that at relatively low temperatures, chain reactions will not develop because thermal energy is insufficient to activate the propagation step. However, Zaikin [97] recently has claimed that application of high dose rates activates chain cracking reactions even at relatively low temperatures without thermal activation energy.

2.2.4 H_2 formation during irradiation

In a series of papers, Wojnarovits, Fejes, and Foldiak investigated the process of hydrogen formation, its mechanism and kinetics during radiolysis of saturated and unsaturated hydrocarbon systems [98–101]. The hydrogen yield was observed to depend strongly on the individual properties of species, originating from the molecular structure. Note that the H_2 liberation mechanism follows either molecular elimination or abstraction by hydrogen atoms [38, 96]. The mechanism and kinetics of molecular hydrogen detachment, as a result of ionizing irradiation, has been discussed by Plotnikov [102]. Despite the case of hydrogen formation during low–temperature radiolysis of hexadecane, which is dose and phase independent, raising temperatures up to 400°C makes hydrogen formation dose–dependent while intensifying the process [103]. Additional hydrogen formation at elevated temperatures may be attributed to formation of alkene molecules during the radiolysis process as the presence of allyl substituents reduces the dissociation energy of adjacent hydrogens.

3. FUNDAMENTALS

This section provides general information about irradiation and energy deposition phenomenon in radiolyzed material. It covers subjects such as charged particles interaction, absorbed dose concept, and dosimetry. Provided discussion helps us to better understand the radiolysis process.

3.1 An Introduction to Irradiation

The application of ionizing incidents, a novel way to combine engineering physics and chemistry, has introduced great opportunities to the developing oil and gas industry. Nowadays, ionizing incidents play an important role in our lives; for instance, the foamed plastics used for noise or shock canceling, digital watch batteries, wire coating material and gamma sterilized disposable hospital equipment are all applications of ionizing irradiation in our daily life. Discovery of X-ray by Wilhelm C. Rontgen in 1895 is considered as a starting point of a new science named as "radiation chemistry" [104]. It is important to note that, as at the early stages of ionizing incident development the radiation sources were not strong enough, most of the effort was focused on radiolysis of gaseous systems. With the advent of larger and more versatile radiation sources in the 1940s, interests in the chemical and physical effects of ionizing incidents increased considerably. During the 1960s and 1970s, the physical processes of energy absorption were analyzed in more detail. The growing mass of information on products and yields was collected and examined systematically to establish patterns of reactivity, and to a lesser extent, possible applications of radiation induced reactions in industry. It is worthwhile mentioning that radiation processing of hydrocarbons attracted considerable attention during the early 1940s when the development of reactor technology required basic information on the stability of lubricants and other components [105].

Ionizing incidents are considered to be an efficient way to deliver energy directly to the electronic structure of the material, resulting in production of ions, secondary electrons, photon or X-ray, excited molecules and free radicals. Considering the lowest energy required to produce ionization of typical material (the energy range of interest spans from 10 eV to 20 MeV), radiation with energy greater than this minimum is classified as "ionizing incidents" [106]. There are five important types of ionizing incidents named as [107]

1. Gamma–ray
2. X–ray
3. Fast electrons
4. Heavy charged particles
5. Neutrons

A moving heavy charged particle imposes electromagnetic forces on atomic electrons and delivers energy to them. This energy may cause ionization or excitation of the target molecules. These particles just give out small portions of their energy in each collision, resulting in an almost continuous energy loss mechanism with minor deflections in their traveling pathway. Although electrons and positrons follow the same mechanism in continuous energy loss, they exhibit substantial deflection in their track due to their small mass [108]. Depending on the situation, electrons may have elastic or inelastic scattering. Inelastic scattering results in energy transfer to the molecules producing excited molecules, secondary and Auger electrons, photons and X–ray, while elastic scattering causes angular deflection in the electron track without any energy loss.

On the opposite side, gamma and X–rays do not gradually lose their energy in their path. They can travel longer distances without having any interaction with an atom. Note that as both x–rays and gamma–rays are electromagnetic radiations,

the fundamental ionization process is identical for both cases. These electromagnetic incidents lose their energy in mechanisms such as photoelectric absorption, Compton scattering, pair production, etc. and do not produce a continuous succession of the ions in their journey. It is worthwhile adding that this manner does not result in the maximum range, despite the phenomenon observed in charged particle interactions [61, 108].

3.2 Absorbed Dose

The absorbed dose (D) is defined as the expectation value of the energy imported to matter per unit mass at a point [107] and is measured in joules (J) per kilograms (kg) or gray (Gy). The older SI unit for absorbed dose was rad.

$$1\ Gy = 1\ \frac{J}{kg} \tag{3.1a}$$

$$1\ Gy = 100\ rad \tag{3.1b}$$

$$1\ kGy = 1\ \frac{watt - sec}{g} \tag{3.1c}$$

$$1\ kGy = \frac{1}{360}\ \frac{kwatt - hr}{kg} \tag{3.1d}$$

The concept of absorbed dose can best be defined in terms of the energy imparted ($d\epsilon$) approach. In a finite volume of dV, which has the mass of dm and volume of dv, the energy imparted is defined as

$$d\epsilon = (R_{in})_u - (R_{out})_u + (R_{in})_c + (R_{out})_c + \sum(Q) \tag{3.2}$$

where $(R_{in})_u$ and $(R_{in})_c$ are the radiant energy of uncharged and charged particles entering the volume, $(R_{out})_u$ and $(R_{out})_c$ are the radiant energy of uncharged and charged particles leaving the volume, and $\sum Q$ is the net energy derived from rest mass in dV (mass→energy positive, energy→mass negative). Radiant energy is

defined as the energy of particles (excluding the rest energy) emitted, transfered, or received. Hence, the amount of absorbed dose (D) can be calculated using Equation 3.3

$$D = \frac{d\epsilon}{dm} \tag{3.3}$$

In this equation, dm corresponds to the mass of the finite volume V which has the infinitesimal volume dv. The average dose ($\bar{D}$) is defined as the total energy imparted to the finite volume V divided by the total mass, m. It is very important to note that the concept of dose deals with the energy deposited in the material and produces any effects attributable to the radiation. In fact, absorbed dose is a measure of that part of energy transferred to the irradiated material which results in the formation of ions and excited species [104]. In order to correlate the amount of deposited energy to the time, we can define the absorbed dose ratio as (t represents time)

$$\dot{D} = \frac{dD}{dt} = \frac{d(\frac{d\epsilon}{dm})}{dt} \tag{3.4}$$

To better understand the concept of absorbed dose, consider a photon $h\nu_1$ entering a control volume (dV). As a result of the Compton interaction, a scattered photon $h\nu_2$ along with an electron leave the control volume. Before leaving the control volume, the electron produces one bremsstrahlung X–ray ($h\nu_3$) and leaves the control volume with the kinetic energy of T (Fig. 3.1). Looking at Equation 3.2, the values of energy imparted, absorbed dose, and dose rate are

$$d\epsilon = h\nu_1 - (h\nu_2 + h\nu_3 + T) + 0 = h\nu_1 - h\nu_2 - h\nu_3 - T$$

$$D = \frac{d\epsilon}{dm} = \frac{h\nu_1 - h\nu_2 - h\nu_3 - T}{dm}$$

$$\dot{D} = \frac{dD}{dt} = \frac{d(\frac{h\nu_1 - h\nu_2 - h\nu_3 - T}{dm})}{dt}$$

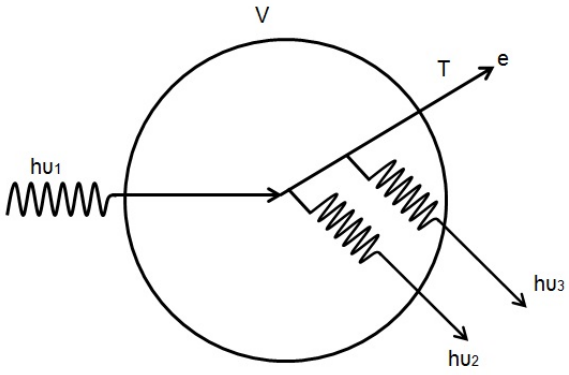

Fig. 3.1.: Absorbed dose in a control volume (reproduced after Attix [107])

3.3 Types of Charged Particle Interaction

Depending on the factors such as the velocity of the collision and the distance between the closest approach of the particles and the target atoms or molecules, the charged particle interactions can be explained in three categories [109]

- Interaction with the electrons of atoms or molecules in the material. The collision is known as inelastic if the individual electrons in the atomic structure of the molecule or atom get enough energy to be excited into higher energy levels or be ejected into an unbound state. For cases in which the exerted energy is less than the smallest molecular energy level difference, energy and momentum are conserved and the collision is assumed to be elastic.

- Interaction with nuclei. This is more likely to happen for the cases of heavy particles

- Interaction with the whole Coulomb field surrounding an atom. In this case, the interaction occurs with the coupled system of nucleus and orbiting electrons.

In ascending orders of time, three stages, named as (1) the physical stage; (2) the physicochemical stage; and (3) the chemical stage follow the absorption of radiation

of radiation energy in a media and lead to the ultimate chemical reactions [110]. Note that the earliest discernible time, obtained from the uncertainty principle is $\sim 10^{-17}s$ which accounts for the production of fast secondary electrons.

3.4 LET, Stopping Power, and Range

Heavy or light charged particles lose their energy to the surrounding media in their way to a destination. The (linear) rate at which energy is lost by the particles plays a part in determining the changes as rapid energy loss causes more excitation to the molecules surrounding the particle track and slower energy deposition leads to a widely separated excitation [104]. Related to what has been mentioned before, linear energy transfer (LET) is defined as the linear rate of loss of energy by ionizing particles traversing a material medium.

Although light charged particles (electrons and positrons) lose their energy almost continuously, similar to the heavy charged particles, they can lose a large fraction of their energy in a single collision resulting in a large deflection, in contrast to the heavy charged particles that have almost straight path though the matter [108]. Stopping power of a medium for a specific ionizing particle is defined as the average linear rate of energy loss of a particle while it is passing through the media and is shown by $-\frac{dE}{dx}$.

Defining $Q_{\min}$ and $Q_{\max}$ as the minimum and maximum energy loss in a single collision respectively, and $W(Q)dQ$ as the probability that a given collision will result in an energy loss between Q and $Q+dQ$, the average energy loss per collision (Q_{avg}) can be calculated using the following formula:

$$Q_{\text{avg}} = \int_{Q_{\min}}^{Q_{\max}} QW(Q)dQ \tag{3.5}$$

Thus, the stopping power is given by

$$-\frac{dE}{dx} = \mu Q_{\text{avg}} = \mu \int_{Q_{\min}}^{Q_{\max}} QW(Q)dQ \tag{3.6}$$

where μ, the macroscopic cross section, is the probability per unit distance of travel that an electronic collision takes place.

When considering electron particles, especially at higher energies, the loss of energy to the media occurs in two ways: either by collision (collision stopping power) or irradiation (radiation stopping power). The collision stopping power formulas for electrons are [108]

$$\left(-\frac{dE}{dx}\right)_{\text{col}} = \frac{4\pi k_0^2 e^4 n}{mc^2\beta^2}\left[\ln\frac{mc^2\tau\sqrt{\tau+2}}{\sqrt{2}I} + F^-(\beta)\right] \tag{3.7a}$$

$$F^-(\beta) = \frac{1-\beta^2}{2}\left[1 + \frac{\tau^2}{8} - (2\tau+1)\ln 2\right] \tag{3.7b}$$

Here, $\tau = \frac{T}{mc^2}$ is the kinetic energy of electron particles expressed in multiples of the electron rest energy mc^2, β is speed of the particle relative to speed of light and I is the mean excitation energy of the medium.

Electromagnetic forces in a in a molecule can cause small electron particles to be accelerated strongly in collisions. It results in the emission of bremsstrahlung, which occurs when the electron pathway in deflected in the electric field of a nucleus or atomic electrons. Unlike collisional energy losses, no single analytic formula exists for calculating the radiative stopping power; however, Equation 3.8 could be used to approximate the radiative stopping power for an electron of total energy E in MeV and element of atomic number Z.

$$\frac{\left(\frac{dE}{dx}\right)_{\text{rad}}}{\left(\frac{dE}{dx}\right)_{\text{col}}} \approxeq \frac{ZE}{800} \tag{3.8}$$

Consequently, the total stopping power would be calculated by adding up the collisional and radiative stopping power.

$$\left(-\frac{dE}{dx}\right)_{\text{tot}} = \left(-\frac{dE}{dx}\right)_{\text{col}} + \left(-\frac{dE}{dx}\right)_{\text{rad}} \tag{3.9}$$

Considering the concept of total stopping power, the range of a charged particle is defined as the expectation value of the pathlength that it follows until it comes to rest and can be approximated using the concept of continuous slowing down approximation range (R_{CSDA}) [107, 109]. For a particle with the kinetic energy of T and density of ρ,

$$R_{\text{CSDA}}(T) = \int_0^T \left(\frac{dT}{\rho dx}\right)^{-1} dT \tag{3.10}$$

The value of R_{CSDA} for low–Z material can be approximated using the following empirical equation [108]:

$$R_{\text{CSDA}}(T) = 0.412 T^{1.27 - 0.0954 \ln T} \tag{3.11}$$

3.5 Dosimetry

Radiation dosimetry is defined as a method to measure the amount of absorbed dose and map the distribution of the energy deposited in a media as a result of radiation exposure. A dosimetry system has two elements: (1) a radiation induced effect, and (2) a device capable of quantifying the induced change in the dosimeter. In fact, any radiation effect or response, that may be quantified in a reproducible manner using a well defined measuring device, can be used as a dosimeter. Several types of dosimeters provide absorbed dose measurement based on two methods: absolute dosimetry and relative dosimetry. The absolute dosimetry is defined as a method by which the absorbed dose is measured directly and no calibration is required from a known radiation field [107]. As an example of this method, we can mention ionization chambers that were also used in this study to calibrate the electron beam

machine. The relative dosimetry, on the other hand, is a method by which a reference or absolute point is defined and all the following measurements are referenced to that particular absolute. Radiochromic films are examples of relative dosimeters. More discussion about the mentioned dosimetry methods is provided in the following sections.

3.5.1 Ionization chamber

Measurement of ionization produced as a result of radiation is one of the favored means of dosimetry. Ionization chambers—the devices used to quantify amounts of absorbed energy—consist of two electrodes separated by a gas filled space in which the incident radiation produces ionization [104]. Fig. 3.2a illustrates charged particles entering an ionization chamber with the potential difference V applied to the chamber plates.

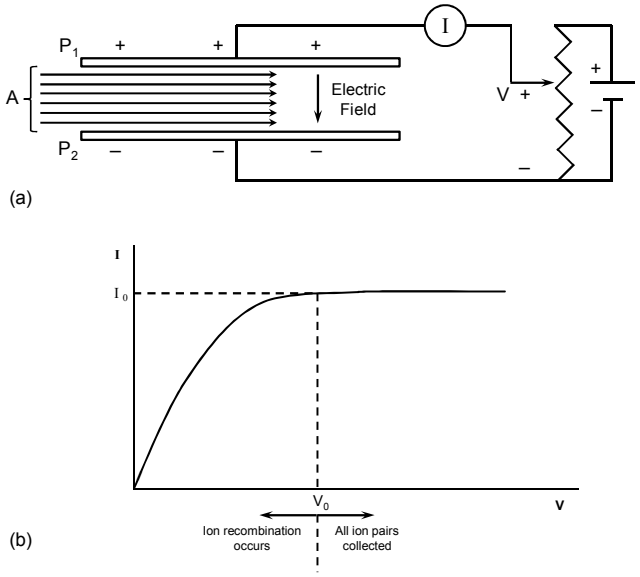

Fig. 3.2.: Ionization chamber design (modified after Turner [108])

Charged particles transfer their energy to the gas molecules in the chamber, ionizing them by ejecting electrons and leaving positive ions. Ejected electrons are also able to generate additional ion pairs if they have sufficient kinetic energy. Related to the strength of the potential difference, the ion pairs will drift apart under its influence and the current I will flow in the circuit. As the electric field between the plates gets stronger, fewer number of formed ions recombine and the majority of them will be absorbed by the chamber plates, resulting in a higher current in the circuit. As shown in Fig 3.2b, the current (I) can be increased by increasing V up to the value of V_0, indicating that all the ion pairs, generated either by the incident radiation and its secondary electrons, will be collected (saturation current I_0) [108]. The saturation current is calculated as

$$I_0 = Ne\dot{\Phi}A = \frac{e\dot{\Phi}AE}{W} \tag{3.12}$$

and the total energy absorption in the gas chamber ($\dot{E_{abs}}$) is

$$\dot{E_{abs}} = \dot{\Phi}EA = \frac{I_0 W}{e} \tag{3.13}$$

where the fluence ,Φ (in $\frac{1}{\text{cm}^2}$), is the number of ionizing particles entering a sphere of unit section area at the point of interest, and $\dot{\Phi}$ (in $\frac{1}{\text{cm}^2.\text{s}}$) is the fluence rate. Also, E and W (in MeV) are the particles energy and amount of energy required to generate a pair of ions in the chamber (the value of W is believed to be independent of irradiated electrons energy; also, note that the ionization potential, which is the least amount of energy required to remove an electron from an unexcited atom, is less than W [111]). N in I_0 calculation formula represents the average number of ion pairs produced by an incident and its secondary electrons and is equal to $\frac{E}{W}$. The recorded ionization current is proportional to the rate at which ions are produced in the gas. Here, what determines the sensitivity of a chamber is the pressure and volume of the gas and associated readout components. Integration of the current, by

allowing it to charge a capacitor, gives the total charge produced by the irradiation, which is proportional to the total number of particles entering the chamber. As a result, ionization measurements can be used to measure both the intensity of the radiation and the total amount of radiation.

3.5.2 Radiochromic dosimeters

Radiochromic dosimeters change color when getting exposed to ionizing irradiation. The color change occurs as a consequence of the interaction of charged particles with a sensitive component in the film [112]. These dosimeters may be found in the form of liquid, gels, or gas. The absorbed dose in radiochromic films related to a quantity known as optical density. In fact, optical density is a measure of the change in color, that occurs upon irradiation. As the film is exposed to irradiation, depending on the absorbed dose, shadows of a specific color develop under irradiation. When compared to other dosimetry systems, radiochromic films provide major advantages. Radiochromic films are relatively insensitive to visible light and offer low energy spectral sensitivity. Their self developing nature and the independence to chemical processing agents make radiochromic films such a convenient and fast means of measuring absorbed dose. In addition to that, their high spatial resolution makes it possible to detect dose at any point or map dose distribution in a two dimensional plane. Although handling of such dosimeters is simple and can be performed under normal room light for a short time, it has been observed that film is sensitive to UV light [113].

4. EXPERIMENTAL METHODOLOGY AND MATERIAL

In this section, we will describe different parts of experimental setup. This includes the irradiation facility, reactor design, petroleum samples characteristics, and the analytical tools to monitor the changes in physical and chemical properties of the heavy petroleum fluids.

4.1 Experimental Setup

4.1.1 Electron accelerator

We have used a Van de Graaff machine (VDG) to generate high energy electron particles (irradiation facilities are located in Biological and Agricultural Engineering Department at Texas A&M University). VDG is an electrostatic accelerator that is capable of producing beams of fast electrons (Fig. 4.1).

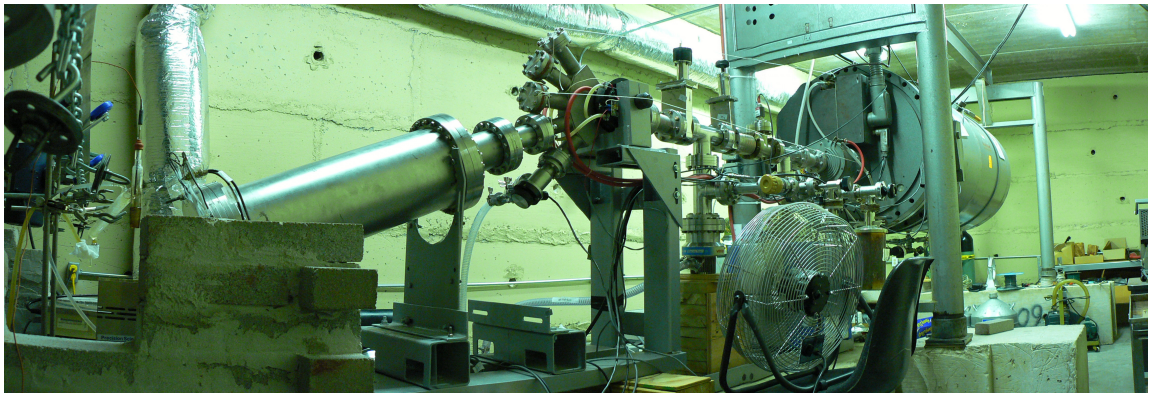

Fig. 4.1.: Van de Graaff machine is used to generate high energy electrons

This machine is able to provide a steady–state beam with a good energy regulation that is generally used for laboratory research [114, 115]. The machine has the capability to generate electrons of energy level in the range of 0.75–2 MeV. We used the energy of 1.35 MeV for all the experiments, as the optimum operating energy for a continuous electron generation. The principle of the operation is based on the mechanical transfer of charges from the ground to a high voltage terminal, which results in generation of a high voltage potential. In a VDG accelerator, the electrons are sprayed into a moving belt vial a corona discharge or physical rubbing in a high pressure atmosphere of insulating gas, using a DC power generator as an electron source. The belt is made of plastic rubber with high dielectric strength and immersed in an insulating gas at high pressure. The electrons or charge collected in the moving belt is transported against the potential gradient to a high voltage metal terminal, where no electric field other than that of charges on the belt exists. The charge is collected at the high voltage terminal upon contact with a metal brush, and the further is accelerated back to the ground [115]. The accelerator consists of three main parts: generator, vacuum system, and control system. The generator is a cylinder shaped tank with the diameter of 0.8 m and length of 1.8 m that is set 1 m above the ground level. Fig. 4.3 shows different parts of the accelerator.

(a) Bending magnet (b) Pressurized tank (c) Exit window

Fig. 4.2.: Different parts of the accelerator tool

4.1.2 Reactor design

The reactor has three major parts:

Reactor body: Glass flask containers or aluminum can containers (an 8 oz aluminum can with approximate wall thickness of 0.2 mm as shown in Fig 4.3a) are two available options for the reactor body. To choose the best case, several factors should be taken under consideration. The first factor is temperature resistance. As temperatures higher than 450°C may be achieved, the container should be able to tolerate very high temperatures. Both the glass flasks and aluminum can containers have the ability to withstand even higher temperatures. Additionally, the reactor body should cause the minimum possible energy attenuation for the passing charged particles. According to Yang [116], an accelerated electron loses about 4% of its energy while passing through the aluminum can reactor walls. However, this value increases to 75% for glass flasks (the energy of charged particles would be absorbed or scattered by the thick walls of the glass containers). Comparing the results, we are able to deliver 3.76 times more energy to the samples which is more favorable in terms of energy efficiency. This is because the thickness of the glass flask is 10 times that of the aluminum can.

Glass insert: To be able to connect the reaction chamber to the condenser unit, we have used a Pyrex glass insert with a 24/40 female joint (Fig. 4.3b). Using the mentioned assembly, we can easily mount and unmount the setup for the next experiments.

Sealant: To prevent leakage, the aluminum can chamber and the glass joint were glued together using a high temperature silicon gasket maker, which is a single component, room temperature vulcanizing gasketing compound designed to provide reliable "formed in place" gaskets for mechanical assemblies. This material cures on exposure to the moisture in the air to form a tough flexible

silicon rubber gasket with the ability to tolerate temperatures up to 600°F. Table 4.1 provides more information about the sealant material [117].

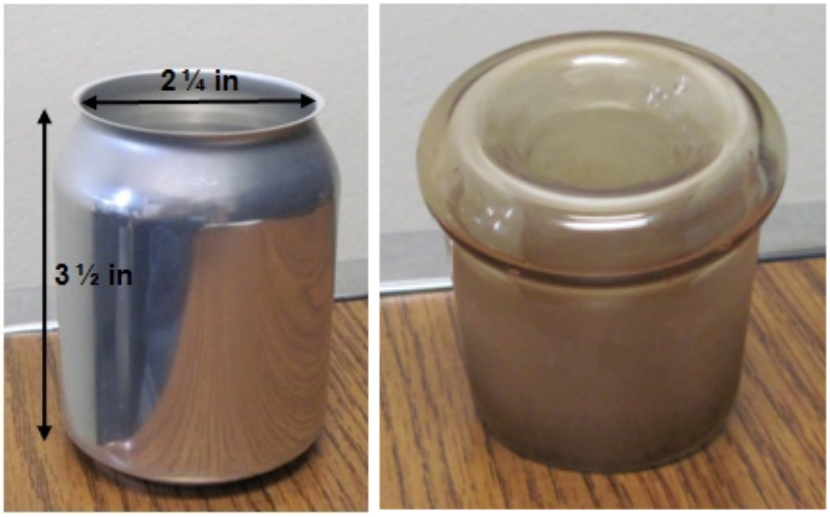

(a) Al reactor (b) Glass insert

Fig. 4.3.: Reactor design

Table 4.1: Silicone gasket maker properties

Chemical type	Acetoxy silicone rubber
Appearance	Red non–sag paste
Odor	Mild acetic
Specific gravity	1.05
Flash point (°C)	> 93
VOC (volatile organic compound) (wt%)	3
Vapor pressure (mmHg)	10

Fig. 4.4 shows the whole reactor setup together. Note that as the gasket maker is not in direct contact with the sample within the can, there is absolutely no contamination due to the sealant material. This setup provides us the following advantages:

- Preventing all kinds of leakage
- No external contamination, as there is no direct contact between the sample and silicon sealant
- High temperature tolerance (copper base temperature may approach 450°C during the experiments)

Fig. 4.4.: Reactor elements: glass insert, Al can, and silicon gasket maker

4.1.3 Condenser unit

Condenser assembly

A glass condenser with a male 24/40 glass joint is connected to the reactor to condense evolved gases into the liquid. Noncondensable gases will also be collected for further analyses. We had two choices for the condenser unit: distillation setup and reflux setup.

The distillation setup (Fig. 4.5) is composed of a reactor connected to a distillatory instrument. Radiation and heat cause heavy petroleum fluids in the reactor to evaporate or crack into lighter vaporizable compounds. Condensable components will condense into the liquid yield collector, and noncondensable gas components will be stored in gas sample bags. As the condensed liquid will be collected somewhere else and it does not remix with the original heavy petroleum sample, it is easier to conduct a liquid analysis on such a light yield. On the other hand, as the evaporated molecules so not return to the reactor, we are unable to expose them further to ionizing particles. This inability to change the residence time of the fluid under the e–beam led to a new design for the radiation reactor, with a reflux condenser.

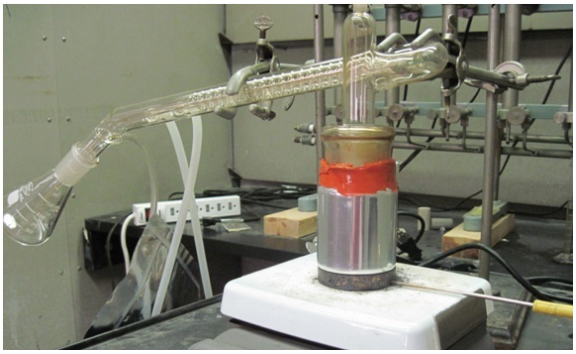

Fig. 4.5.: Distillation setup

The reflux setup (Fig. 4.6) is made up of a glass condenser with an outlet for noncondensable gases. The major difference between the distillation and reflux setup is that in the latter one, the evolved gas will not condense in a separate collector; instead, it returns to the reactor again to gain incremented exposure to heat and irradiation, resulting in a more efficient cracking. However, having heavy and light molecules mixed together imposes restrictions on liquid product analysis and requires more complicated analytical techniques.

Fig. 4.6.: Initial reflux setup without any modification for additional thermocouples

A water circulation system is employed to keep the temperature in the condenser constant and condense evolved gas into liquid. The inlet is fed by a pump connected to the condenser to provide 0°C water at a constant rate. Noncondensable gases will be collected in specially designed 0.5 and 1.5 liter FlexFoil sample bags (Fig. 4.7). The bag is made of four layers of foil material to prevent permeation into and out of it. These kinds of bags provide light and moisture protection to store low

molecular weight chemicals such as hydrogen or methane without losses. The bags feature a single polypropylene fitting that can be used for both a syringe port with PTFE-lined septum or a hose connection and acts as a shut–off valve for the hose connection.

Fig. 4.7.: Gas sample bag

The bottom section of the can is not flat, so to introduce the heat from the hot plate uniformly, we have employed a copper base with a flat bottom (Fig. 4.8). The top portion has the shape of the bottom of the can so they fit each other easily. To be able to control the temperature of the experiment, we pierced a hole in the copper base to insert a "K–type" thermocouple. Using the temperature data from the copper base, we can make sure that the temperature stays constant for different experiments.

To provide the required heat for thermal and radiation thermal cracking, a temperature control hotplate with an operating temperature range of 10–540°C was used.

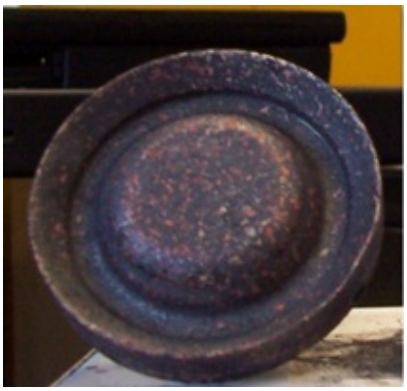

Fig. 4.8.: The copper base fits the bottom of the can and provides uniform heat to the reactor

Modification of the reflux setup

Using the previous reflux setup, the only temperature we could measure was the copper base temperature. This temperature does not give us accurate information about the fluid temperature. To gather more information about the temperature inside the reactor, some modifications have been done on the original reflux setup (Fig. 4.9).

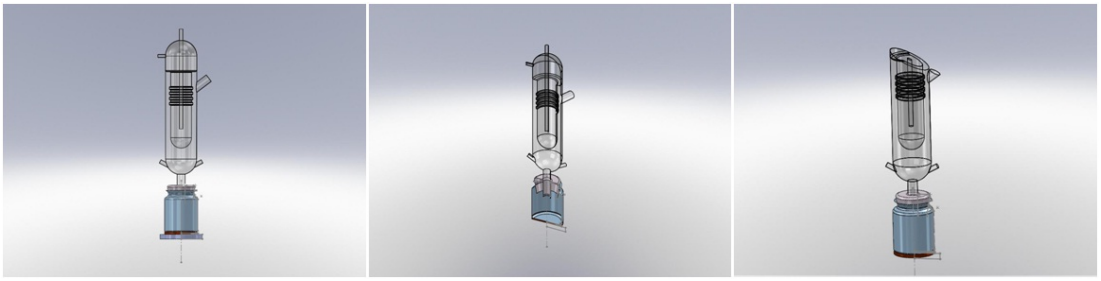

(a) Side view (b) Cross section 1 (c) Cross section 2

Fig. 4.9.: Modified reflux setup

The condenser column was adapted to have two glass handles on both sides. It allows passing the additional thermocouples through the side holes into the reactor. The liquid temperature was measured with a "K–type" thermocouple. Knowing the temperature inside the reactor, the whole upgrading process can be precisely monitored. It also provides more information about the reactions inside the reactor. Additionally, a "J–type" thermocouple was employed to record the vapor temperature throughout the experiments. Gas temperature data provide a substantial contribution to quantify the intensity of the reactions.

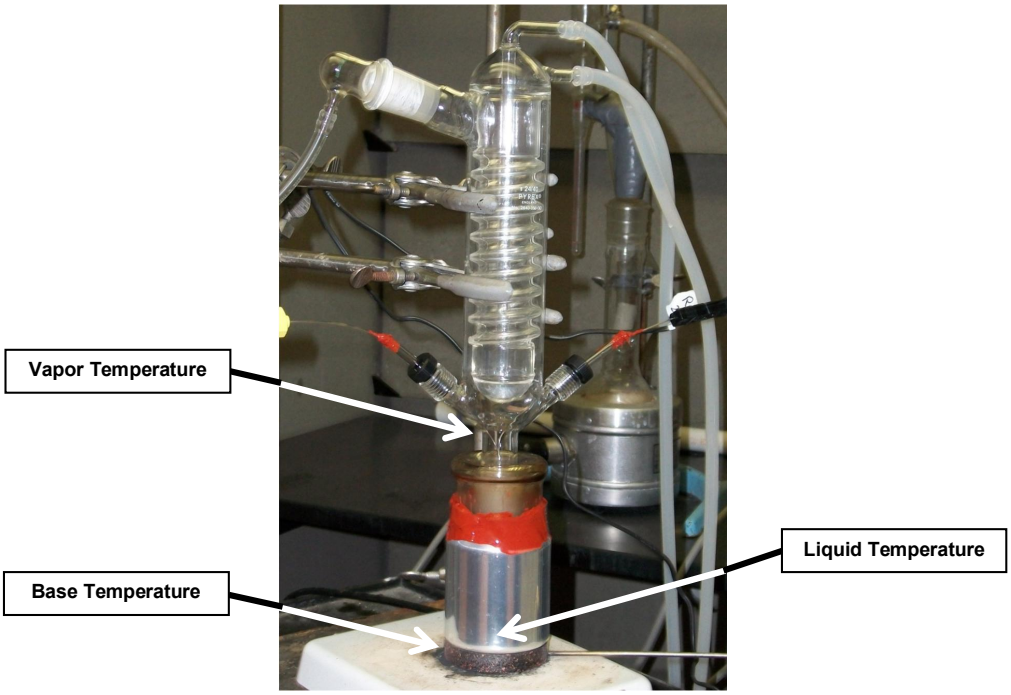

Fig. 4.10.: Thermocouples arrangement

The new setup has two side holes covered with welded glass hands of 2 inches length. Thermocouples were glued with a high temperature silicon gasket maker to

a 2 inch glass tube with an OD of quarter inches to hold them on the sides. But, as the surface area of the thermocouples is small, the rubber was not able to hold the thermocouple setup as firmly as required. So, we decided to use epoxy resin and hardener, which provide a solid setup that keeps the thermocouples from any further movements inside the glass tube. Thermocouples and the connected glass tubes are mounted on the glass hands via special plastic caps. Using the plastic caps, we are able to slightly adjust the length of the thermocouple that goes into the reactor; consequently, we can adapt the setup to handle minor changes in reactor dimensions. Fig. 4.11 depicts the thermocouple, plastic cap, glass tube, and the other parts all connected together. To prevent any possible leakage, an O–ring was used under the plastic cap. The combination of the O–ring assembly along with the epoxy resin guarantees a very promising seal for this part of the condenser.

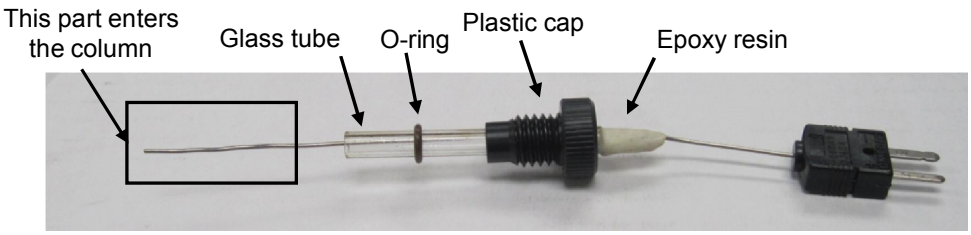

Fig. 4.11.: Temperature measurement assembly

All the temperature data were collected using a data acquisition module with five thermocouple inputs [118]. The module reads the temperature each 10 seconds and stores it in a laptop connected to it. For the purpose of our experiments, temperatures were recorded with two significant digits for all K and J type thermocouples.

4.1.4 Thermal and radiation thermal cracking experiments

To investigate the effect of electron particles on heavy petroleum fluids, we conducted two types of experiments. Thermal cracking (TC) and radiation thermal cracking (RTC). Both experiment types took place at similar reactor temperatures and environmental conditions, and the only difference between the runs is that it includes only heating for TC and simultaneous heating and irradiation for RTC. To be able to provide more energy to the samples, all the experiments were done in reflux mode. Fig. 4.12 shows the reaction chamber along with the accelerator's exit window. After calibrating the VDG machine, irradiation hot spots were determined and the location of the reactor was adjusted in a way to absorb the highest possible number of electron particles. Depending on the required dose, the duration of experiments varied from 1 to 2 hrs. In the case of 10 kGy absorbed energy, the experiments lasted for one hour while two–hour experiments provided an absorbed dose of 20 kGy.

Depending on the objectives of each experiment, the liquid temperature was adjusted to take the values in the range of 200 to 400°C. To find the proper sample size for the experiments, two important factors should be taken into account. The volume of the liquid in the reactor should not be too small as it causes the liquid level to drop below the minimum level for the optimum dose absorption. Furthermore, when using small volumes of heavy petroleum samples, thermal cracking may be the dominating process as we provide considerable amounts of heat to a small volume of the sample. On the other hand, the current configuration of the VDG machine is not appropriate for massive objects or large amounts of liquid samples. Finally, after some trials, we ended up using 30 gr of petroleum samples in the reactor for each experiment.

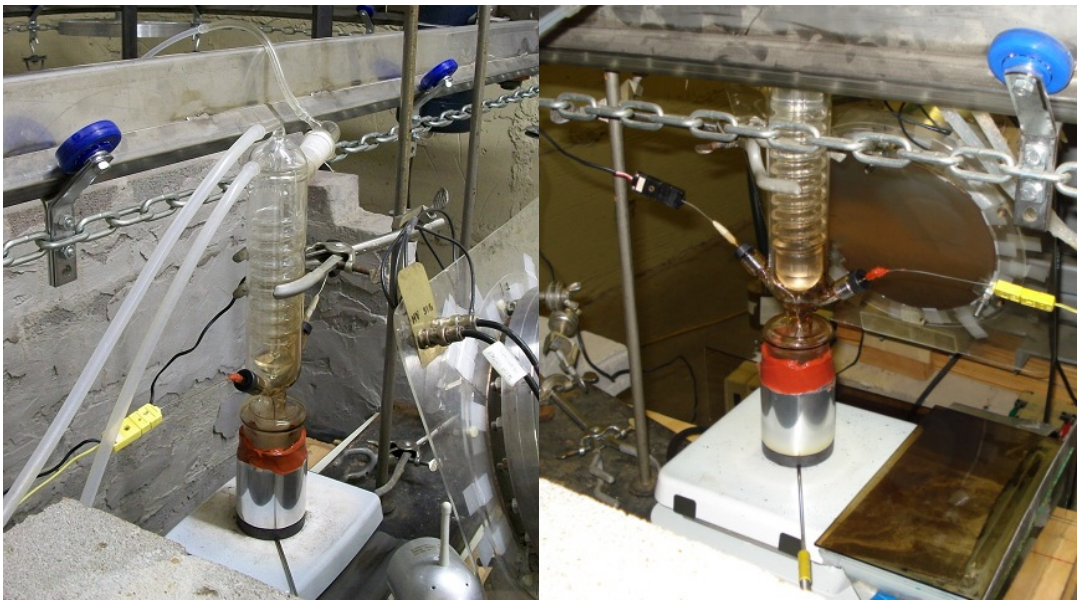

(a) (b)

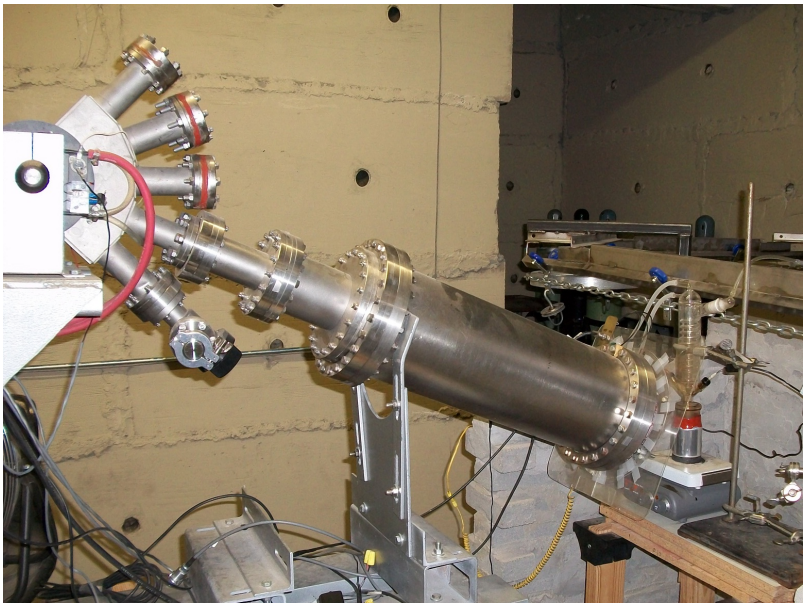

(c)

Fig. 4.12.: The reaction chamber in front of the accelerator's exit window

It is important to add that before starting the experiments, we performed a number of pre–runs to check the integrity of the heater, thermocouples, and experiment tools. Consequently, six heating experiments with different performance capacities of the heater (max, 0.75, and 0.5 power) were performed, and at the same time, the source voltage and copper base temperature were recorded. To make sure that any probable temperature deviation between replications does not correlate to the possible chemical reactions in the reactor, we have used water as our reaction fluid in pre–runs (as an experiment proceeds, there are some reactions occurring within the reactor causing the properties of the samples to change, and these changes may be a potential source of temperature variation inside the reactor). Looking at the temperature profile, we can see that, as expected before, temperatures of similar runs are similar to each other, which assures the integrity of instruments (Fig. 4.13).

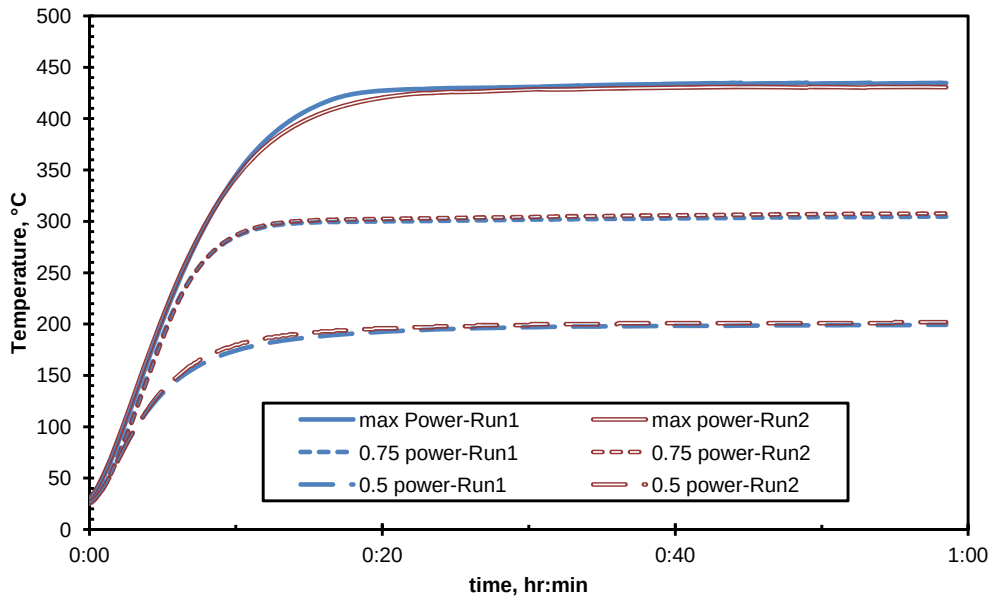

Fig. 4.13.: Copper base temperature for different heater powers shows quite stable performance of the instruments

4.2 Petroleum Samples

In this study, we used three different petroleum samples with distinct characteristics that allowed acquiring valuable information on radiation induced reactions of different hydrocarbon species and probable synergetic effects (Table 4.2). The results show that radiolytic behavior of hydrocarbons and the stability of post–irradiation products vary for different molecules, depending on the structure of the samples and the experimental circumstances. The current section provides detailed characteristics of the samples used in this study.

Atmospheric Residuum (AR) is a sticky liquid with a high concentration of heavy hydrocarbons and asphaltene. The fluid is composed of 62% deasphalted oil and 38% pitch. Fig. 4.14 shows the viscosity and Fig. 4.15 provides the simulation distillation analysis of AR fluid. According to the graphs,the sample has an extremely high viscosity and a high concentration of heavy hydrocarbon molecules. Looking at the graphs more precisely, we can see that only around 70% of all the AR boils before 720°C while 30% of the sample has not still evaporated at temperature of 720°C. To have an idea about the heaviness of the sample, it is worthwhile adding that 720°C refers to the boiling point of paraffinic C_{100} (the value is just an indicator of this group and the true boiling point of C_{100} and its isomers depends on their structure). This means that almost 30% of the whole liquid component is made of components heavier that than C_{100}.

Deasphalted Oil (DAO) is a stream of the AR produced by sending the feed through a pilot scale solvent deasphalting unit. The liquid is much lighter than the AR but still too heavy in comparison to regular oil and heavy oil samples. Fig. 4.16 and 4.17 show viscosity and simulated distillation of the DAO sample. According to the graph, 10% of the DAO fluid boils after 720°C, which refers to C_{100}^{+} hydrocarbons (Table 4.2 provides more information about the samples).

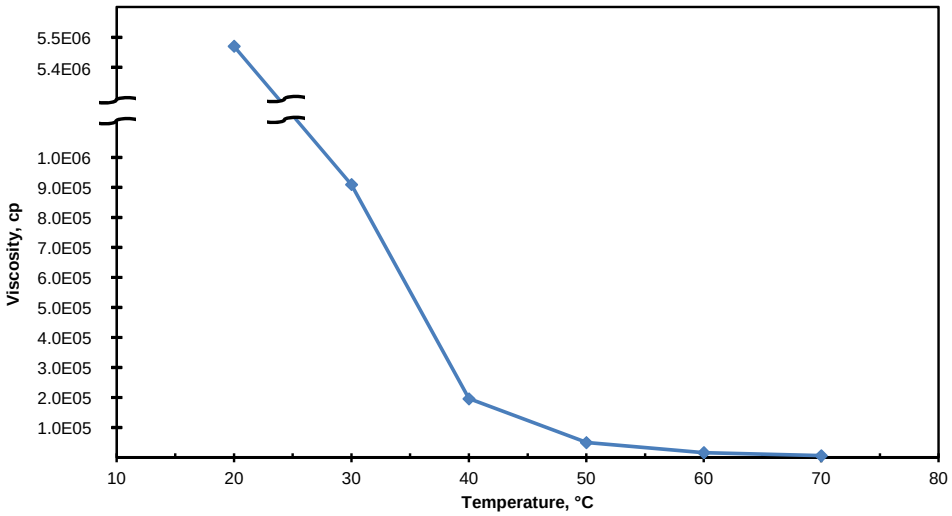

Fig. 4.14.: Viscosity of the untreated AR measured at different temperatures

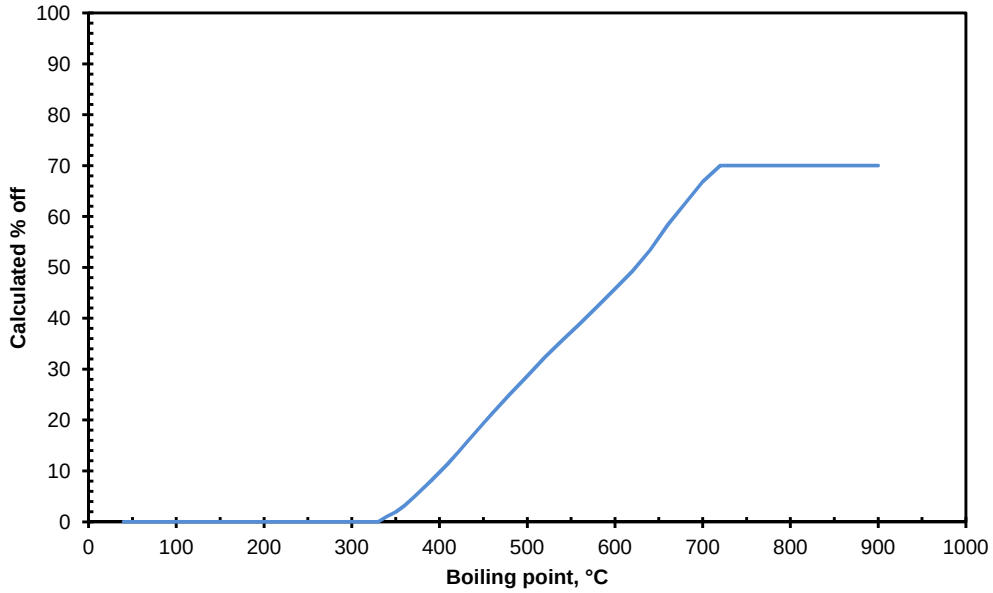

Fig. 4.15.: Simulated distillation of the untreated AR demonstrates extremely heavy nature of the fluid

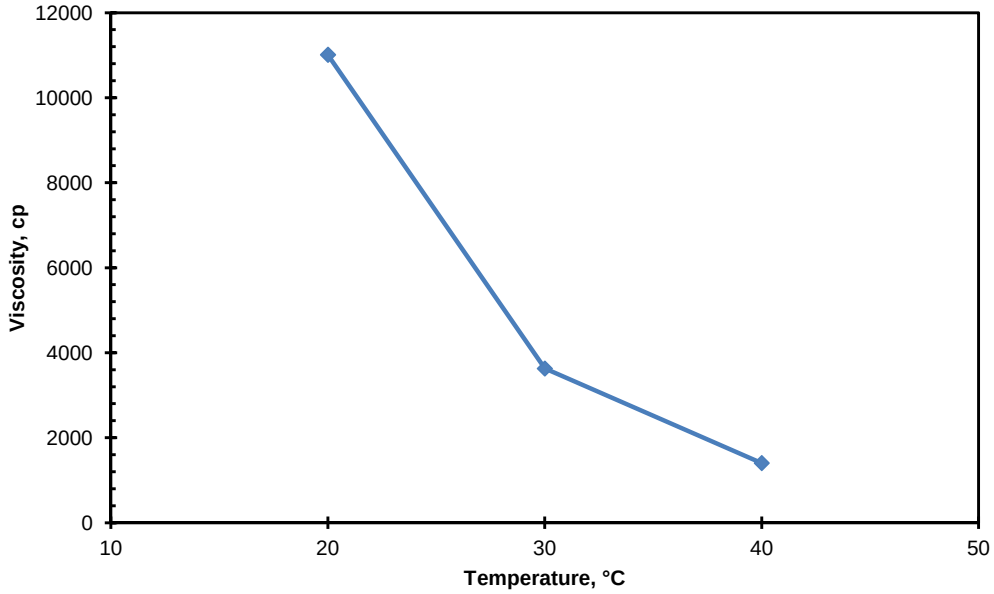

Fig. 4.16.: Viscosity of the untreated DAO measured at different temperatures

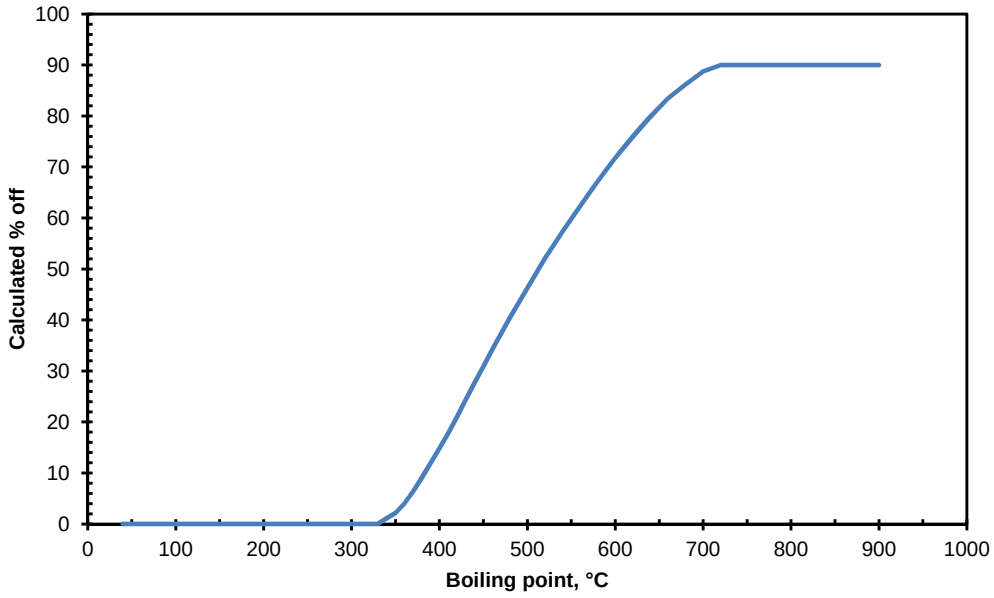

Fig. 4.17.: Simulated distillation of the untreated DAO demonstrates the heavy nature of the fluid

Table 4.2: Heavy petroleum samples specifications

Sample	AR	Pitch	DAO				
			Full range	Cut 11	Cut 13	Cut 14	VR
Cutpoints (°F)	650+	–		785–	785–900	900–1028	1028+
Yield (wt%)	–	38	62	15.8	24.9	17.9	41.2
°API (60°F/60°F)	7.4	14.8	14.5	18.4	15.8	14.1	12
S.G. (60°F/60°F)	1.0187	0.9672	0.9692	0.9440	0.9606	0.9718	0.9861
Density (gr/cc)	1.0177	0.9663	0.9682	0.9430	0.9596	0.9707	0.9850
Sulfur, X–ray (wt%)	5.15	7.25	3.74	3.01	3.24	3.73	4.40
Ash content (wt%)	0.054	0.170	0.002	–	–	–	0.021
Pour point (°F)	95	–	45	0	20	25	65
C_7 insolubles (wt%)	10.43	38.60	0.06	–	–	–	0.16
C_5 insolubles (wt%)	18.32	56.28	0.16	–	–	–	0.04
CHNS (wt%)	–	99.63	99.75	99.84	99.78	99.88	99.39
Carbon (wt%)	83.6	82.31	85.55	85.21	85.21	84.78	84.12
Hydrogen (wt%)	10.27	9.06	11.09	11.69	11.49	11.39	11.11
Nitrogen (wt%)	0.43	1.10	0.25	<0.15	<0.15	0.20	0.32
Sulfur (wt%)	5.10	7.16	2.86	2.94	3.08	3.51	3.84

Pitch is the solid remainder of the deasphalting process and forms 38 wt% of the original AR (Fig. 4.18).

Fig. 4.18.: Pitch sample

4.3 Analytical Methods

We have employed three analytical methods to be able to monitor the physical and chemical changes that are brought about as a result of irradiation. Radiation induced physical and rheological changes were analyzed using viscometers, densitometers, and gas chromatography instruments. One of the most important objectives of this study is to characterize radiolytic reactions of heavy hydrocarbons to be able to control the upgrading process and accomplish the highest throughput while reducing the operation costs. Achieving these objectives demands in–depth knowledge about the radiolysis reaction mechanism, chemical changes, and the dominating variables. The gas chromatography test results developed in this research provided us comprehensive information about the chemical distribution of the products after different treatment scenarios. The following section discusses the methods we employed to analyze radiation products.

4.3.1 Viscosity and density

To measure the viscosity of the samples before and after the treatments, we have used cone and plate Brookfield LVDV–III Ultra and HBDV–III Ultra viscometers. A programmable refrigerated bath was also used to measure the viscosity at desired temperatures. This type of viscometer is generally used when only small sample volumes are available. The rotating viscometer measures fluid parameters of shear stress and viscosity at given shear rates. The viscometer has a cone spindle, which is driven through a calibrated spring. The viscous drag of the fluid against the cone spindle is measured by the spring deflection. Then, a rotary transducer measures the spring deflection [119]. The range of the viscosity is determined by the rotational speed of the cone spindle, the size and shape of the spindle, the container in which the cone spindle is rotating, and the full–scale torque of the calibrated spring. Depending on the type of the spindle, the LVDV–III machine is capable of measuring the viscosities in the range of 15 to 6,000,000 cp and the HBDV–III machine covers the range of 800 to 320,000,000 cp. In this study, the CPE–52 spindle was used to measure the viscosity of heavy petroleum fluids. Using the CPE–52 allows to measure the viscosities in the range of 50 to 7,864,000 cp [119]. An appropriate selection requires measurements made between 10 to 100 on the instrument percent torque scale. In other words, to measure high viscosity, choose a slow speed of spindle rotation. If the chosen speed results in a reading above 100%, then either the speed should be reduced or a spindle with smaller diameter should be replaced. To make sure that the viscosity measurements reflect the real values accurately, we graphed shear stress versus shear rate data and calculated the viscosity using linear regression. More information regarding the viscosity calculation and calibration process is provided in Appendix A.

Density of the samples were measured using the Anton Paar SVM 3000 machine, where the required determination of the sample density is undertaken by the integrated density measuring cell which works on the proven principle of the oscillation

U–tube (also used in Anton Paar's DMA series of density meters) [120]. The density measurement in SVM 3000 complies with the ASTM D7042 standard.

4.3.2 Gas chromatography

We used gas chromatography machines to analyze the gases evolving during RTC and TC experiments. The analyses were performed using a refinery gas analyzer (RGA, Agilent 7890A) and a gas chromatograph–mass selective detector (GC–MSD, Agilent 6890). The RGA machine is equipped to the advanced electronic pneumatic control (EPC) modules and high performance GC oven temperature control. The machine is capable of supporting two inlets, three detectors, and four detector signals simultaneously. The column oven operates at the temperature range of +4°C to +450°C, while using cryogenic cooling will decrease the starting temperature to –80°C. Light liquid and gas samples can be analyzed with a flame ionization detector (FID) and two thermal conductivity detectors (TCD). The FID (responds to most organic compounds) has the minimum detectable level of 1.5 pg C/s (for tridecane) and operates at temperatures up to 450°C. On the other hand, the TCD (a universal detector that responds to all compounds, excluding the carrier gas) has the minimum detectable level of 400 pg tridecane/ml with the maximum temperature of 400°C. The GC–MSD machine has the same functionality but benefits from a mass selective detector, which has outstanding detection capabilities and provides promising analyses, especially from a qualitative point of view. More information on GC instruments and operation parameters can be found in Appendix B.

4.3.3 Simulated distillation (SIMDIS)

Simulated distillation (SIMDIS) is a gas chromatography technique which separates individual hydrocarbon components in the order of their boiling point, and is used to simulate the time–consuming laboratory–scale physical distillation procedure,

known as true boiling point (TBP) distillation [121]. The separation is accomplished with a nonpolar chromatography column using a gas chromatograph, equipped with an oven and injector, which can be temperature programmed. A flame ionization detector is used for detection and measurement of the hydrocarbon analytes. The results of SIMDIS analysis provide a quantitative percent mass as a function of the boiling point of the hydrocarbon components in the sample. SIMDIS is valuable for, and can improve results from, computer modeling of refining processes for improvements in design and process optimization. The boiling point with the yield profile data of these materials are used in operational decisions made by refinery engineers to improve product yields and product quality.

In this study, the SIMDIS method ASTM D7169[1] was used to determine boiling point distribution of the cut point intervals of crude oil and residues using high temperature gas chromatography. The test is used to determine boiling point distribution of the hydrocarbons up to n-C_{100} with the corresponding elution temperature of 720°C. GC oven initial temperature should be set at −20°C with the initial hold time of 0 min. The oven is heated at the rate of 15°C/min to the final temperature of 425°C and held for 10 minutes. The column has a length of 5 m, an inner diameter of 0.53 mm with a stationary phase thickness of 0.15 µm and a carrier (mobile) phase flow of 25 ml/min passing through it.

[1]Standard Test Method for Boiling Point Distribution of Samples with Residues such as Crude Oils and Atmospheric and Vacuum Residues by High Temperature Gas Chromatography [122]

5. RESULTS AND DISCUSSION

This section discusses the results of TC and RTC experiments on two different petroleum samples. The products were analyzed for physical and chemical changes. At the end, the dependence of radiation throughput on various factors and the stability of the treated hydrocarbons are analyzed.

5.1 Solvent Diluted Samples

As discussed in the previous section, the samples in this study are composed of quite heavy molecules, that exhibit very high viscosity. Dealing with such a heavy fluid always poses a lot of problems. Thus, at first, we decided to dilute the fluids before RTC and TC experiments. Dissolving the samples into a strong solvent has two advantages:

- As the samples, specially the AR fluid, have a severely sticky nature, it is really difficult to transfer them or prepare them for each experiment. The sample container should be submerged into a hot water bath for a specific time duration to be able to transfer it into the reactor. Dissolving the samples into a solvent helps us to overcome the fluid transportation problems.

- Second, as the samples have large hydrocarbon molecules such as asphaltene and resins, dilution with a strong solvent will help to break the larger molecules into smaller species, and ionizing electron particles may be more effective for these molecules.

One of the strongest solvents we can use for high asphaltic fluids is naphtha. Full range naphtha is a fraction of oil boiling between 30 to 200°C mostly formed of C_5 to C_{12} hydrocarbons, sulfur, and small amounts of nitrogen. Depending on the boiling point of the components, naphtha can be either light (boiling in the range of 30 to 90°C) or heavy (boiling point temperature in the range of 90 to 200°C). The term

medium naphtha is used occasionally for the case of fractions boiling below 150°C and contains C_7 to C_9. Hydrocarbon components such as paraffins, olefins, naphthenes, and aromatics constitute a major portion of naphtha composition while sulfur and nitrogen form the most important heteroatom components in the naphtha [123]. Although naphtha has a significant capability to dissolve heavy hydrocarbon fluids, difficulties arise when dealing with its strong pervasive odor. Naphtha smells quite strong even for a short term exposure. Consequently, the use of naphtha in academic and laboratory environments can be pretty problematic. In an effort to replace naphtha with another potential solvent, we tried a couple of other components to dissolve pitch samples at various temperatures. Among all the solvents, xylene did a better job as it was able to dissolve a considerable amount of heavy hydrocarbons and did not cause any of the problems we had with naphtha. Although toluene was also a potential solvent for mentioned purposes, its carcinogenic nature prevented us from any further experiment on this solvent. After choosing the right solvent, we performed a couple of tests with different solvent to solute ratios for the pitch and AR samples, but the results of the experiments turned out to be substantially dominated by the solvent. In fact, the solvent domination interferes with the analysis of the radiolysis products and we can not accurately figure out the changes that have happened to the heavy hydrocarbon molecules as a result of radiation–induced upgrading. Hence, the diluent was taken out for the rest of experiments.

5.2 Irradiation of Deasphalted Oil (DAO)

To investigate the effect of ionizing electron particles on heavy deasphalted oil, we have performed RTC and TC experiments and analyzed the results for any physical and chemical change. The duration of the TC and RTC experiments was 2 hours and the liquid temperature was kept at 385°C throughout the run time. While TC experiments used heat as the sole source of cracking energy, heating and irradiation

took place simultaneously during the RTC tests and the amount of 20 kGy energy was absorbed by the fluid.

5.2.1 Physical and rheological properties

Fig. 5.1 provides the viscosity of the DAO fluid, treated in different ways, measured at two temperatures.

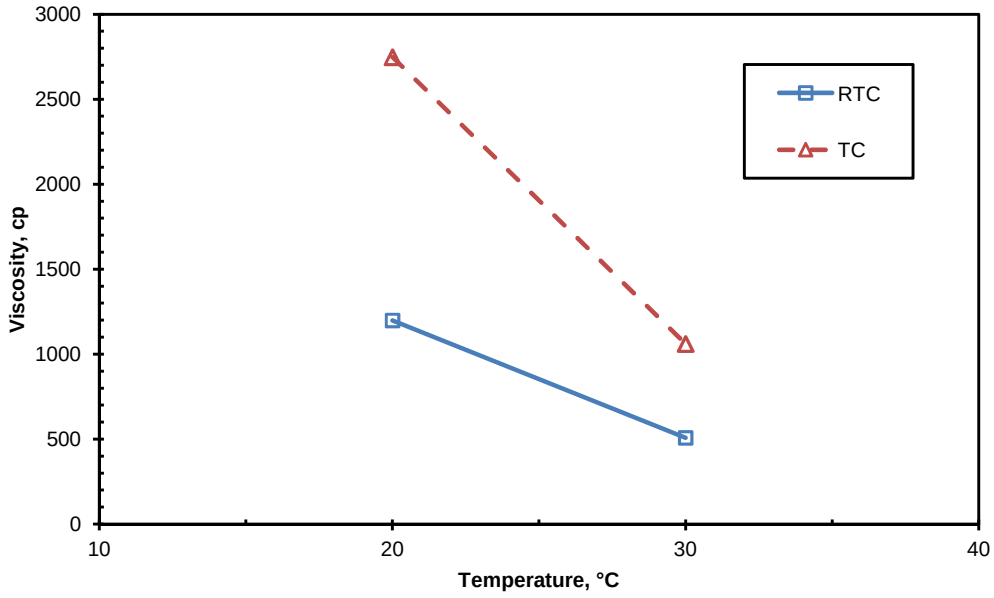

Fig. 5.1.: Further viscosity reduction is achieved when DAO samples are exposed to electron irradiation

The graph shows that irradiation has lowered the viscosity of the fluids substantially. A viscosity reduction of 55% (viscosity decreased from 2750 cp to 1200 cp) for irradiated samples is evidence of intensified cracking as a consequence of ionizing irradiation. The effectiveness of irradiation, as an efficient means of delivering energy

to the electronic structure of the molecules, becomes more pronounced since the thermal energy is coupled tightly to translational, rotational, and vibrational modes; and only a small portion of the energy goes into the electronic structure of the absorber. In fact, irradiation will impact initiation as one of the most energy–intensive steps in chain reactions. This intensified cracking results more lighter molecules in the final product and causes the viscosity of the irradiated DAO fluid to reduce considerably. The following sections provide more details about the similarities and differences of thermal and radiation–induced cracking. Although different in viscosity, RTC and TC products have similar API gravities (Table 5.1).

Table 5.1: RTC and TC products of DAO have similar density values

Properties	RTC	TC
°API (60°F/60°F)	14.70	14.44
Density, at 60°F (gr/cc)	0.9669	0.9685
$\Delta\mu(\mu_{DAO} - \mu)$, at 70°F (cp)	9813.5	8264.5

5.2.2 Simulated distillation analysis

Fig. 5.2 provides detailed information of the boiling point distribution of hydrocarbon components in treated and untreated heavy oil samples (the horizontal axis represents the boiling temperature and the vertical axis specifies weight percent of the components with a boiling point temperature *equal* or *less* than that specific temperature). The results show that TC and RTC products have a higher concentration of light components than the original untreated DAO. Now, consider the boiling temperature of 430°C (this temperature corresponds to the boiling point

of paraffinic C_{28}). The points at which a vertical line from $T = 430°C$ intersects RTC, TC, and DAO lines represents the weight percent of the components boiling off before 430°C. Looking at the graph, 24.5 wt%, 31.5 wt%, and 36.5 wt% of DAO, TC, and RTC fluids comes out of the mixture respectively. TC products have 7 wt% more light components (C_n, $n \leq 28$) than the DAO fluid that causes the viscosity to decrease from 11000 cp for DAO to 2750 cp for TC (at 20°C). On the other hand, the concentration of C_n ($n \leq 28$) is 5 wt% higher in RTC than TC, which can be evaluated as the lighter nature of irradiated samples. The presence of 5 wt% more lighter components in RTC fluid reduces the viscosity from 2750 cp for TC to 1200 cp for RTC (at 20°C). Higher concentration of light molecules in RTC samples is because irradiation reinforces the cracking process.

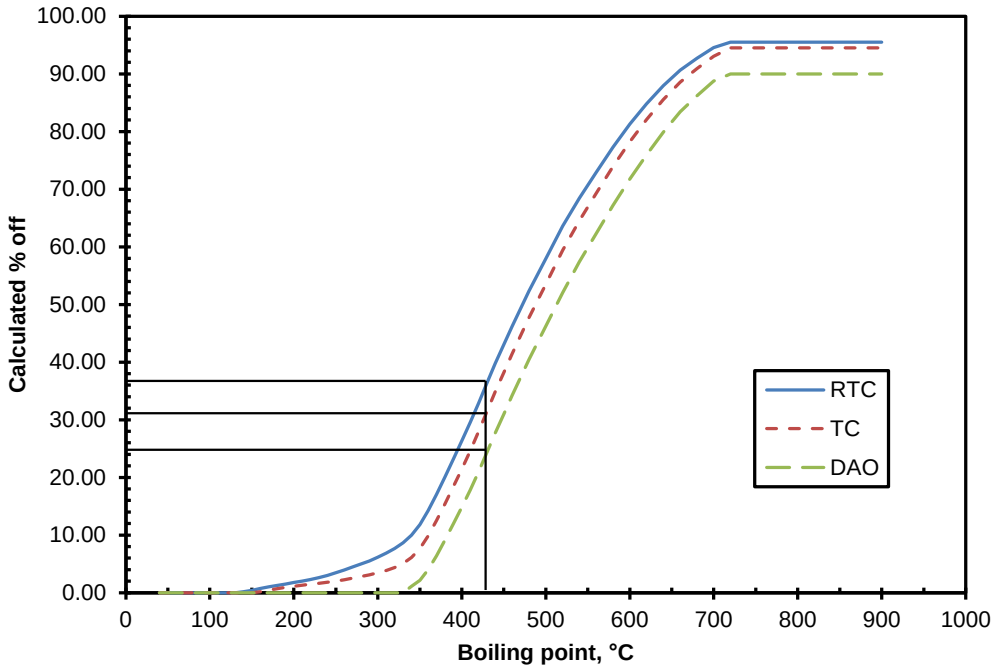

Fig. 5.2.: Intensified cracking of DAO samples as a result of electron irradiation is clear in SIMDIS analysis results

To better understand the changes that happen to the DAO fluid after TC and RTC experiments as well as the similarities and dissimilarities of these treatment scenarios, Fig. 5.3 provides the percent difference of the boiled off weight fraction in RTC and untreated DAO along with that of TC and DAO, graphed as a function of temperature.

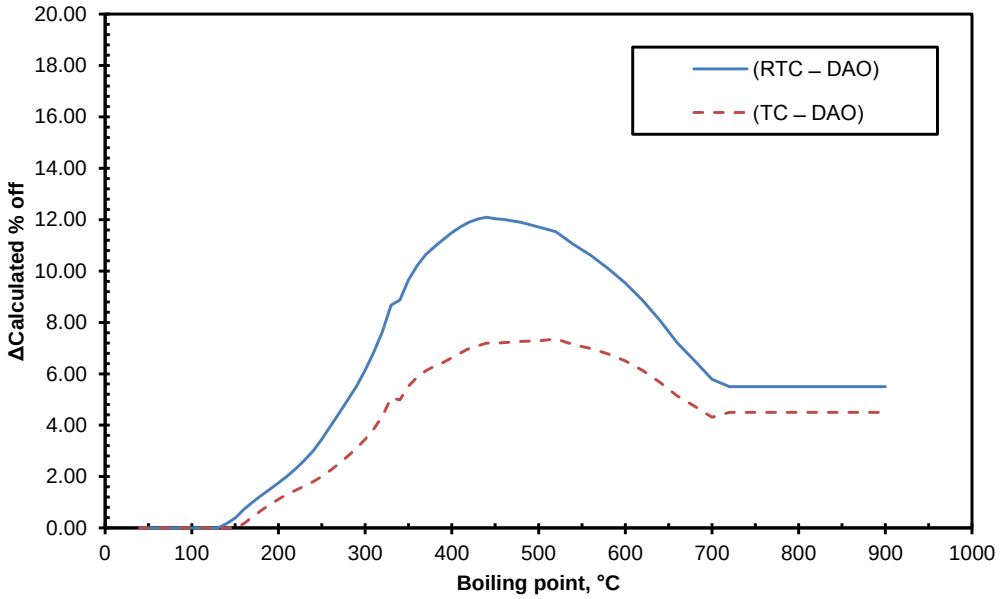

Fig. 5.3.: Irradiation improves the cracking process without any major change in the reaction pathway

This graph can be discussed from two perspectives. First of all, if we look at the trend line for the RTC and TC fluids, there is an apparent upward shift from TC to RTC for the case of components boiling at $T > 150°C$. It is, as mentioned before, interpreted as the lighter nature of RTC products, which is a consequence of enhanced cracking. On the other hand, the positive slope of the lines at temperatures below 430°C indicates that we have a higher concentration of lighter components in RTC

and TC than in the untreated DAO. The negative slope of the lines for $T > 430°C$ is, however, analyzed as more concentration of components in this boiling point range for untreated DAO fluids compared to RTC or TC. Keeping in mind that 430°C corresponds to the boiling point of C_{28}, we can claim that the *net* effect of both treatment scenarios is to crack C_{28}^{+} components into lighter species. However, this is not the most important conclusion that can be drawn from the provided graph. Considering the trend lines more precisely, it is apparent that both treatments follow a similar pattern, an increase starting by 150°C that reaches to a maximum at 430°C followed by a decrease to 720°C (that is the upper limit of the boiling temperature in ASTM D7169). Additionally, the relative ratio of the concentration of different hydrocarbon molecules in the TC sample is the same as that of the RTC sample. It can be concluded from the discussion that although irradiation improves cracking, it does not change the reaction mechanism in favor of molecules with a specific boiling point or molecular weight. Fig. 5.4 more explicitly represents the similarities of RTC and TC products (despite the two previous graphs, the Y axis here represents the weight percent of components that have a specific boiling point and it does not contain components with lower boiling points). At $T < 430°C$, RTC has a higher concentration of light components. When the temperature goes above 430°C, the RTC line falls below the TC line meaning that larger percentage of heavier components in the RTC fluid is cracked into lighter components, fully backing the idea that radiation reinforces the cracking process. The graph also shows that thermal and radiation thermal treatments generate products with similar boiling point distribution, fully backing the idea that radiation does not change the reaction pathway. The subsequent sections on gas and light liquid analysis provide more evidence to support the claimed mechanism for radiation–induced reactions.

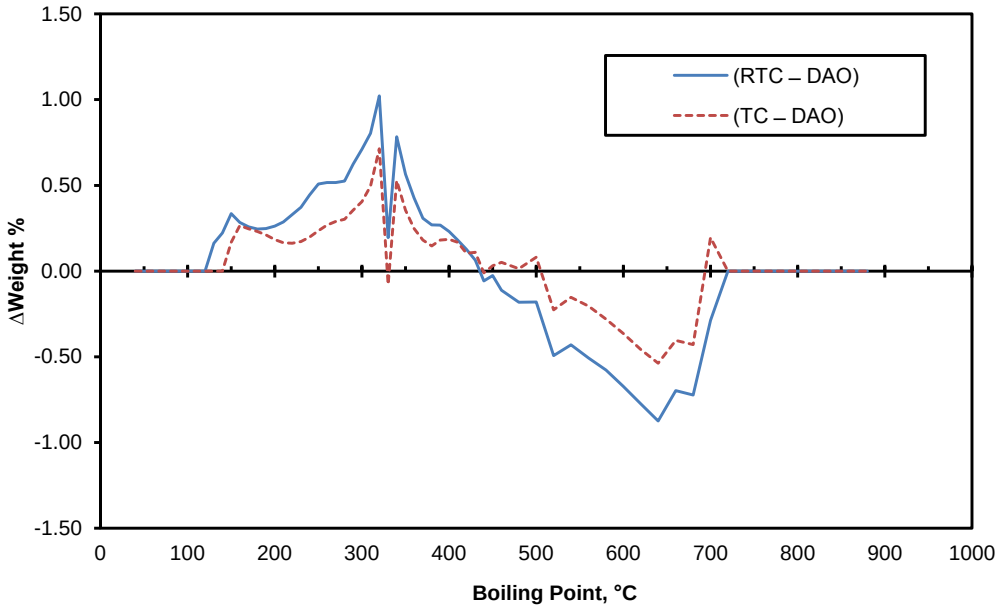

Fig. 5.4.: Boiling point distribution of RTC and TC samples show quite similar pattern

5.2.3 Evolved gas analysis

Before starting the results of gas analysis, it is important to clarify a special point regarding the experimental setup. As mentioned earlier, we have used a "J type" thermocouple to monitor the temperature of the evolved gas during the tests. Due to the nature of the reflux experiment, all the condensable gas will be condensed into the liquid phase and noncondensable gas will be collected as gas samples. However, the concentration of vapor molecules is not that much in the vicinity of the vapor thermocouple and consequently, the temperature read by the thermocouple is not accurately reflecting the vapor's real temperature; rather, temperature of the vapor thermocouple is directly related to the amount of gas evolved during the tests. The higher amount of evolved gas, the higher the temperature would be (The thermo-

couple will be exposed to more gas molecules and the temperature gets closer to real temperature of gas molecules). Additionally, the thermocouple is located close to the 0°C cooling water tank, located inside the condenser, and temperature would be affected by that part as well. Hence, rather than correlating the temperatures to the real temperature of the gas molecules, we use the data from the "J type" thermocouple as an index to represent the amount of evolved gas during the experiments (because of this reason we call it the "quantifier thermocouple").

Investigation of gas samples helps us to better understand the reaction mechanism. In this study, gas samples were analyzed from two perspectives: quantitative and qualitative. The quantitative point of view gives us information about the amount of gas evolved during the RTC and TC experiments. On the other hand, the qualitative analysis discusses the chemical composition of the evolved gas to inspect the similarities and differences. Fig. 5.5 depicts the temperature data acquired from the quantifier thermocouple during RTC and TC experiments.

The higher thermocouple readings in RTC means a higher amount of noncondensable gas. This can be also seen from the gas sampling bags. RTC sample bags were inflated almost two times more than that of TC bags. Gas molecules are, in fact, the product of the upgrading process, when heavy complex molecules break into smaller compounds; hence, more amounts of liberated gas in RTC is analyzed as reinforced cracking, which is a result of electron irradiation. Now, consider the distribution of different hydrocarbon molecules in gas samples (Fig. 5.6). The graph shows that both gas samples have similar composition; this leads to the conclusion that similar reactions take place when either thermal or radiation thermal cracking are employed as a means of reducing viscosity of heavy petroleum fluids.

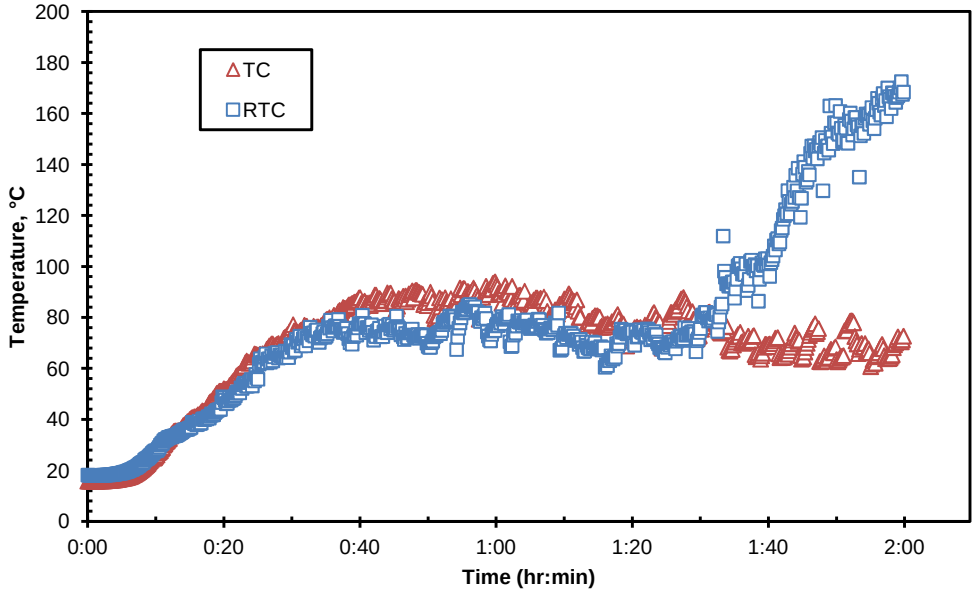

Fig. 5.5.: Higher temperature of the quantifier thermocouple indicates more evolved gas for RTC

Although the amount of evolved hydrogen in TC experiments was lower that the GC instrument's threshold, we can see that there is a traceable amount of hydrogen in RTC gas. When hydrocarbons are exposed to ionizing irradiation, the charged particles deliver their energy to the molecules, resulting in the formation of excited species. Such an excited molecule can be potential source of H_2 molecules. Radiation–induced hydrogen has two origins. It may be formed either through molecular elimination or hydrogen atom mechanism [38,96,98,101]. For the case of molecular elimination, the excited hydrocarbon (A^*) loses a H_2 molecule, resulting in an unsaturated molecule ($A_{unsaturated}$). This process is also called unimolecular hydrogen formation.

$$A^* \rightarrow A_{unsaturated} + H_2 \tag{5.1}$$

On the other hand, we may consider a model for the production of hydrogen in which a C–H bond is initially broken in an excited molecule or ion to produce hydrocarbon radical and H atom. The hydrogen atoms posses a range of kinetic energies, but most are sufficiently excited to abstract on their first collision (also defined as hot hydrogen atoms). If the abstraction takes place from another molecule, the process is called bimolecular hydrogen formation. If the abstraction occurs from the same carbon atom or an adjacent one on the same molecule from which the hot hydrogen atom has been released, the process will be indistinguishable from the molecular elimination (both processes are unimolecular). Hydrogen atoms, that do not react on their first collision, are defined as epithermal or thermal, depending on their kinetic energy. With a few exceptions, epithermal and thermal hydrogens will react similar to each other. Epithermal hydrogen atoms will undergo more than one collision before abstracting, and on each collision will get partially deactivated. The probability of their reaction on the following collisions is therefore decreased, and these atoms will be scavengable. Compared to the hot atoms, the contribution of thermal atoms to the hydrogen yield is not that significant.

$$A^* \rightarrow \dot{A} + \dot{H} \tag{5.2}$$

$$\dot{H} + A \rightarrow H_2 + \dot{A} \tag{5.3}$$

Where A is a hydrocarbon molecule and A^* represents the excited state of that molecule.

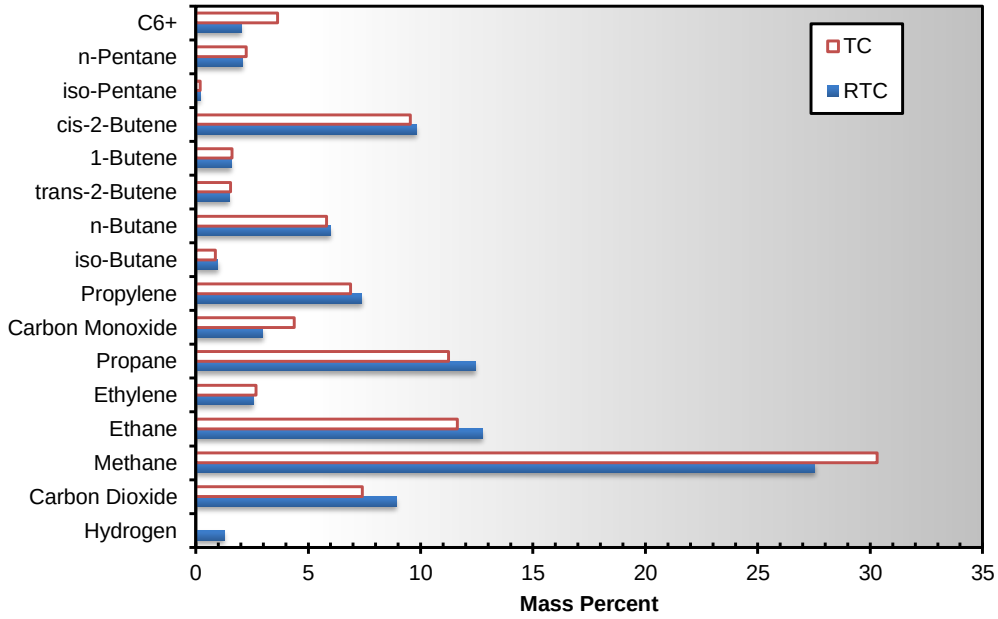

Fig. 5.6.: RTC and TC gas products have similar component distribution in DAO experiments

5.2.4 Light liquid fraction analysis

The following section discusses the composition of the liquid products with boiling points less than 250°C, which are excluded and analyzed using chromatographic techniques. Having detailed information about the light liquid components, we can get valuable knowledge about the mechanism of RTC and TC treatments. According to Fig. 5.7, the distribution of different hydrocarbon species in both treatment scenarios are similar to each other. Aromatic molecules are the most abundant group and form 20 wt% of light liquid components. Mono–aromatics, i–paraffins, and n–olefins stand after aromatics with wt% of 14, 13, and 10, respectively, for both TC and RTC products. On the other hand, both cases have very small concentrations of di–olefins, naphtheno–olefins, indanes, indenes, and naphthalenes.

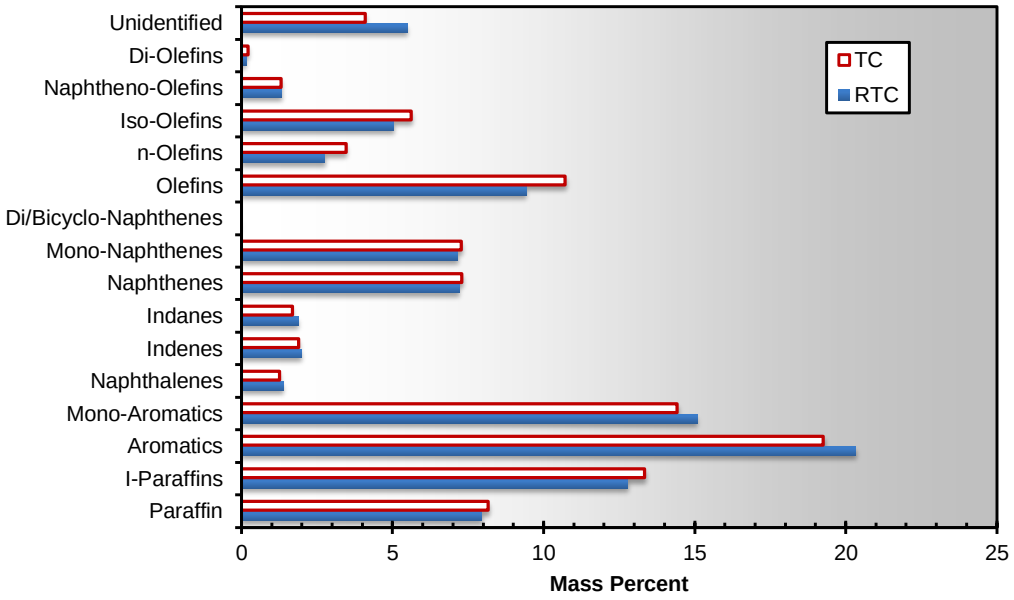

Fig. 5.7.: Distribution of different hydrocarbon groups in light liquid components shows similar composition for RTC and TC products of the DAO fluid

Fig. 5.8 represents the carbon number distribution of the light liquid products. Again, irradiated and unirradiated samples share similar patterns. C_8–C_{12} have the highest concentration while the concentration of C_{13} decreases steeply.

Moreover, we have analyzed mass distribution of different hydrocarbon groups in light liquid products to acquire better idea on probable changes that may happen to a specific group of components as a result of irradiation (Fig. 5.9). Except for the paraffins (the composition of light and heavy hydrocarbons differs slightly in RTC and TC cases) and n–Olefins (C_4 concentration is higher in TC), the other groups (iso–paraffins, mono–aromatics, mono–naphthenes, iso–olefins, and naphtheno–olefins) exhibit similar composition distribution. The analyses performed on light liquid products interestingly confirm the results of SIMDIS and gas analysis, supporting the claimed theory about the role of irradiation on chain reactions and the fact that the reaction path will not alter by radiolytic methods.

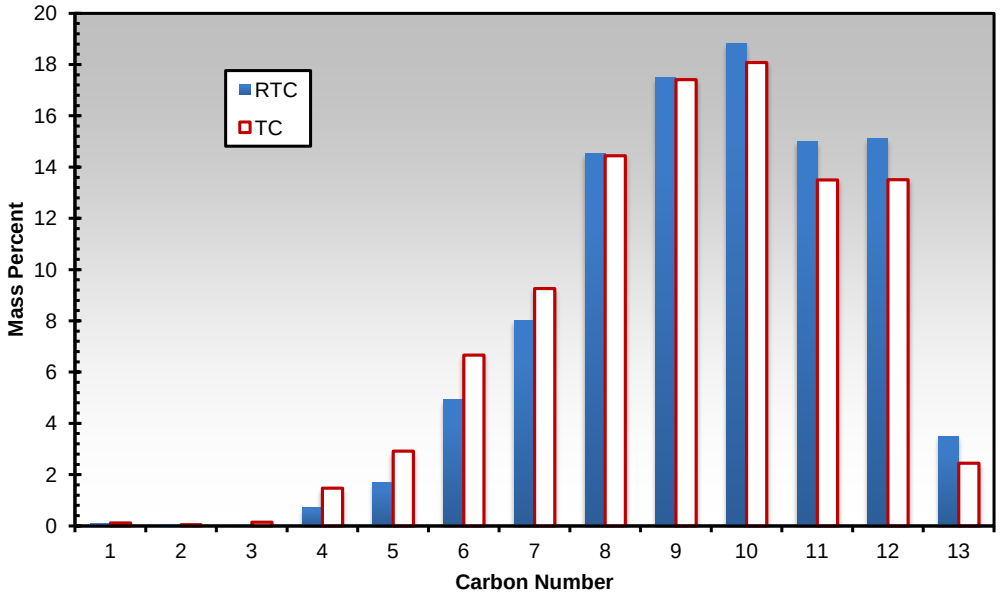

Fig. 5.8.: Carbon number distribution of light liquid products in the radiolyzed DAO fluid looks similar to that of the thermally cracked products

5.3 Irradiation of Highly Asphaltic Atmospheric Residuum (AR)*

In this set of experiments, we investigated radiation–induced reactions of highly asphaltic atmospheric residuum fluids. The duration of the TC and RTC experiments was 1 hour and the liquid temperature was kept at 380°C throughout the run time. While TC experiments used heat as the sole source of cracking energy, heating and irradiation took place simultaneously during the RTC tests and the amount of 10 kGy energy was absorbed by the fluid.

*Reprinted with permission from "Utilization of Charged Particles as an Efficient Way To Improve Rheological Properties of Heavy Asphaltic Petroleum Samples" by M. Alfi, P. Da Dilva, M. Barrufet, and R. Moreira. Paper presented at SPE Latin American and Caribbean Petroleum Engineering Conference (LACPEC 2012). Copyright 2012 by SPE.

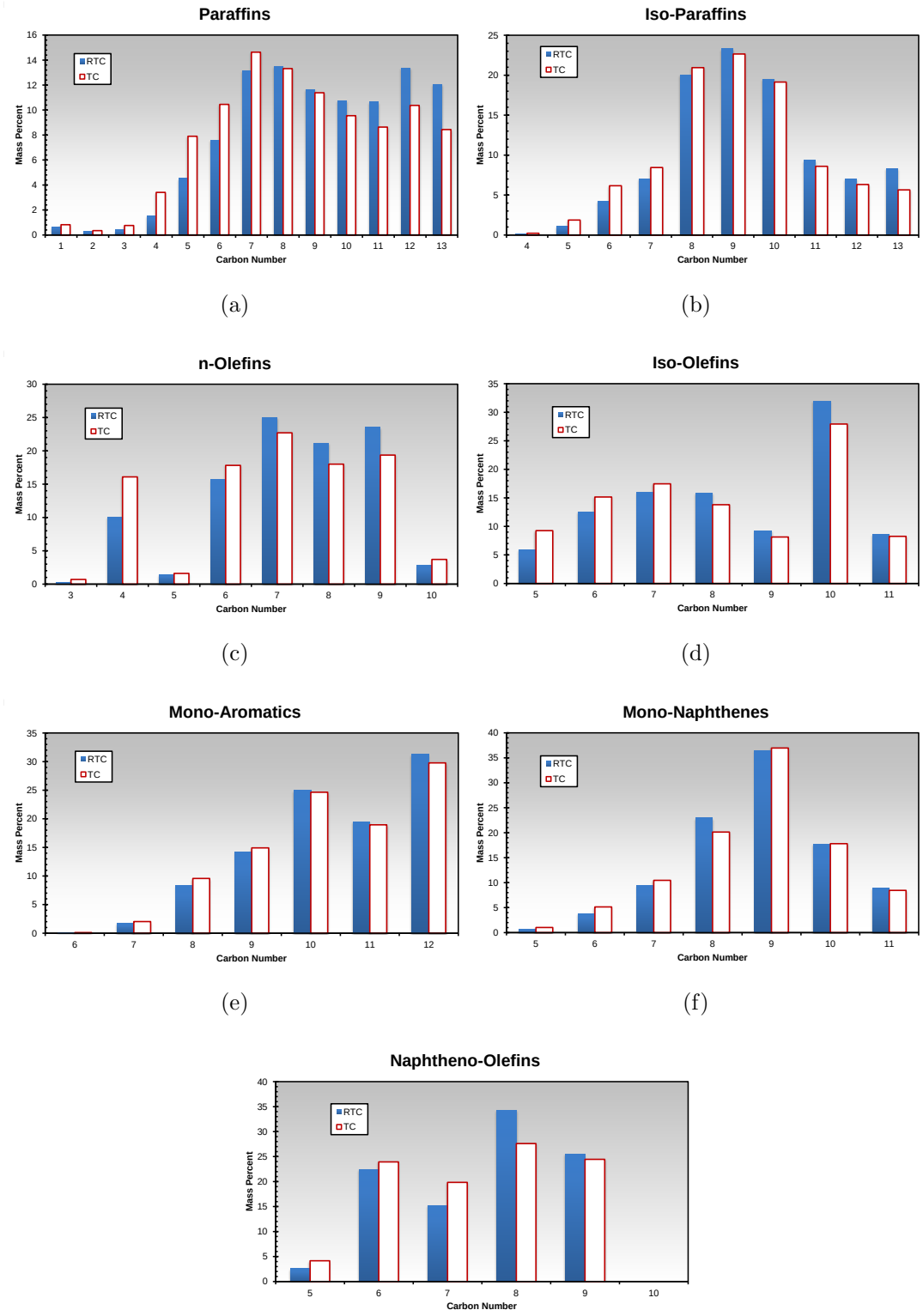

Fig. 5.9.: Mass distribution of the different hydrocarbon groups in light liquid products shows the similarities of TC and RTC in the DAO fluid

5.3.1 Physical and rheological properties

To monitor the rheological changes brought about as a consequence of irradiation, the viscosity of RTC and TC samples were measured at different temperatures (Fig. 5.10).

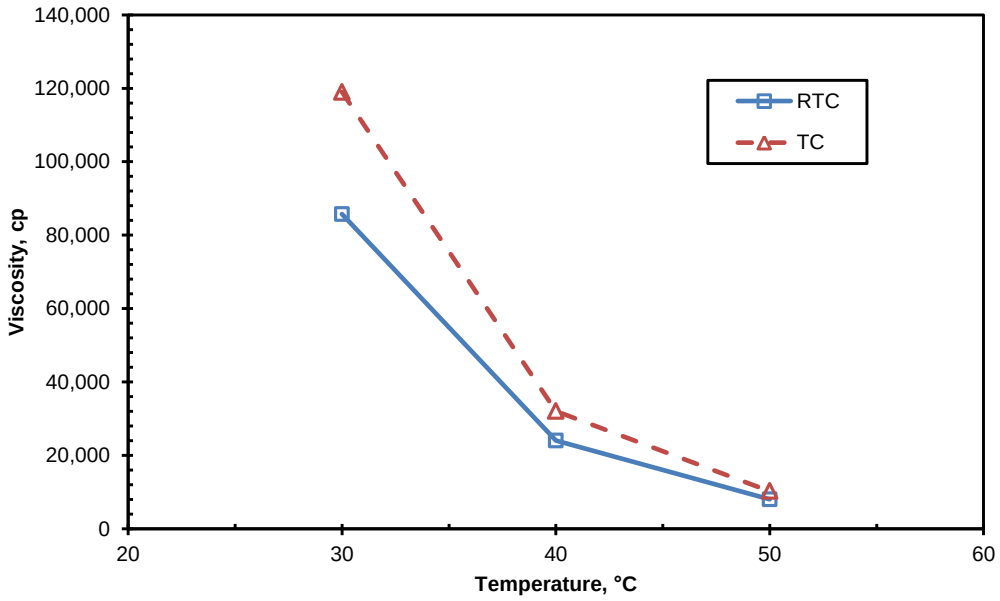

Fig. 5.10.: Radiation thermal cracking intensifies the viscosity reduction of highly asphaltic AR fluids

Looking at Fig. 5.10, it is apparent that electron irradiation further reduces the viscosity of heavy oil samples with respect to TC. In fact, ionizing irradiation will intensify cracking of larger molecules into smaller species. As the molecules become smaller, the intra–layer adhesive forces diminish, leading to a less–viscous fluid. Using ionizing electron particles, 30% viscosity reduction has been achieved due to a more efficient cracking process (viscosity has decreased from 120000 cp to

85000 cp). Ionizing electron particles are capable of delivering their entire energy to the electronic structure of the absorber, resulting in an energy–efficient generation of reactive species, which initiate chemical reactions. Although heat provides enough energy required for C–C bond cleavage and generation of free radicals, the process is way less efficient when compared to ionizing irradiation. In fact, irradiation will impact initiation as one of the most energy–intensive steps in chain reactions. Although RTC and TC samples exhibit different viscosities, they have similar API values (Table 5.2). Although viscosity measurements imply that irradiation will improve rheological properties of heavy petroleum fluids, we need to know more details about the RTC and TC products to judge the differences in the reaction mechanism of thermal and radiation thermal cracking.

Table 5.2: RTC and TC products of AR have similar density

Properties	RTC	TC
°API (60°F/60°F)	7.67	7.45
Density, at 60°F (gr/cc)	1.0167	1.0183
$\Delta\mu(\mu_{AR} - \mu)$, at 70°F (cp)	823500	790250

5.3.2 Simulated distillation analysis

SIMDIS analyses provide detailed information on distribution of the hydrocarbon molecules in liquid products, helping us to get better insight toward the reaction mechanism. Looking at Fig. 5.11, the horizontal axis represents the boiling temperature and the vertical axis specifies the weight percent of the components with boiling point temperatures *equal* or *less* than that specific temperature. Both RTC and TC

samples show an upward shift from the untreated AR fluid which is an indication of the higher percentage of light components in those samples. Comparing RTC and TC experiments, RTC has a slightly higher concentration of lighter components than TC. As an example, for the boiling point of 600°C, from the graph, about 2 wt% difference between RTC and TC does not appear to be significant. However, when one compares it to the original untreated AR and notices that 7.2 wt% difference between AR and TC causes the viscosity of the sample to reduce from 900×10^3 to 120×10^3 cp (87% viscosity reduction), it is conceivable that 2 wt% difference in TC and RTC is capable of decreasing the viscosity from 120×10^3 to 85×10^3 cp (30% viscosity reduction). In addition, due to limitations of the current SIMDIS method, any viscosity changes related to the degradation of large aromatic aggregates into C_{100}^{+} components cannot be traced in SIMDIS results (Fig. 5.11 shows that around 20 wt% of the components in the treated samples has more than 100 carbon atoms). A higher concentration of light molecules in RTC products is attributed to the intensified cracking accomplished as a consequence of ionizing irradiation.

To find more information about the differences between TC and RTC mechanisms, Fig. 5.12 provides the percent difference of the boiled off weight fraction in the RTC and untreated AR along with that of the TC and AR, graphed as a function of temperature. The graph helps us to gain better information on each scenario. The upward trend of both treatment scenarios at $T < 650$°C reveals that both RTC and TC products have a higher concentration of light components compared to the AR case; however, the downward trend of the graphs for $T > 650$°C can be interpreted as the point where heavier compounds of the AR fluid break into lighter molecules as a result of RTC and TC treatments and the process ends up with lower concentrations of molecules with boiling point temperatures greater than 650°C in the treated AR. Thus, we can conclude that the *net* effect of both treatments is to crack molecules with $T_b > 650$°C into molecules of a less–complex structure.

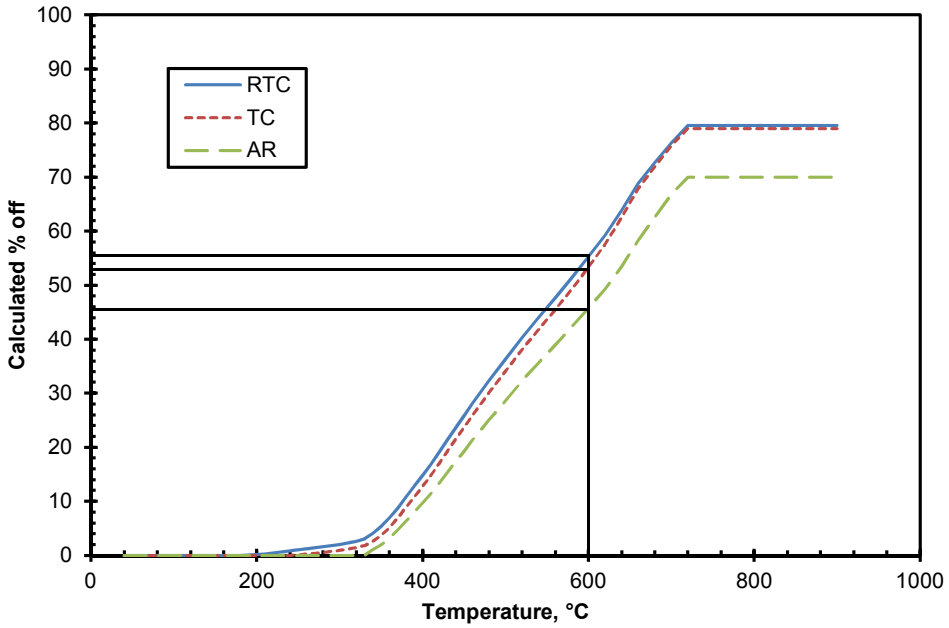

Fig. 5.11.: SIMDIS analyses show that irradiated AR samples have a higher concentration of light components

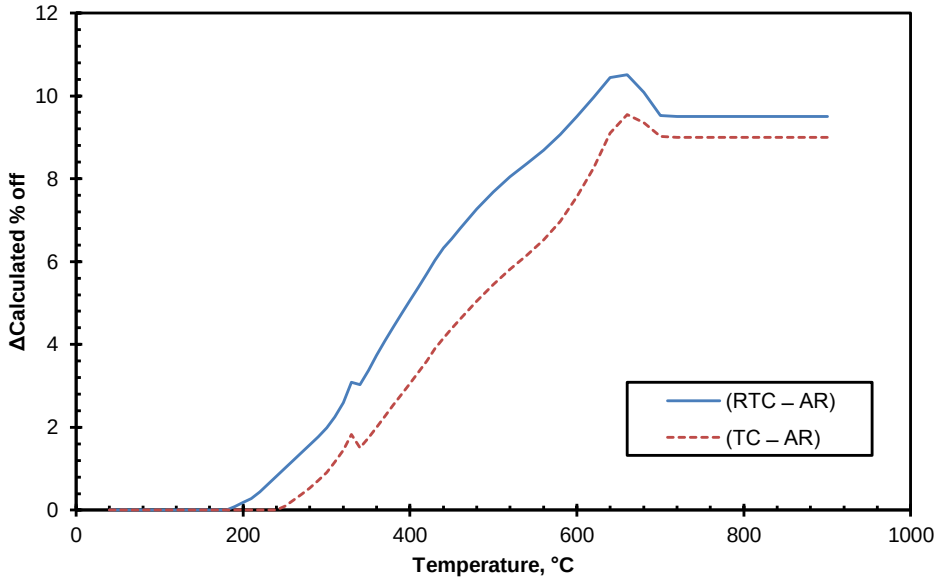

Fig. 5.12.: The overall distribution of RTC and TC products are similar

The upward shift of the RTC case compared to the TC can be described as intensified cracking from electron–induced reactions, although both cases exhibit a similar trend (an increase followed by a decrease starting at 650°C). Moreover, the relative ratio of the concentration of different hydrocarbon molecules in the TC sample is the same as that of the RTC sample, indicating that radiation does not significantly change the reaction pathway in favor of molecules with a specific boiling point or molecular weight. However, there are some distinctions between TC and RTC trend lines stating at $T = 550$°C. To better analyze it, the difference in boiling distribution of AR with RTC and TC are graphed in Fig. 5.13 (despite the two previous graphs, the Y axis here represents the weight percent of components that have a specific boiling point and it does not contain components with lower boiling points).

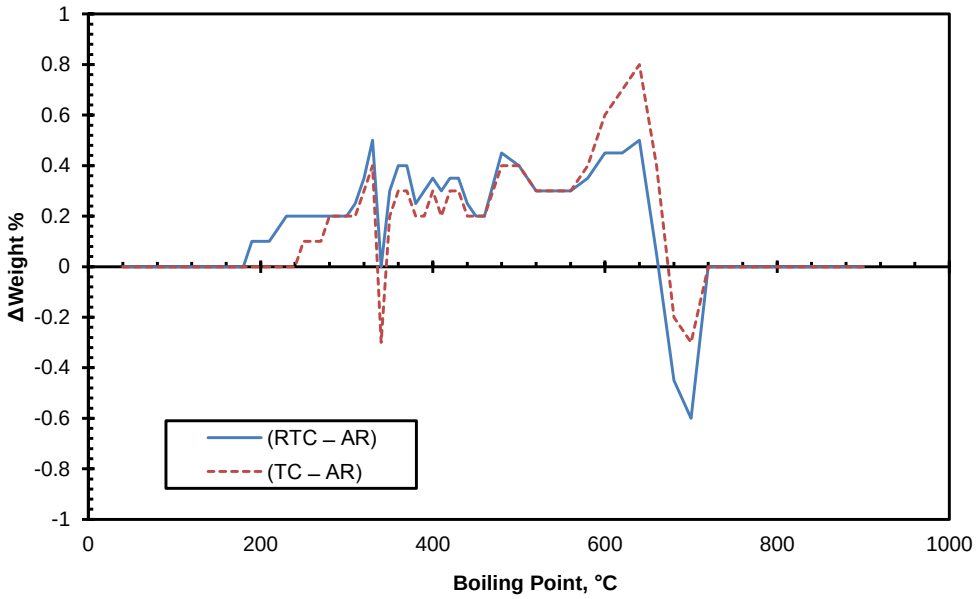

Fig. 5.13.: Boiling point distribution of RTC and TC experiments in AR samples shows distinctive patterns in the temperature range of 550–650°C

For lower boiling points, RTC and TC fluids exhibit the same trend with a slight upward shift in radiated samples, indicating the higher concentration of lighter components. At 550°C, the TC fluid's line begins to deviate from that of RTC with a steep increase in the weight of compounds boiling within the temperature range of 550–650°C. In fact, the RTC sample has a lower concentration of components boiling in this temperature range. This behavior can be explained as radiation–induced degradation of aromatics in asphaltene aggregates and consequent changes in the relative concentration of resulting hydrocarbons. Aromatic components have lower ionization and excitation potentials, and in mixtures with other hydrocarbon molecules, they provide protection effects when exposed to ionizing irradiation. This protection effect happens through charge scavenging by the aromatics or energy transfer to the aromatics. As a result, the aromatic components may undergo further degradation. Investigation of light components in liquid components provides us more details about the differences in RTC and TC products of highly asphaltic petroleum fluids.

5.3.3 Light liquid fraction analysis

To understand the reaction mechanism, similarities, and distinctions, light components of the liquid products (boiling point less than 250°C) are excluded and analyzed using chromatographic techniques. Fig. 5.14 provides the mass distribution of different hydrocarbon species in TC and RTC products. The graph shows that although both treatments have similar backbones, there are detectable differences especially for I–Paraffins. The similar overall trend line can be interpreted as identical chain cracking reaction mechanism for both TC and RTC without any significant change in reaction pathway as a result of irradiation. However, the dissimilarities correlate to the degradation of the aromatic molecules as a result of ionizing electron particles. Now, consider the mass distribution of different carbon numbers (Fig. 5.15).

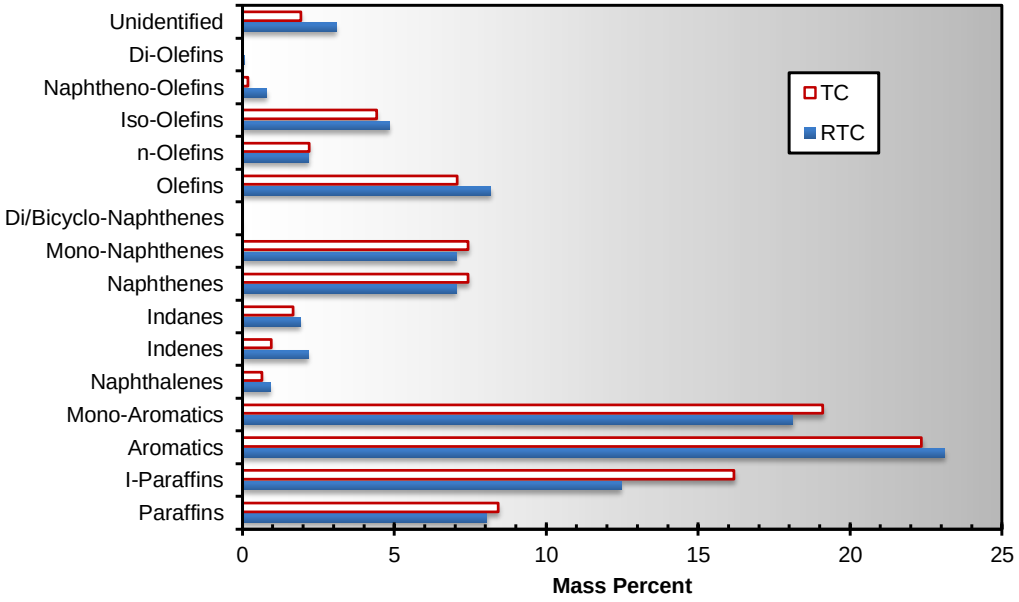

Fig. 5.14.: Distribution of different hydrocarbon groups in light liquid components of the AR fluid exhibits differences in RTC and TC products

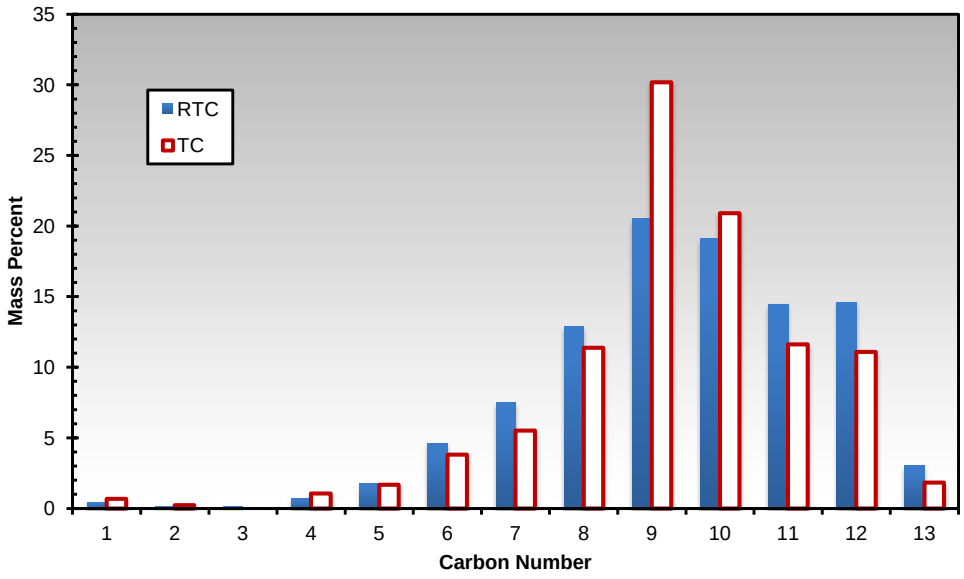

Fig. 5.15.: Carbon number distribution of the medium–weight hydrocarbons in the radiolyzed fluid looks different from that of the thermally cracked fluid

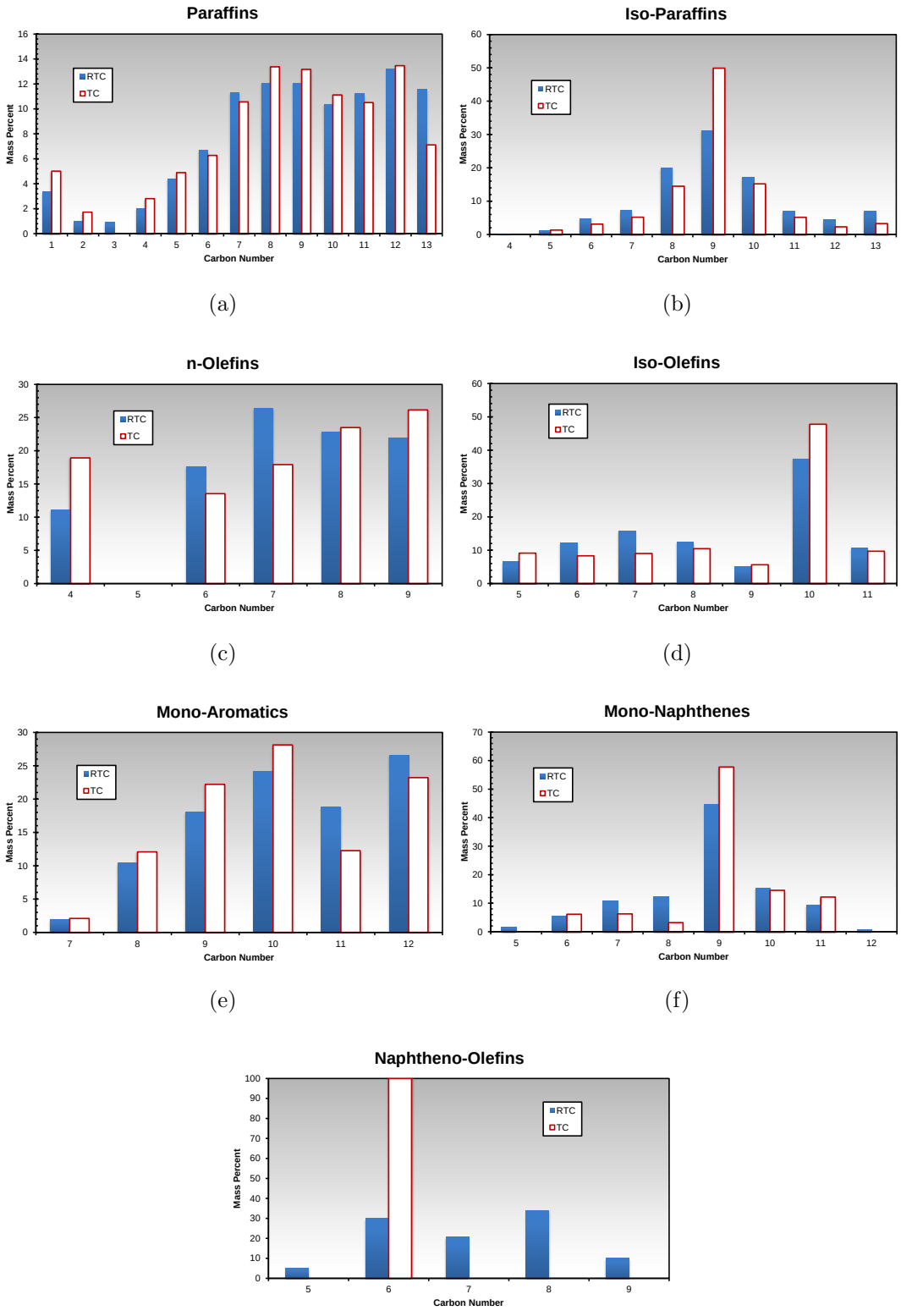

Fig. 5.16.: Mass distribution of the different hydrocarbon groups in light liquid products shows dissimilarities for TC and RTC experiments in the AR fluid

Fig. 5.15 shows the differences in product pattern of RTC and TC experiments more clearly (the distinctive pattern become pronounced for the case of medium carbon numbers). While the C_8 to C_{12} molecules in the RTC fluid have similar mass percents, the concentration of the C_9 is way above the other molecules in the TC product.

To find detailed information about the product pattern of RTC and TC samples, and investigate the probable effects of irradiation on specific hydrocarbon species, we have compared mass distribution of components in different hydrocarbon groups of light liquid products (Fig.5.16). Among all the groups, iso–paraffins, n–olefins, mono–naphthenes, and naphteno–olefins clearly show the difference in product pattern of two treatment scenarios. Looking at iso–paraffins, we can see that the concentration of the C_9 hydrocarbon is much higher in the TC compared to the RTC. This distinct pattern is also observed for the light and medium components of n–olefins and medium components of mono–naphthenes. While naphtheno–olefins in TC products are completely composed of hydrocarbons with six carbon atoms in their structure, the naphtheno–olefins in RTC products exhibit more diversity. To conclude, the results of different analyses show that although electron irradiation does not change the mechanism of the chain reaction, it intensifies the cracking process and brings some changes to the large asphaltene molecules.

5.4 Factors Affecting Radiation Throughput

The following section discusses the effective parameters that can affect radiation throughput. Although there are a number of important factors that may influence the radiolysis process, we have chosen the reaction temperature, irradiated dose, and additives as the most important ones.

5.4.1 Reaction temperature effects

The effect of reaction temperature on the radiation throughput is investigated in this section. Finding out the optimum operating temperature, we are able to lower the operating cost of radiation thermal cracking while not destructing the radiolysis output. We have performed RTC and TC experiments on the DAO sample at four different liquid temperatures (this is the temperature of the liquid inside the can, measured by a "K–type" thermocouple). The liquid temperature started at 230 ± 1.5°C to simulate low–temperature radiation thermal cracking. Medium–temperature cracking experiments were performed at 270 ± 1.5°C and 320 ± 2.5°C while the high–temperature test was done at the liquid temperature of 380 ± 2.5°C. Like the previous tests, the liquid temperature was the same for both TC and RTC experiments and the only difference between the runs referred to the presence of irradiation in RTC cases. In the TC case, the fluid was heated for 2 hours while in the RTC experiment heating and irradiation took place simultaneously and the amount of 20 KGy energy was absorbed by the fluids.

Fig. 5.17 and Table 5.3 provide the viscosity of the RTC and TC products (measured at 20 and 30°C) at different reaction temperatures. It is apparent that for low temperatures, irradiation does not cause any improvement to the viscosity of heavy petroleum fluids. To analyze the results and see the differences, we have combined the data from all the graphs into a single graph (Fig. 5.18). The solid black line in the graph represents the viscosity of the original untreated DAO. At lower temperatures, both treatments increase the viscosity of the samples by 10%. This can be attributed to the polymerization of the hydrocarbon molecules to form heavier components. Somewhere between 320 to 380°C, cracking reactions become activated, causing the viscosity to decrease in both experiments. However, this reduction is more pronounced for the case of irradiated samples.

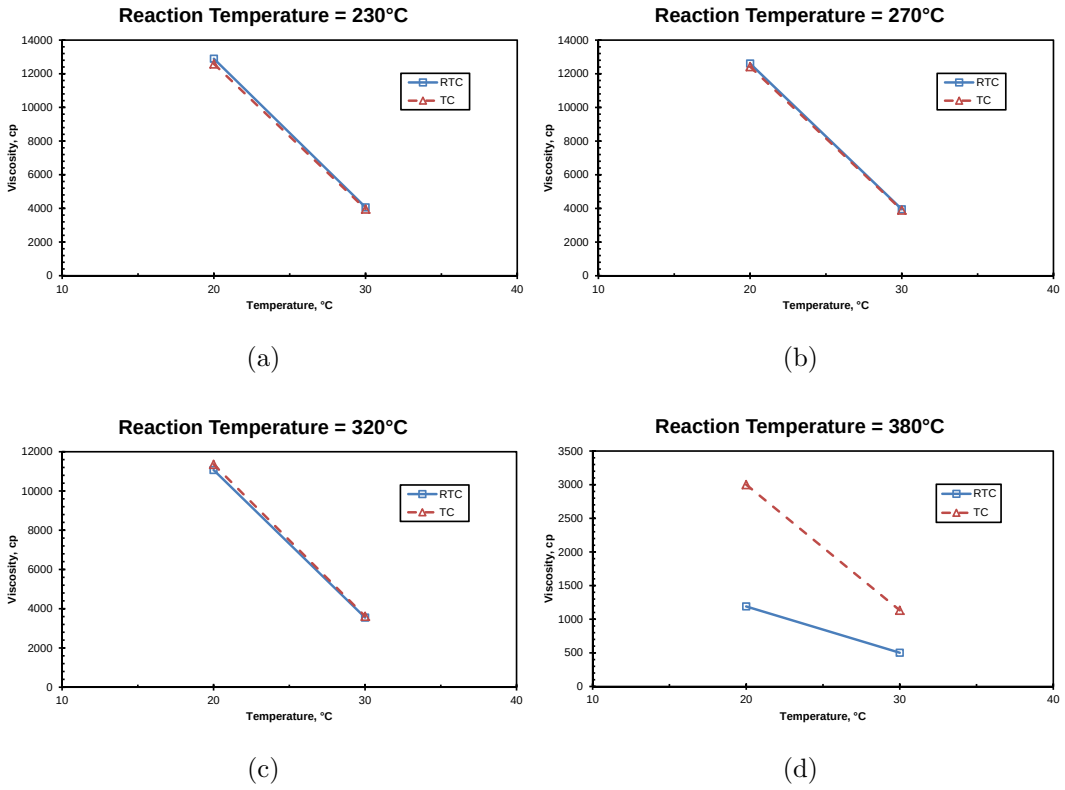

Fig. 5.17.: Electron irradiation does not assist the viscosity reduction process at low temperatures

Table 5.3: Viscosity values of the DAO fluid at different reaction temperatures

Temperature (°C)	μ at 20°C (cp)			μ at 30°C (cp)		
	RTC	TC	RVR	RTC	TC	RVR
230	12891±100	12584±100	–2.4	4062±30	3961±30	–2.5
270	12606±100	12425±100	–1.5	3947±30	3904±30	–1.1
320	11070±100	11362±100	2.6	3548±30	3617±30	1.9
380	1190±10	3001±25	60.3	502±10	1133±10	55.7

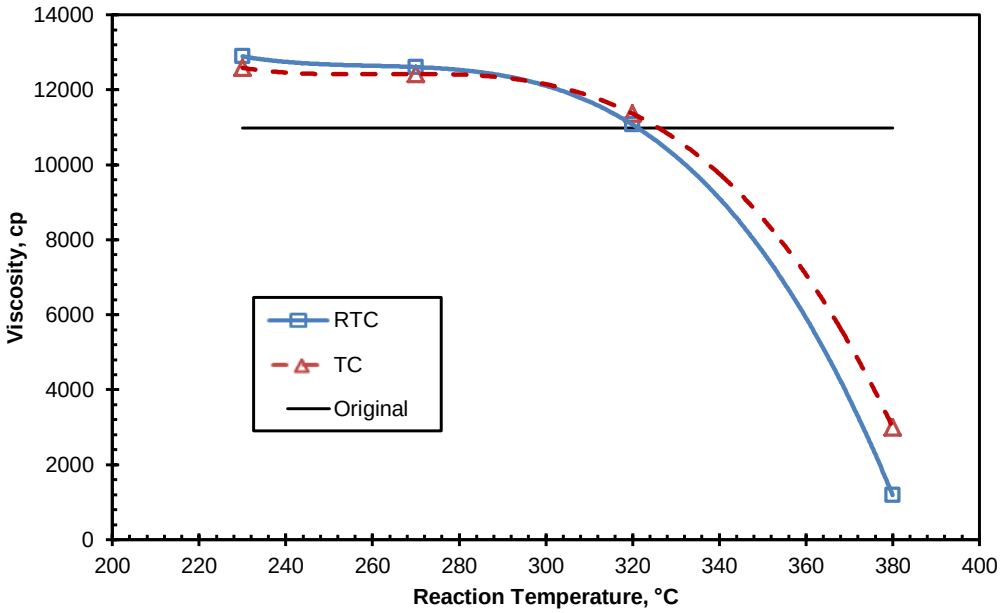

Fig. 5.18.: Low temperature RTC and TC increase the viscosity while at higher temperatures viscosity reduction is observed for both the cases

To better evaluate the impact of temperature on hydrocarbon irradiation, we have defined relative viscosity reduction (RVR) as the relative reduction in the fluid viscosity, achieved as a result of radiation–induced reactions (Equation 5.4).

$$\text{RVR} = \frac{\mu_{TC} - \mu_{RTC}}{\mu_{TC}} \times 100 \tag{5.4}$$

Fig. 5.19 pictures the values of RVR at different temperatures. The negative values at low temperatures mean that the viscosity of the RTC product is higher than that of TC. It is interpreted as reinforced polymerization in irradiated samples. On the other hand, irradiation improves the upgrading process at higher temperatures because of the more efficient energy delivery process. The following discussion explains the theory behind the observed behavior.

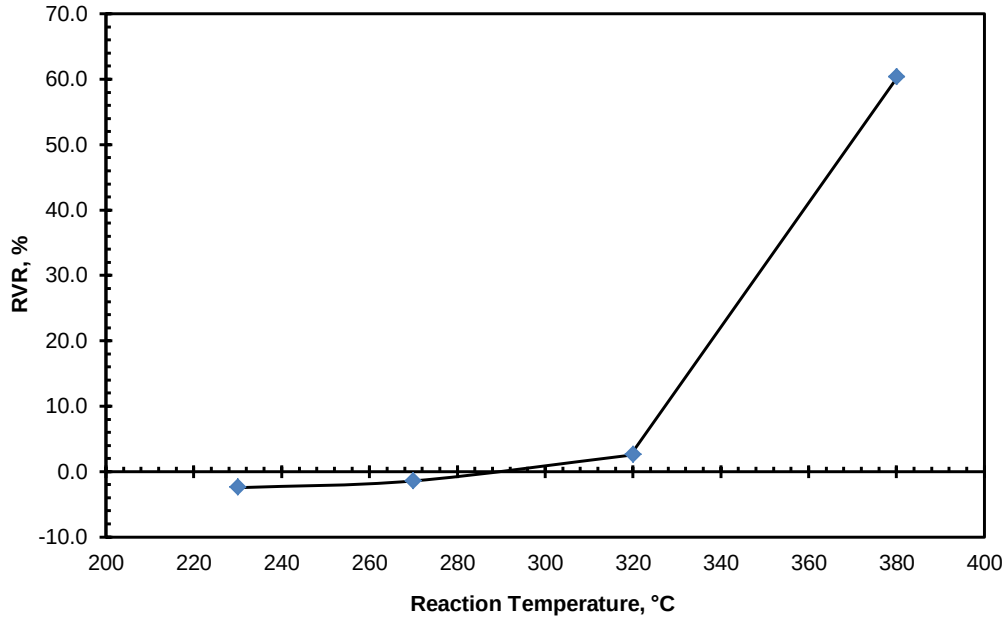

Fig. 5.19.: Intensified polymerization (at $T < 320°C$) and intensified cracking (at $T > 320°C$) is observed for the radiolyzed fluids

Noticing the interaction of high energy electron particles with the media helps to understand the observed behavior. As mentioned earlier, electron particles give out their energy to the surrounding molecules while passing through a media, causing ionization or excitation to the target molecules. Depending on the situation, electrons may have elastic or inelastic scattering. Inelastic scattering results in energy transfer to the molecules, producing excited molecules and ions, secondary and Auger electrons, photon, and X–ray, while elastic scattering causes deflection in the electron track without any energy loss.

Appearance of electric chargers is one of the most obvious consequences of exposing materials to ionizing radiation. Ionizing incidents result in abstraction of electrons from the molecules and creation of positive ions in a so called "ionization" process. The electrons abstracted from the irradiated molecules will be pulled by

ions of positive charge strongly, resulting in charge recombination. Recovered ionization potential generates highly excited molecules with energy levels much higher than the bond strength. The remaining energy, that is deposited by ionization irradiation, causes "excitation" for the molecules exposed to radiation (Equations 5.5 and 5.6) [66, 124, 125].

Ionization:

$$\mathrm{AB} \rightsquigarrow \mathrm{AB}^{+} + \dot{e} \tag{5.5}$$

Excitation:

$$\mathrm{AB} \rightsquigarrow \mathrm{AB}^{*} \tag{5.6}$$

These primary reactions result in development of secondary reactions (Equation 5.7a–g) where the ions, secondary electrons, and excited species exchange energy and charge with nearby neighbors, resulting in generation of short–living intermediate components which may finally evolve into new stable products (Fig. 5.20)

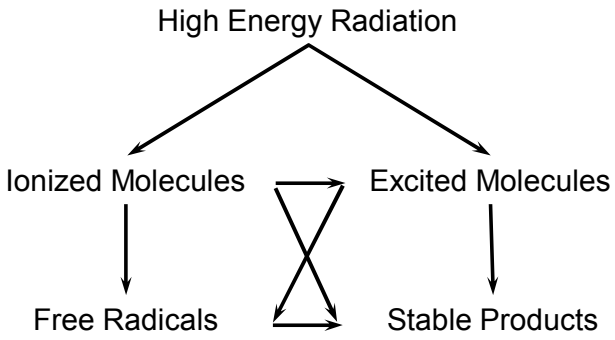

Fig. 5.20.: Schematic representation of primary and secondary radiolysis events (regenerated after Cleland [125])

$$AB^+ + e^- \rightarrow AB^* \tag{5.7a}$$

$$AB^* \rightarrow A^{\cdot} + B^{\cdot} \tag{5.7b}$$

$$AB^{+\cdot} \rightarrow A^+ + B^{\cdot} \tag{5.7c}$$

$$A^{\cdot} + BR \rightarrow AR + B^{\cdot} \tag{5.7d}$$

$$A^{\cdot} + C \rightarrow AC^{\cdot} \tag{5.7e}$$

$$A^{\cdot} + B^{\cdot} \rightarrow AB \tag{5.7f}$$

$$AB^* \rightarrow C + D \tag{5.7g}$$

Where $\rightsquigarrow$ stands for irradiation, AB^* and AB^+ represent excited molecules and positive ions respectively, $\dot{e}$ is a free electron, $A^{\cdot}$ and $B^{\cdot}$ denote free radicals, C and D are stable molecules, and R is a substitute. Two different charged particles with opposite charges combine according to Equation 5.7a to form excited or even superexcited species. Excited molecules, which are unstable due to their high energy level, may then dissociate into free radicals (Equations 5.7b and 5.7c). Generated free radicals may undergo abstraction reactions (Equation 5.7d) or propagation by addition interactions (5.7e). Note that free radicals are very active species with high energy levels and short living time; they demand special isolation techniques to be employed for any mechanistic interpretation [126]. Finally, stable products may be formed as a result of reactions such as radical recombination (Equation 5.7f) or molecular dissociation (Equation 5.7g). These reactions do not represent the whole set of probable reactions and include just those most often encountered in industrial applications [125].

Having all the prerequisites available, generated free hydrocarbon radicals may start a series of chain reactions causing hydrocarbon molecules to upgrade [30, 51].

Chain reactions are comprised of three main stages known as chain initiation, propagation (reaction process), and termination.

- Initiation

$$C_n \rightarrow C_i{}^{\cdot} + C_j{}^{\cdot} \tag{5.8}$$

Any reaction proceeding by a free radical mechanism must include some radical–producing reactions, which are generally referred to as initiation reactions, and these initiator derived radicals (species resulting from hydrocarbon radiolysis along with the ones generated by thermal hydrocarbon cracking) react with the reactants producing reactant–derived radicals. Considering the chain reaction of hydrocarbons, the energy consumed for cracking initiation in the form of heat or ionizing irradiation will not change the product enthalpy. In fact, this initiation energy is consumed to create a large concentration of active radicals necessary for chain initiation. Assume the initial concentration of radicals to be a specific value, using electron irradiation as a way to generate that concentration of active radicals, the energy is directly transferred to the molecules. Comparing this energy to the amount of heat required to produce the same concentration of active radicals, one can conclude that the consumed energy in the form of heat is excessively higher. The feedstock should be heated to high temperatures to deliver relatively small amount of energy into the molecules. So, consuming the same amount of energy, the concentration of active radicals generated in the chain initiation step is much higher in RTC than TC. The initiation step is followed by two groups of reactions, the first being those in which products are formed in a chain sequence of propagating reactions named as the propagation or chain process, which is the dominant part of chain reactions where the reactants are converted into the products in a sequence of reactions. The second is the termination step where the active radicals come together and form non–active species. Although each of the chain sequences must have involved some termina-

tion reactions, the amount of products in these processes is negligible compared to products of the chain sequence [127].

- Propagation (chain process)

$$\text{Hydrogen exchange: } \mathrm{C}_i{}^{\cdot} + \mathrm{C}_n \rightarrow \mathrm{C}_i\mathrm{H} + \mathrm{C}_n{}^{\cdot} \tag{5.9}$$

$$\beta \text{ scission: } \mathrm{C}_n{}^{\cdot} \rightarrow \mathrm{C}_k{}^{\cdot} + 1\text{–Alkene} \tag{5.10}$$

Where k can be any value in the range $1 \leq k < n$.

$$\text{Radical addition: } \mathrm{C}_n{}^{\cdot} + 1\text{–Alkene} \rightarrow \mathrm{C}_{n+}{}^{\cdot} \tag{5.11}$$

The free radicals generated in the initiation step (with either thermal or radiation origin) have the ability to propagate through a series of chain development reactions. Each active radical can serve as the starting point for hundreds or thousands of consecutive reactions. In other words, the final result of a series of chain reactions is substantially dominated by the products of the chain propagation step. The dominating reactions of the propagation step (in hydrocarbon cracking chain reactions) exhibit an endothermic nature. It means that they require an activation energy to develop further in favor of generating lighter species.

- Termination

$$\mathrm{X}^{\cdot} + \mathrm{Y}^{\cdot} \rightarrow \mathrm{XY} \tag{5.12}$$

Where $\mathrm{X}^{\cdot}$ and $\mathrm{Y}^{\cdot}$ can be any of the radical species formed during the initiation or propagation steps.

Now, let us consider four different scenarios, low temperature ($T \leq 270°\mathrm{C}$) and high temperature ($T \geq 380°\mathrm{C}$) thermal and radiation thermal cracking. When working at low temperatures, as the required activation energy for chain development is not supplied, the chain reaction stays abortive. The free radicals, generated either

through thermal or radiolytic processes, will not take part in cracking reactions. However, high energy radicals will stabilize through the formation of heavier species in polymerization reactions. The higher the concentration of the reactive free radical, the more probable the formation of polymerization products would be. Consequently, higher degrees of polymerization occur in RTC as electron irradiation intensifies the formation of reactive free radicals. This is reflected in the higher viscosity of RTC products at lower reaction temperatures. On the other hand, when the temperature goes above a threshold, it provokes endothermic reactions, activating the chain propagation step. Eventually, hydrocarbon cracking will happen as a result of a chain process. As mentioned earlier, chain propagation plays an important role in composition distribution of the final product and is fed by the reactive free radicals created during the initiation step. The higher concentration of free radicals in the RTC case provides the essential requirements for an intensified cracking process when compared to the TC case.

5.4.2 Irradiation dose

Irradiation dose is one of the most important factors affecting the results of radiation thermal cracking that can be viewed from two different standpoints. First, knowing the relationship between irradiation dose and experiment throughput, we are able to determine the best operating conditions with the highest output. Second, it is obvious that delivering more energy—in the form of irradiated dose—causes higher operation costs. Hence, there should be a balance between the process outcome and the energy expense for that outcome. This section is aimed to investigate the effect of absorbed dose on radiation throughput. To do so, we have irradiated DAO samples at two different absorbed doses (10 and 20 kGy). As the electron generation machine operates at a constant energy rate, the duration of experiments varies depending on the absorbed energy values (1 hour for 10 kGy and 2 hours for 20 kGy) and the amount of thermal energy delivered to each sample differs for the two irradiation

tests. Consequently, we are not able to compare directly the RTC products with different absorbed dose values. Alternatively, to be able to evaluate the effect of irradiation dose on radiolysis throughput, we have used relative viscosity reduction (RVR) as a way to evaluate the viscosity reduction achieved by ionizing irradiation (Equation 5.4). The results of different irradiation doses are shown in Table 5.4.

$$\text{RVR} = \frac{\mu_{TC} - \mu_{RTC}}{\mu_{TC}} \times 100 \tag{5.4}$$

Table 5.4: Higher absorbed doses provide more intensified cracking (RVR is calculated at 20°C)

Irradiated dose, kGy	RVR, %
10	30.04
20	56.37

From Table 5.4, it is apparent that increasing irradiation dose from 10 kGy to 20 kGy will substantially improve the viscosity reduction. However, to study the radiolytic behavior of heavy petroleum samples and the effect of absorbed dose more extensively, we need to perform more experiments. The viscosity enhancement may follow a linear trend with the absorbed dose (Fig. 5.21a), or higher absorbed doses may further intensify the cracking process, increasing the slope of the RVR curve (Fig. 5.21b). On the contrary, as reported by some authors [8], the effect of irradiated dose may come to saturation after a specific amount of absorbed energy and higher doses will just increase operating costs (Fig. 5.21c).

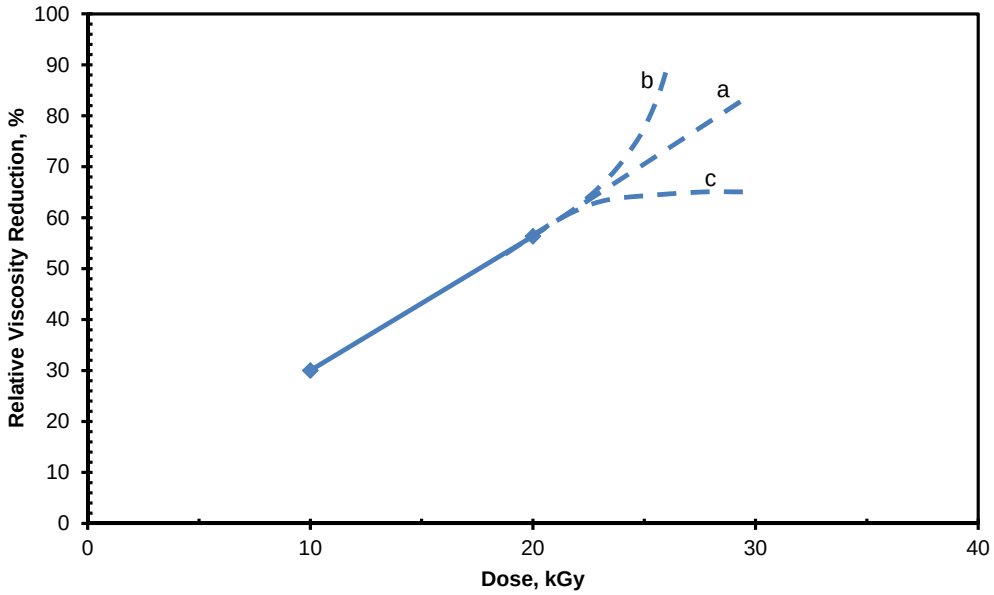

Fig. 5.21.: RVR may increase linearly with absorbed dose values (a), follow a concave curve (b), or come to saturation at a specific amount of absorbed energy (c)

5.4.3 Additives

The following section investigates the impact of different additives, with distinct chemical characteristics, on thermal and radiation thermal cracking of heavy deasphalted oil. The duration of experiments was 2 hours and the amount of 20 kGy energy was delivered to the fluids. In this study, ethanol and butanol (as alcohols), glycerol (as a polyol), and tetralin (as a hydroaromatic) are used as additives and were added to the DAO sample with the ratio of 1:59. Table 5.5 provides the viscosity of TC and RTC samples in mixture with different additives.

Table 5.5: Viscosity values of the DAO fluid in mixture with different additives

Additive	μ at 20°C (cp)		μ at 30°C (cp)	
	RTC	TC	RTC	TC
Tetralin	4042±30	5260±35	1484±10	1860±15
Butanol	4287±30	5648±35	1534±10	2012±15
Glycerol	4416±30	4451±30	1606±10	1606±10
Ethanol	3662±30	5210±35	1363±10	1855±15

Except for glycerol, radiation is observed to decrease the viscosity of DAO fluids. The RTC and TC experiments have the lowest viscosities when ethanol is used as the additive. The interesting part of the graphs refers to the glycerol experiments, where the viscosity of RTC and TC products take very similar values. In this study, additives are aimed to play an active role in chain propagation reactions by providing the necessary components of an effective upgrading. However, compared to the other additives, glycerol is observed to interfere with the radiolysis process. In fact, the presence of even a small portion of glycerol suppresses radiation–induced reactions. Fig 5.22 represents the viscosity of RTC and TC products at 20°C. Note that because of the lighter nature of the additives in comparison to the DAO fluid, the ultimate reaction temperature of RTC and TC experiments in mixtures fell in the range of medium–temperature reactions (300°C). To compare these results with that of the original DAO irradiation, we have interpolated the viscosity values of the irradiated DAO at 300°C, using Figure 5.18, and labeled the results as the "no additive" case. According to the graph, the viscosity of the RTC products with additives is lower than the no additive case. However, it can be seen that additives reduce the viscosity for both TC and RTC cases. In other words, when using additives, cracking chain–reactions become activated even at lower reaction temperatures; consequently, both TC and RTC treatments result in samples with lower viscosity values at the reaction

temperature of 300°C. Note that at the same reaction temperature, chain reactions are not activated for the no additive case.

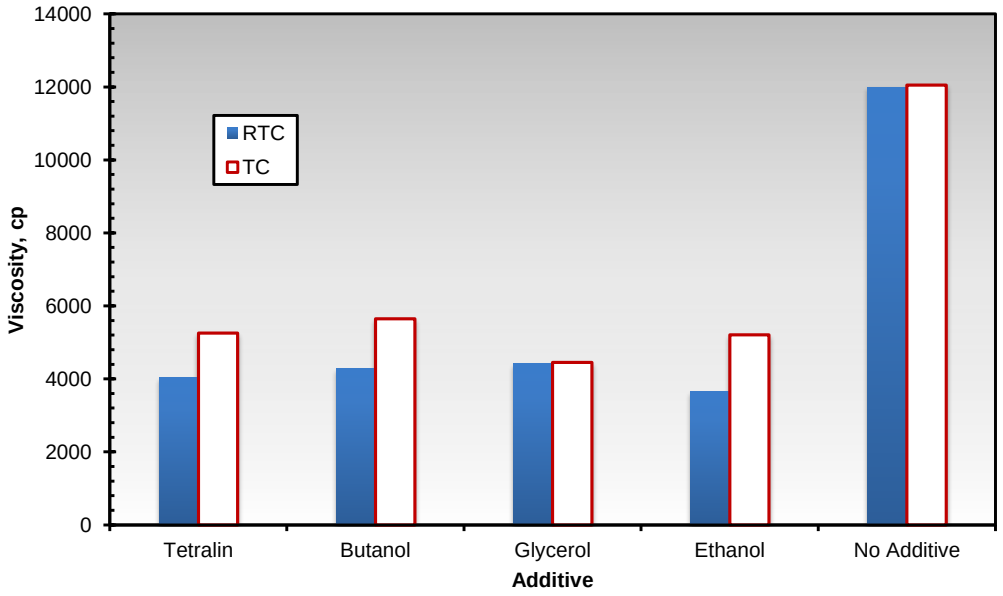

Fig. 5.22.: The viscosity of RTC and TC experiments in the presence of additives is way lower than the no additive case

Although distinctive, the viscosities of the additive experiments are not substantially different, especially for tetralin, butanol, and glycerol. This may lead to a belief that these additives offer the same contribution to the radiation–induced chain reactions, when being exposed to ionizing particles. To better investigate the differences, Figure 5.23 represents the relative viscosity reduction (Equation 5.4) for the different scenarios. Note that the RTC results reflect the contribution of the thermal and irradiation components to the upgrading process. Using RVR, the contribution of the thermal cracking to the fluid viscosity reduction is ruled out, so we can better discuss the effectiveness of the ionizing particles in the presence of different addi-

tives. Figure 5.23 indicates that the contribution of ethanol, butanol, and tetralin to the radiolysis process is similar (around 25% viscosity reduction is achieved when irradiation is coupled to thermal treatment).

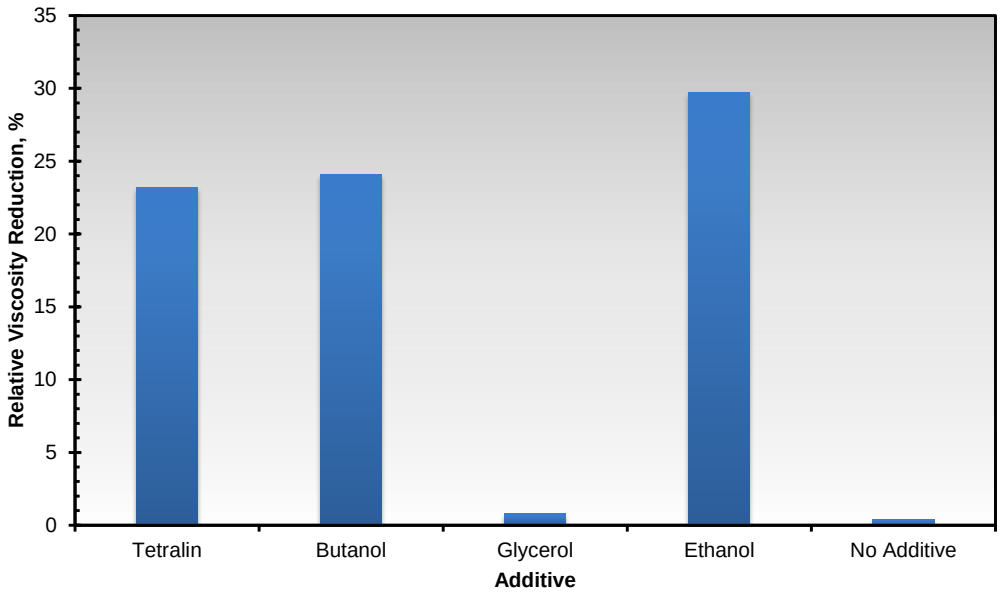

Fig. 5.23.: Ethanol, tetralin, and butanol show similar RVR factors while glycerol neutralizes the effect of ionizing particles and keeps the level of radiation–induced upgrading down

As mentioned earlier, RTC and TC experiments show comparable viscosity values in the presence of glycerol. In fact, the entire viscosity reduction for the irradiated glycerol samples is achieved by the thermal component in the RTC experiment. Similarly, RTC and TC products of the no additive case take comparable viscosity values. However, the nature of the observed behavior is different for these two cases. The low viscosity of the TC product in the glycerol case is evaluated as activated thermal cracking for this mixture at the reaction temperature of 300°C. So, the sim-

ilar viscosities of RTC and TC products show that glycerol neutralizes the effect of high energy ionizing particles, suppressing the radiation–derived cracking reactions (these radiation–induced processes are known as intensifiers in chain reactions). On the other hand, higher viscosity values for both TC and RTC products in the no additive case are interpreted as inactive cracking chain–reactions at this temperature. In fact, ionizing particles can generate highly reactive radical species but these components are not capable of carrying out the chain processes.

5.5 Aging Effects

One of the most important purposes of this study is to investigate the effect of a potential heavy oil upgrading and visbreaking technique on the rheological properties of heavy petroleum fluids. To come up with an affordable solution for the viscous fluid transportation problems, the stability of the products with time should be taken under consideration. Thus, a successful upgrading scenario has two different phases. The first part refers to the moment of upgrading and the throughput of the process (it has been already discussed in previous sections); the second part corresponds to the time after upgrading and probable changes. To find out the aging effects of each treatment scenario, the viscosity of the samples was measured at different time intervals until 120 days from the experiments. Note that all the samples were kept at same environmental conditions. According to Figure 5.24, RTC and TC products of the DAO fluid show a stable trend without any viscosity alteration with time indicating that no further reaction takes place in the samples. Figure 5.24 depicts also the viscosity alteration of AR samples with time. The time–stable nature of the RTC product is reflected in its steady viscosity trend. This indicates the successfulness of radiation–induced cracking as a heavy oil treatment method. In contrast, the viscosity of TC samples exhibit unstable characteristics with time; it increases at the beginning and ends up in a plateau. To be able to explain the observed behavior, we should consider both DAO and AR fluids together. As we can see from Figure

5.24, RTC products (either DAO or AR, regardless of the fluid characteristics) show a promising product stability. However, the results of TC products depend on the nature of the irradiated fluid. While the DAO samples are stable, the viscosity of the AR fluid increases with time substantially (90% increase). The difference in the characteristics of two heavy petroleum fluids gives a clue about this behavior. As mentioned earlier, the DAO fluid is a stream of the AR produced by sending the feed through a pilot scale solvent deasphalting unit. So, the explanation for this kind of response correlates to the asphaltene molecules in the AR liquid.

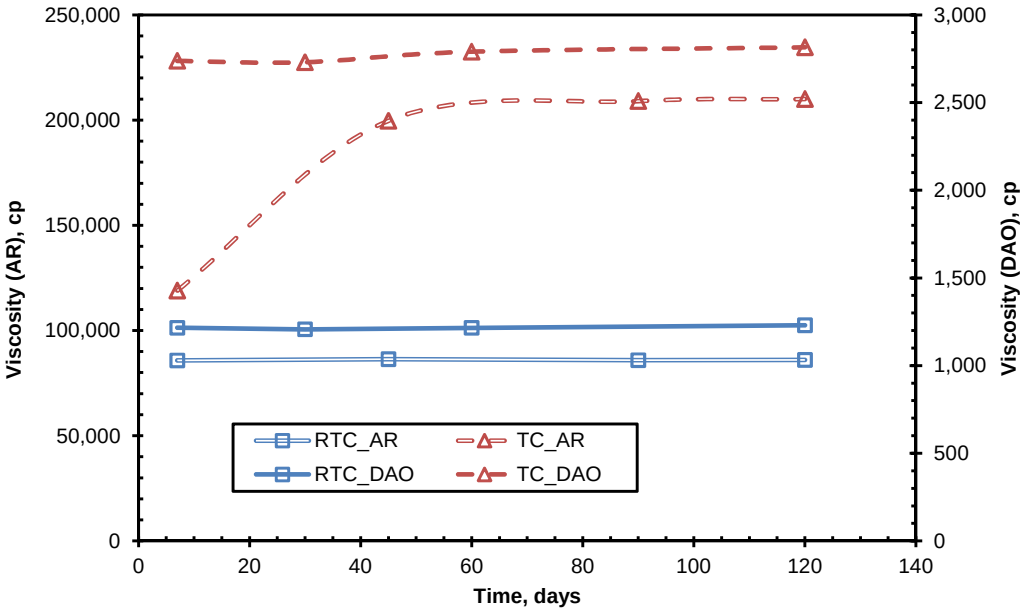

Fig. 5.24.: RTC products exhibit a time–stable nature regardless of the type of the irradiated fluid, however, TC products show an unstable nature for the fluids with a high asphaltene content

A hypothesis to explain this behavior takes into account the structure of asphaltene aggregates as well as the effect of ionizing irradiation. The asphaltene structure

consists of two dimensional fabrics of condensed aromatics, combined in a 3D network [128–130]. The number of rings in a single asphaltene fused ring system has been an area of uncertainty with early estimated ranging from a few rings to 20 [131]. However, the structure of a individual molecules strongly depends of the origin and thermodynamical conditions at which the molecules have been formed. A descriptive framework can be developed that accounts for, and is consistent with, a large body of the works. It suggests a "like your hand" structure for asphaltene molecules, composed of a single fused aromatic core and peripheral alicyclic and alkane substituents [132]. Note that different heteroatoms such as sulfur, nitrogen, and oxygen play an indispensable role in asphaltene molecule structure. Figure 5.25 provides a postulated molecular structure of the asphaltene molecule, proposed for the residue of a Venezuelan crude.

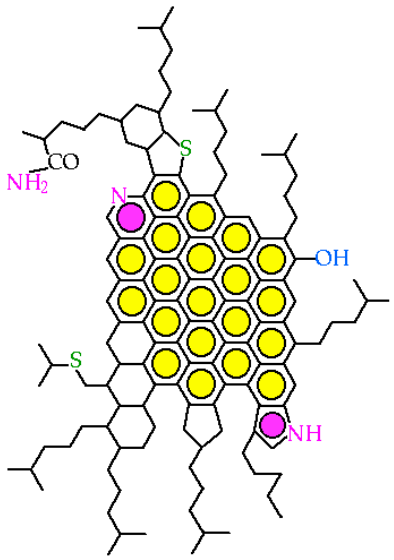

Fig. 5.25.: Postulated molecular structure of a single asphaltene molecule, proposed for the residue of a Venezuelan crude [133]

Taking one step ahead, individual layers of hydrocarbons, mainly composed of aromatic molecules, join together to form unit cells (aggregates) that can further grow into larger associations of nuclei (Fig 5.26). Vander Waals, columbic, and repulsive interactions are the dominant intermolecular forces, keeping the integrity of the structure [134].

The results of studies on radiolysis of aromatic components demonstrate the protection effects of aromatics and hydroaromatics in mixtures with other hydrocarbons [37, 82, 83]. In the presence of aromatic components, (with lower excitation and ionization potentials), protection occurs either through charge scavenging by the aromatics (Equation 5.13) or energy transfer to the aromatics (Equation 5.14). As a result, the aromatic components may undergo further degradation. This additional step is proposed to be responsible for the distinct distribution of gas products and light liquid components in RTC and TC products of atmospheric residuum (section 5.3.3), as well as smaller sizes of aromatic aggregates in the RTC samples compared to the TC samples.

$$C_n^+ + A \rightarrow C_n + A^+ \tag{5.13}$$

$$C_n^* + A \rightarrow C_n + A^* \tag{5.14}$$

Where C_n^+ stands for positive hydrocarbon ions, C_n^* represents excited hydrocarbons, and A is aromatic molecule.

Both TC and RTC treatments of heavy asphaltic fluids deliver energy to the asphaltene aggregates, breaking them into lighter units. However, ionizing particles intensify decomposition of asphaltene aggregates in favor of smaller units. After the experiments, depending on the size of the aromatic units, intermolecular forces may be able to bring the molecules together and reform larger asphaltene aggregates. Because of the larger size of the aromatic units in the TC fluid, attractive forces are strong enough to aggregate them into larger structures. Consequently, the viscosity of the fluid increases with time. On the opposite side, radiation–induced degradation

of the asphaltene aggregates results in molecules of smaller sizes with weaker intermolecular forces. Unlike the TC case, attractive forces are not strong enough in RTC products to reinforce association of asphaltene molecules into larger structures with higher viscosities. Figure 5.27 represents the explained process schematically. The observed behavior introduces RTC as a reliable upgrading technique, which provides stable properties for the treated products even after a long time.

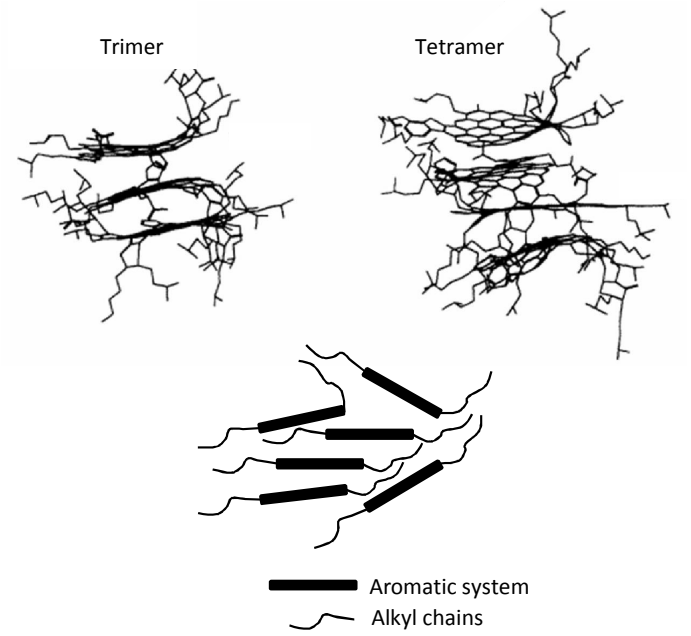

Fig. 5.26.: Proposed schematic structure of asphaltene aggregates (modified after Andreatta et al. and Rogel [132, 135])

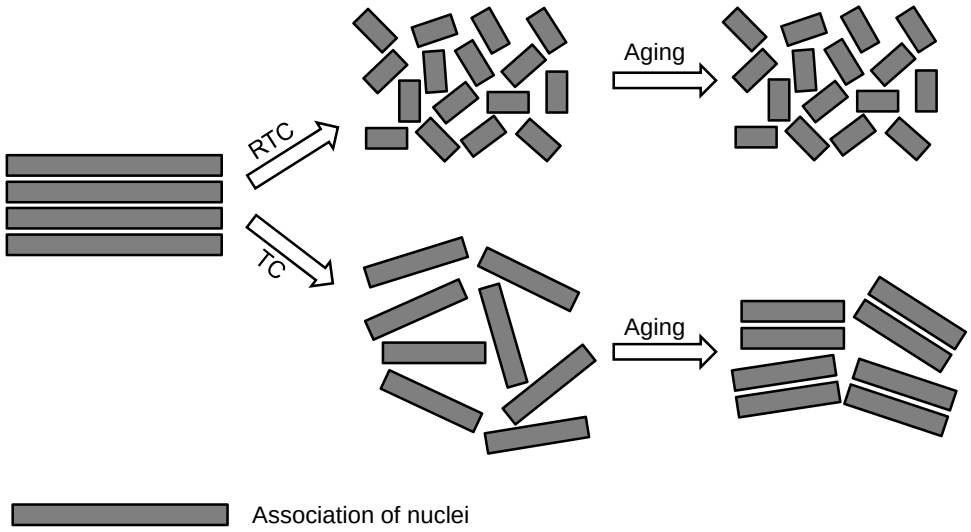

Fig. 5.27.: Smaller size of the aromatic units in the irradiated samples keeps them from aggregating into larger structures

6. CONCLUSIONS AND FUTURE WORK

The effect of accelerated electron particles on thermal treatment of heavy asphaltic and deasphalted petroleum fluids was investigated in this study. The products were analyzed by their physical and chemical properties. Viscosity and density measurements were used as indices of radiation–induced physical changes. To monitor the chemical changes due to electron irradiation, we have used GC and GC–MSD instruments. Moreover, the results of SIMDIS analysis helped us to evaluated composition distribution of RTC and TC products. Combining the analysis of physical and chemical changes, we are able to objectively judge the mechanism of radiolysis reactions and the effect of petroleum composition on radiolysis throughput.

Radiation–induced reactions of heavy deasphalted samples show that high energy particles intensify the cracking process. In fact, charged particles improve the upgrading process in favor of low–viscous samples. However, the samples exhibit comparable densities. Reinforced cracking is also reflected in the results of SIMDIS analyses, where RTC products have higher concentration of light components than TC. On top of that, it was concluded, from the composition distribution of RTC and TC products, that although irradiation has improved the cracking process, the reaction pathway would not change as a result of irradiation. This was also confirmed by information earned from the analysis of the light liquid fraction and evolved gas components.

Although similar in overall trend, there are some differences in the results of heavy asphaltic fluids and deasphalted samples. Similar to the previous case, irradiation of asphaltic samples intensifies the cracking process and lowers the viscosity of the products. The mechanism of RTC and TC experiments in asphaltic samples, nevertheless, shows detectable differences that can be attributed to the fact that radiation plays an active role in degradation of aromatic structures. The results of the light liquid components also confirmed the proposed theory.

Reaction temperature and its influence on radiation output was also investigated in this study. According to the results, radiation would not be effective unless above a specific threshold temperature. In fact, radiation–induced chain reactions would be effective at sufficiently high temperatures and below that, the chain reactions would not be activated.

The experiments show that higher amounts of absorbed dose will further decrease the viscosity of the samples. However, more investigations are required to make a general conclusion. In another section, we analyzed the effect of different additives. Interestingly, glycerol was observed to cancel out the effect of radiation.

At the end, we analyzed the stability of irradiated and unirradiated samples. Regardless of the sample type, irradiated samples exhibit a time–stable nature. On the other hand, the TC products of asphaltic fluid show unstable characteristics with time. This behavior can be attributed to the aggregation of aromatic structures in favor of larger associations of nuclei.

Although this study provides great deal of information about radiation induced reactions of different hydrocarbon fluids and consequent physical and chemical changes, there are still a number of issues that should be taken into account. One of the most important factors is the irradiation facility. The Van de Graaff machine, which is used for this research, has the optimum operating condition of generating electrons of 1.35 MeV energy. However, we might be interested in finding the effect of electrons with other energies on radiolysis process to find out the best operating conditions with respect to the heavy petroleum samples. In addition to that, while the current Van de Graaff machine provides us a constant irradiation dose rate through the whole, we may want to investigate the effect of absorbed dose rate on the process. Different dose rates can provide distinct destructive effects even if the total amount of delivered energy is identical for all the cases. According to what is observed in this study, ionizing electron particles are capable of breaking asphaltene aggregates into smaller structures with lower amount of inter–molecular attractive forces. However,

to be able to better analyze the effect of ionizing incident on asphaltene structure, we should employ specific analytical tools that guarantee precision information about radiation–induced reaction of complex asphaltene structures.

REFERENCES

[1] P. Stark, K. Chew, B. Fryklund, The role of unconventional hydrocarbon resources in shaping the energy future, in: International Petroleum Technology Conference, Dubai, UAE, 4–6 December 2007.

[2] C. Pauchon, Editorial, Oil & Gas Science and Technology (2004) 453–454.

[3] P. E. Koppel, W. L. Mazurek, A. Harji, Project scenarios for bitumen upgrading, in: SPE International Thermal Operations and Heavy Oil Symposium and International Horizontal Well Technology Conference, Calgary, Canada, 4–7 November 2002.

[4] M. Gray, Upgrading Petroleum Residues and Heavy Oils, Marcell Dekker, New York, 1986.

[5] T. I. Aksenova, D. K. Daukeev, B. M. Iskakov, Y. A. Zaykin, N. R. Mazhrenova, A. S. Nurkeeva, Investigations on radiation processing in Kazakhstan, Radiation Physics and Chemistry 46 (4-6, Part 2) (1995) 1401–1404.

[6] G. Mirkin, R. F. Zaykina, Y. A. Zaykin, Radiation methods for upgrading and refining of feedstock for oil chemistry, Radiation Physics and Chemistry 67 (3-4) (2003) 311–314.

[7] R. F. Zaykina, Y. A. Zaykin, T. B. Mamonova, N. K. Nadirov, Radiation–thermal processing of high–viscous oil from Karazhanbas field, Radiation Physics and Chemistry 60 (3) (2001) 211–221.

[8] R. F. Zaykina, Y. A. Zaykin, G. Mirkin, N. K. Nadirov, Prospects for irradiation processing in the petroleum industry, Radiation Physics and Chemistry 63 (3-6) (2002) 617–620.

[9] A. V. Bludenko, A. V. Ponomarev, V. N. Chulkov, I. A. Yakushev, R. S. Yarullin, Electron–beam decomposition of bitumen–gas mixtures at high dose rates, Mendeleev Communications 17 (4) (2007) 227–229.

[10] G. B. Skripchenko, V. I. Sekrieru, N. K. Larina, Z. S. Smutkina, O. K. Miesserova, V. A. Rudoi, Action of radiation on heavy petroleum and oil products, Solid Fuel Chemistry 20 (Compendex) (1987) 54–58.

[11] F. Cataldo, Y. Keheyan, S. Baccaro, The effect of gamma–irradiation of anthracite coal and oil bitumen, Journal of Radioanalytical and Nuclear Chemistry 262 (2) (2004) 443–450.

[12] Y. A. Zaykin, R. F. Zaykina, Stimulation of radiation–thermal cracking reactive ozone–containing mixtures, Radiation Physics and Chemistry 71 (1-2) (2004) 475–478.

[13] F. Cataldo, Y. Keheyan, S. Baccaro, Gamma radiolysis of a heavy petroleum fraction, Journal of Radioanalytical and Nuclear Chemistry 258 (3) (2003) 537–541.

[14] D. Yang, J. Kim, P. Silva, M. A. Barrufet, R. Moreira, J. Sosa, Laboratory investigation of e–beam heavy oil upgrading, in: Latin American and Caribbean Petroleum Engineering Conference, Cartagena de Indias, Colombia, 31 May–3 June 2009.

[15] D. Yang, J. Kim, P. Silva, M. Barrufet, R. Moreira, Electron beam (e–beam) irradiation improves conventional heavy-oil upgrading, in: SPE Annual Technical Conference and Exhibition, Florence, Italy, 19–22 September 2010.

[16] Y. A. Zaykin, R. F. Zaykina, J. Silverman, Radiation–thermal conversion of paraffinic oil, Radiation Physics and Chemistry 69 (3) (2004) 229–238.

[17] G. Foldiak, Radiolysis of liquid hydrocarbons, Radiation Physics and Chemistry 16 (6) (1980) 451–463.

[18] M. Alfi, P. Da Silva, M. Barrufet, R. Moreira, Utilization of charged particles as an efficient way to improve rheological properties of heavy asphaltic petroleum fluids, in: SPE Latin America and the Caribbean Petroleum Engineering Conference, Mexico City, Mexico, 16–18 April 2012.

[19] M. Alfi, P. Da Silva, M. Barrufet, R. Moreira, Electron induced chain reactions of heavy petroleum fluids–effective parameters, in: SPE Heavy Oil Conference, Calgary, Canada, 12–14 June 2012.

[20] G. Skripchenko, G. Golovin, V. Sekrieru, Effect of gamma–radiation on structure, reactivity and process of liquefaction of brown coals, Coal science : Proceedings of the Eighth International Conference on Coal Science 2 (1995) 1379–1387.

[21] P. N. Kuznetsov, L. I. Kuznetsova, Y. V. Obukhov, N. K. Kuksanov, Studies on the effect of irradiation by accelerated electrons on the hydrogenation reactivity of brown coal, Fuel 80 (15) (2001) 2203–2206.

[22] P. N. Kuznetsov, N. K. Kuksanov, L. I. Kuznetsova, Effect of irradiation by an accelerated electron beam on the reactivity of brown coal for conversion into low molecular products, Vacuum 62 (2-3) (2001) 247–250.

[23] K. Ouchi, Y. Kawana, T. Masuda, N. Yuki, S. Toyoda, Y. Sanada, K. Yamaguchi, Y. Yoshida, H. Honda, Effect of cobalt–60 gamma radiation on coals. I. analysis of decomposition gases (1963).

[24] H. Mitsui, Y. Shimizu, Radiation–thermal cracking of coal, Radiation Physics and Chemistry 18 (3-4) (1981) 817–826.

[25] K. Ouchi, Y. Kawana, T. Masuda, N. Yuki, S. Toyoda, Y. Sanada, K. Yamaguchi, Y. Yoshida, H. Honda, Effect of cobalt–60 gamma radiation on coals. II. changes in physical and chemical properties, Fuel (England) 42 (1963) 105–112.

[26] I. Mustafaev, L. Jabbarova, K. Yagubov, N. Gulieva, Radiation–thermal refining of oil–bituminous rocks, Journal of Radioanalytical and Nuclear Chemistry 262 (2) (2004) 509–511.

[27] M. W. Haenel, U. B. Richter, S. Solar, N. Getoff, On the possibility of coal degradation by ionizing radiation: radiation–induced C–C bond cleavage in 1,2 diarylenthanes as model compounds of coal, Coal science : Proceedings of the Eighth International Conference on Coal Science 1 (1995) 445–449.

[28] G. Wu, Y. Katsumura, C. Matsuura, K. Ishigure, J. Kubo, Comparison of liquid–phase and gas–phase pure thermal cracking of n–hexadecane, Industrial & Engineering Chemistry Research 35 (12) (1996) 4747–4754.

[29] G. Wu, Y. Katsumura, C. Matsuura, K. Ishigure, J. Kubo, Radiation effect on the thermal cracking of n–hexadecane. 1. products from radiation–thermal cracking, Industrial & Engineering Chemistry Research 36 (Compendex) (1997) 1973–1978.

[30] G. Wu, Y. Katsumura, C. Matsuura, K. Ishigure, J. Kubo, Radiation effect on the thermal cracking of n–hexadecane. 2. a kinetic approach to chain reaction, Industrial & Engineering Chemistry Research 36 (9) (1997) 3498–3504.

[31] V. A. Tyshchenko, Chemistry of the radiation effect on hydrocarbon media, Chemistry and Technology of Fuels and Oils 39 (3) (2003) 145–147.

[32] J. P. Manion, M. Burton, Radiolysis of hydrocarbon mixtures, The Journal of Physical Chemistry 56 (5) (1952) 560–569.

[33] A. V. Topchiev, K. P. Lavrovsky, L. S. Polack, A. M. Brodsky, Y. A. Kolbanovsky, Studies in radiation chemistry of petroleum hydrocarbons and applications of radiation to petroleum industry and petrochemical synthesis, in: Proceedings of the Fifth World Petroleum Congress, Jun 1959, World Petroleum Congress – Proceedings, 1959, pp. 121–129.

[34] R. Salovey, W. E. Falconer, Radiation–induced reactions in n–hexadecane, The Journal of Physical Chemistry 69 (7) (1965) 2345–2350.

[35] A. V. Topchiev, Radiolysis of Hydrocarbons, Elsevier Publishing Co., Amesterdam, 1964.

[36] G. M. Panchenkov, A. V. Purilov, G. I. Zhuravlev, D. P. Shcherbakov, S. V. Sal'tsov, Study of the basic principles of radiation–thermal cracking of n–hexadecane, High Energy Chemistry 15 (5) (1981) 331–334.

[37] Y. S. Soebianto, T. Yamaguchi, Y. Katsumura, K. Ishigure, J. Kubo, T. Koizumi, Protection in radiolysis of n–hexadecane–1. radiolysis of pure liquid n–hexadecane, International Journal of Radiation Applications and Instrumentation. Part C. Radiation Physics and Chemistry 39 (3) (1992) 251–256.

[38] W. E. Falconer, R. Salovey, Comparison of radical and nonradical processes in the condensed–phase radiolysis of n–hexadecane, J. Chem. Phys. 44 (9).

[39] A. V. Topchiev, L. S. Polak, V. Y. Glushnev, G. G. Popov, e. al., Radiation–thermal cracking of petroleum hydrocarbons, Neftekhimiya 2 (2) (1962) 196–210.

[40] I. Santar, Primary yields in hydrocarbons: Basic information for understanding the radiolytic mechanisms, in: Symposium on the Mechanisms of of Hydrocarbon Reactions, 5-7 June, 1973, Hungary, 1973, p. 65.

[41] S. J. Rzad, P. P. Infelta, J. M. Warman, R. H. Schuler, Kinetics of electron scavenging and ion recombination in the radiolysis of hydrocarbon solutions, Journal of Chemical Physics 52 (1970) 3971–83.

[42] Y. A. Zaikin, R. F. Zaikina, W. J. Chappas, Effect of electron beam pulse characteristics on the rate of radiation–thermal cracking of petroleum feedstock, in: 8th International Topical Meeting on Nuclear Applications and Utilization of Accelerators, July 29–August 2, 2007, pp. 701–707.

[43] A. D. Trifunac, M. C. Sauer, I. A. Shkrob, D. W. Werst, Radical cations in radiation chemistry of liquid hydrocarbons, Acta Chemica Scandinavica 51 (1997) 158–166.

[44] G. I. Zhuravlev, S. V. Voznesenskaya, I. V. Borisenko, L. A. Bilap, Radiothermal effect on heavy crude–oil residues, High Energy Chemistry 25 (1) (1991) 20–23.

[45] Y. A. Zaikin, R. F. Zaikina, Effect of radiation–induced isomerization on gasoline upgrading, in: 8th International Topical Meeting on Nuclear Applications and Utilization of Accelerators, July 29, 2007 - August 2, 2007, pp. 993–998.

[46] A. V. Topchiev, L. S. Polak, K. P. Lavrovsky, A. M. Brodsky, et al., Radiative-Thermal cracking of petroleum hydrocarbons, in: Proceedings of the 6th World Petroleum Congress on Base Stocks from Petroleum and Natural Gas for Chemical Industry, 1963, World Petroleum Congress – Proceedings, 1963, pp. 75–89.

[47] M. M. Melikzade, K. M. Yakubov, N. M. Alieva, Combined influence of gamma-radiation and temperature on hydrocarbon composition of cuts from secondary processing of petroleum feedstock, Chemistry and Technology of Fuels and Oils 13 (9-10) (1977) 707–708.

[48] I. V. Il'gisonis, A. N. Koldashov, M. V. Sal'nikov, Experimental plant for radiation–thermal cracking of hydrocarbons, Atomic Energy 23 (5) (1967) 1229–1230.

[49] A. Brodskii, N. Zvonov, K. Lavrovskii, V. Titov, Radiation thermal conversion of petroleum fractions, Neftekhimiya (U.S.S.R.) 1 (1961) 370–381.

[50] J. G. Carroll, R. O. Bolt, J. A. Bert, A survaey of the radical stability of hydrocabon fuels, Aeronautical Engineering Review 17 (3) (1958) 61–65.

[51] M. F. Hoare, T. A. Garbett, R. E. Pegg, The effect of gamma radiation on the thermal decomposition of light paraffinic hydrocarbons (1959).

[52] G. Foldiak, Z. Horvath, Radiation–chemistry of saturated–unsaturated hydrocarbon systems .5. liquid–phase gamma–radiolysis of C3–hydrocarbons, Acta Chimica Academiae Scientarium Hungaricae 86 (4) (1975) 385–396.

[53] Z. Horvath, G. Foldiak, Radiation–chemistry of saturated–unsaturated hydrocarbon systems .6. liquid–phase gamma–radiolysis of C4–hydrocarbons, Acta Chimica Academiae Scientarium Hungaricae 86 (4) (1975) 397–411.

[54] A. V. Ponomarev, I. E. Makarov, N. R. Saifullin, A. S. Syrtlanov, A. K. Pikaev, Electron–beam radiolysis of gaseous propane in the presence of water under circulation conditions, Radiation Physics and Chemistry 65 (1) (2002) 71–78.

[55] A. V. Ponomarev, I. E. Makarov, A. K. Pikaev, N. R. Saifullin, A. S. Syrtlanov, The formation of oxygen–containing compounds upon radiolysis of gaseous propane under circulation conditions in the presence of water, Doklady Physical Chemistry 381 (1) (2001) 267–270.

[56] A. V. Ponomarev, Electron–beam radiolysis of gaseous alkanes under circulation conditions: Gas–to–liquid transformation, Radiation Physics and Chemistry 78 (1) (2009) 48–56.

[57] F. Lampe, Irradiation reactions in hydrocarbon gases, Nucleonics 18 (4) (1960) 60–65.

[58] A. Ponomarev, A. Tsivadze, Gas–to–liquid conversion of alkanes by electron beam radiolysis, Doklady Physical Chemistry 411 (2) (2006) 345–351.

[59] I. Makarov, A. Ponomarev, B. Ershov, Radiation–induced synthesis of branched liquid alkanes, High Energy Chemistry 41 (2) (2007) 55–60.

[60] A. V. Ponomarev, A. S. Syrtlanov, A. K. Pikaev, Condensable products of radiolysis of multicomponent mixtures of gaseous alkanes, Doklady Physical Chemistry 372 (1-3) (2000) 68–71.

[61] G. W. Crawford, J. F. O'Briant, Effect of gamma radiation on pure hydrocarbons: Methane, Texas Petroleum Research Committee–Oil Recovery Conference–Proceedings (1958) 189–198.

[62] V. A. Potanina, L. G. Zherdeva, V. A. Gorbatch, A. G. Siryuk, Y. S. Zaslavskii, T. P. Ponomareva, N. A. Smirnyagina, Effect of ionizing radiation on naphthenic hydrocarbon in lubricating oils, Chemistry and Technology of Fuels and Oils 12 (1976) 752–758.

[63] V. A. Potanina, V. A. Gorbach, A. G. Siryuk, Y. S. Zaslavskii, T. P. Ponomareva, Effect of ionizing radiation on aromatic hydrocarbons in lubricating oils, Chemistry and Technology of Fuels and Oils 15 (1977) 558–562.

[64] R. F. Zaykina, Y. A. Zaykin, Radiation technologies for production and regeneration of motor fuel and lubricants, Radiation Physics and Chemistry 65 (Compendex) (2002) 169–172.

[65] M. A. Scapin, C. Duarte, M. H. O. Sampa, I. M. Sato, Recycling of the used automotive lubricating oil by ionizing radiation process, Radiation Physics and Chemistry 76 (11-12) (2007) 1899–1902.

[66] A. Chapiro, Radiation Effects in Polymers, Elsevier, Oxford, 2004, pp. 1–8.

[67] A. A. Miller, E. J. Lawton, J. S. Balwit, The radiation chemistry of hydrocarbon polymers–polyethylene, polymethylene and octacosane, Journal of Physical Chemistry 60 (5) (1956) 599–604.

[68] T. F. Williams, Modes of radiation–induced cross–linking in hydrocarbon polymers, Nature 186 (4724) (1960) 544–545.

[69] Y. Okada, Irradiation of Hydrocarbon Polymers in Nitrous Oxide Atmosphere, Advances in Chemistry, AMERICAN CHEMICAL SOCIETY, WASHINGTON, D.C., 1967, pp. 44–56.

[70] H. Mohan, R. M. Iyer, Gamma–radiation induced polymerization of methyl–methacrylate in aliphatic–hydrocarbons–kinetics and evidence for incorporation of hydrocarbon in the polymer–chain, Radiation Physics and Chemistry 34 (5) (1989) 829–837.

[71] K. Ema, Y. Izumi, Y. Kawakami, T. Yamamoto, Effect of atmospheric hydrogen on the radiation–induced gas evolution from polybutadiene, International Journal of Radiation Applications and Instrumentation. Part C. Radiation Physics and Chemistry 38 (3) (1991) 339–342.

[72] Y. Tabata, Cross-Linking of Hydrocarbon Polymers and Their Model Compounds, ACS Symposium Series, American Chemical Society, Washington, DC, 1991, pp. 31–43.

[73] T. Czvikovszky, Degradation effects in polymers, in: Advances in radiation chemistry of polymers, Notre Dame, Indiana, USA, 2003, pp. 91–102.

[74] O. Gueven, An overview of current developments in applied radiation chemistry of polymers, in: Advances in radiation chemistry of polymers, Notre Dame, Indiana, USA, 2003, pp. 33–39.

[75] B. W. Hutzler, L. D. B. Machado, A. B. Lugao, A. Villavicencio, Properties of irradiated PVC plasticized with non–endocrine disruptor, Radiation Physics and Chemistry 57 (3-6) (2000) 381–384.

[76] J. Kubo, K. Otsuhata, Inhibition of radiation degradation of polyolefins by hydroaromatics, Radiation Physics and Chemistry 39 (Compendex) (1992) 261–268.

[77] E. J. Lawton, A. M. Bueche, J. S. Balwit, Irradiation of polymers by high-energy electrons, Nature 172 (4367) (1953) 76–77.

[78] L. Sanche, Irradiation of organic and polymer films with low-energy electrons, Nuclear Instruments and Methods in Physics Research Section B: Beam Interactions with Materials and Atoms 208 (2003) 4–10.

[79] N. I. Alekhina, S. Z. Levinson, S. V. Voznesenskaya, N. I. Kuritsina, N. S. Oreshkova, L. O. Kogan, Radiational–thermal stability of hydrocarbons of aromatic oil obtained by adsorptive treatment, Chemistry and Technology of Fuels and Oils 23 (1987) 241–244.

[80] D.-H. Han, T. Stuchinskaya, Y.-S. Won, W.-S. Park, J.-K. Lim, Oxidative decomposition of aromatic hydrocarbons by electron beam irradiation, Radiation Physics and Chemistry 67 (2003) 51–60.

[81] B. Y. Chung, J. Y. Cho, C. H. Song, B. J. Park, Degradation of naturally contaminated polycyclic aromatic hydrocarbons in municipal sewage sludge by electron beam irradiation, Bulletin of Environmental Contamination and Toxicology 81 (2008) 7–11.

[82] Y. S. Soebianto, Y. Katsumura, K. Ishigure, J. Kubo, T. Koizumi, Protection in radiolysis of n–hexadecane–2. radiolysis of n–hexadecane in the presence of additives, International Journal of Radiation Applications and Instrumentation. Part C. Radiation Physics and Chemistry 40 (6) (1992) 451–459.

[83] S. Tabuse, Y. Izumi, T. Kojima, Y. Yoshida, T. Kozawa, M. Miki, S. Tagawa, Radiation protection effects by addition of aromatic compounds to n-dodecane, Radiation Physics and Chemistry 62 (1) (2001) 179–187.

[84] J. Kubo, New functional material produced from petroleum, Erdol & Kohle Erdgas Petrochemie 46 (10) (1993) 360–365.

[85] J. Kubo, Radical scavengers from heavy hydrocarbons, CHEMTECH 26 (1996) 29–34.

[86] J. G. Speight, The Desulfurization of Heavy Oils and Residua, Marcel Dekker, Inc., New York, 1999.

[87] R. F. Zaykina, Y. A. Zaykin, T. B. Mamonova, N. K. Nadirov, Radiation methods for demercaptanization and desulfurization of oil products, Radiation Physics and Chemistry 63 (3-6) (2002) 621–624.

[88] S. Farooq, C. N. Kurucz, T. D. Waite, W. J. Cooper, S. R. Mane, J. H. Greenfield, Waste treatment, Wat. Sci Tech. 26 (5-6) (1992) 1265–1274.

[89] A. G. Chmielewski, J. Licki, Application of electron beam from accelerator to purification of exhaust gases from combustion of high–sulphur fossil fuels, Environment Protection Engineering 34 (2008) 51–59.

[90] M. F. Ali, S. Abbas, A review of methods for the demetallization of residual fuel oils, Fuel Processing Technology 87 (7) (2006) 573–584.

[91] Y. A. Zaykin, R. F. Zaykina, G. Mirkin, On energetics of hydrocarbon chemical reactions by ionizing irradiation, Radiation Physics and Chemistry 67 (2003) 305–309.

[92] P. J. Lucchesi, B. L. Tarmy, R. B. Long, D. L. Baeder, J. P. Longwell, High temperature radiation chemistry of hydrocarbons, Industrial and Engineering Chemistry 50 (6) (1958) 879–884.

[93] J. Franck, E. Rabinowitsch, Some remarks about free radicals and the photochemistry of solutions, Transactions of the Faraday Society 30 (0) (1934) 120–130.

[94] P. J. Lucchesi, D. L. Baeder, J. P. Longwell, Radiation promoted hydrocarbon reactions, in: Proceedings of the Fifth World Petroleum Congress, Jun 1959, World Petroleum Congress – Proceedings, 1959, pp. 97–107.

[95] I. Mustafaev, N. Gulieva, The principles of radiation–chemical technology of refining the petroleum residues, Radiation Physics and Chemistry 46 (4-6) (1995) 1313–1316.

[96] T. Gaumann, S. Rappoport, A. Ruf, Effect of temperature in the radiolysis of paraffins, The Journal of Physical Chemistry 76 (25) (1972) 3851–3855.

[97] Y. A. Zaikin, Low–temperature radiation–induced cracking of liquid hydrocarbons, Radiation Physics and Chemistry 77 (2008) 1069–73.

[98] G. Foldiak, L. Wojnarovits, Radiation chemistry of saturated–unsaturated hydrocarbon systems, 1. processes of hydrogen formation, Acta Chimica Academiae Scientarium Hungaricae 67 (2) (1971) 209–219.

[99] L. Wojnarovits, G. Foldiak, Radiation chemistry of saturated–unsaturated hydrocarbon systems .2. hydrogen formation during radiolysis of liquid C6–C8 hydrocarbon mixtures, Acta Chimica Academiae Scientarium Hungaricae 67 (2).

[100] L. Wojnarovits, P. Fejes, Radiation chemistry of saturated–unsaturated hydrocarbon systems, 3. kinetic study of hydrogen formation, Acta Chimica Academiae Scientiarum Hungaricae 69 (1971) 177–201.

[101] G. Foldiak, L. Wojnarovits, Radiation chemistry of saturated–unsaturated hydrocarbon systems .4. effect of cyclic structure on radiation–chemical hydrogen evolution from hydrocarbons with 5 to 8 carbon atoms, Acta Chimica Academiae Scientarium Hungaricae 70 (1-2) (1971) 23–39.

[102] V. G. Plotnikov, Radiation–chemical stability of molecular systems; reactions of monomolecular detachment of hydrogen atoms and dissociative attachment of electrons, Radiation Physics and Chemistry 26 (5) (1985) 519–525.

[103] G. Wu, Y. Katsumura, H_2 evolution in hexadecane irradiated at high temperatures, Radiation Physics and Chemistry 58 (3) (2000) 267–269.

[104] R. G. Woods, A. K. Pikaev, Applied Radiation Chemistry: Radiation Processing, A Wiley-Interscience, New York, 1994.

[105] G. Foldiak, Radiation Chemistry of Hydrocarbons, Elsevier, Amesterdam, 1981.

[106] G. F. Knoll, Radiation Detection and Measurements, John Wiley, New York, 2000.

[107] F. H. Attix, Introduction to Radiological Physics and Radiation Dosimetry, John Wiley and Sons Inc., New York, 1994.

[108] J. E. Turner, Atoms, Radiation, and Radiation Protection, Pergamon Press, New York, 2007.

[109] F. A. Smith, A Primer in Applied Radiation Physics, World Scientific Publishing Co., Singapore, 1999.

[110] A. Mozumder, Fundamentals of Radiation Chemistry, Academic Press, San Diego, 2000.

[111] S. Lovell, An Introduction to Radiation Dosimetry, University Press, Cambridge, 1979.

[112] G. Shani, Radiation Dosimetry: Instrumentation and Methods, CRC Press, Boca Raton, 2001.

[113] M. Stevens, J. Turner, R. Hugtenburg, P. Butler, High–resolution dosimetry using radiochromic film and a document scanner, Physics in Medicine and Biology 11 (41) (1996) 2357–2365.

[114] E. J. Wilson, Introduction to Particle Accelerators, Oxford University Press, Oxford, 2001.

[115] S. Humphries, Principles of Charged Particle Acceleration, John Wiley, New York, 1986.

[116] D. Yang, Heavy oil upgrading from electron beam (e-beam) irradiation, Ph.D. thesis (2009).

[117] D. Boyd, Material safety data sheet, high temperature rtv red silicone gasket maker (2009).

[118] OMB–DAQ–54/55/56, USB data acquisition modules reference manual.

[119] Brookfield DV–III ultra, programmable rheometer, operating instructions.

[120] Anton Paar SVM 3000/G2, Stabinger Viscometer, reference manual.

[121] D. C. Villalanti, J. C. Raia, J. B. Maynard, High–temperature Simulated Distillation Applications in Petroleum Characterization, John Wiley & Sons, Ltd, 2006.

[122] A. D7169-11, Standard test method for boiling point distribution of samples with residues such as crude oils and atmospheric and vacuum residues by high temperature gas chromatography (2011).

[123] G. Antos, A. M. Aitani, Catalytic Naphtha Reforming, CRC Press, New York, 2004.

[124] B. M. Tolbert, R. M. Lemmon, Radiation decomposition of pure organic compounds, Radiation Research 3 (1) (1955) 52–67.

[125] M. R. Cleland, Radiation processing: basic concepts and practical aspects, Industrial Irradiation Technology 1 (3) (1983) 191–218.

[126] R. H. Schuler, Scavenger methods for free radical detection in hydrocarbon radiolysis, The Journal of Physical Chemistry 62 (1) (1958) 37–41.

[127] E. S. Huyser, Free–Radical Chain Reactions, John Wiley & Sons, Inc., New York, 1970.

[128] J. P. Dickie, T. F. Yen, Electron microscopic studies on petroeum asphaltics (September 11–16 1966).

[129] J. P. Dickie, T. F. Yen, Macrostructures of the asphaltic fractions by various instrumental methods, Analytical Chemistry 39 (14) (1967) 1847–1852.

[130] T. F. Yen, J. G. Erdman, S. S. Pollack, Investigation of the structure of petroleum asphaltenes by x–ray diffraction, Analytical Chemistry 33 (11) (1961) 1587–1594.

[131] H. Groenzin, O. C. Mullins, Molecular size and structure of asphaltenes from various sources, Energy & Fuels 14 (3) (2000) 677–684.

[132] G. Andreatta, C. C. Goncalves, G. Buffin, N. Bostrom, C. M. Quintella, F. Arteaga-Larios, E. Pérez, O. C. Mullins, Nanoaggregates and structure–function relations in asphaltenes, Energy & Fuels 19 (4) (2005) 1282–1289.

[133] G. Mansoori, Nanoscal structures of asphaltene molecule, asphaltene steric–colloid and asphaltene micells & vesiceles, tigger.uic.edu/∼mansoori/asphaltene.molecule_html (2011).

[134] J. Murgich, Intermolecular forces in aggregates of asphaltenes and resins, Petroleum Science and Technology 20 (9-10) (2002) 983–997.

[135] E. Rogel, Studies on asphaltene aggregation via computational chemistry, Colloids and Surfaces A: Physicochemical and Engineering Aspects 104 (1) (1995) 85 – 93.

[136] R. P. W. Scott, Introduction to Analytical Gas Chromatography, Marcel Dekker, Inc., New York, 1998.

[137] L. S. Ettre, Nomenclature for chromatography, Pure and Appl. Chem. 65 (4) (1993) 819–872.

APPENDIX A

VISCOSITY CALCULATION/VISCOMETER CALIBRATION

Viscosity is the measure of the internal friction of fluid. This internal friction is caused when a layer of fluid moves in relation to another layer. The greater the friction, the larger the amount of force that is required to initiate this movement. Fig. A.1 helps us to define viscosity more precisely. In this case, two parallel planes of the fluid with equal areas "A" are separated by a distance dx and are moving at different speeds V_1 and V_2. Defining the value of $\frac{dv}{dx}$ as the shear rate (it describes the shearing that the fluid experiences when the layers move with respect to each other) and $\frac{F}{A}$ as the shear stress, μ in Equation A.1 is known as the fluid viscosity.

$$\frac{F}{A} = \mu \frac{dv}{dx} \tag{A.1}$$

Therefore, we can define viscosity as $\mu = \frac{\text{Shear stress}}{\text{Shear rate}}$

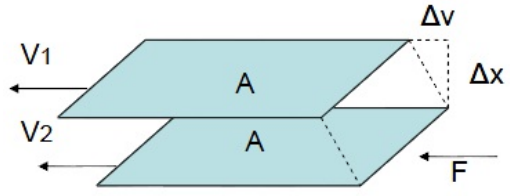

Fig. A.1.: Deformation of a liquid under the action of a tangential force

Most instruments designed to measure viscosity can be classified in two general categories: tube and rotational types (Fig. A.2). The selection of a particular instrument must be based on the type of analysis required and the characteristics of the fluid to be tested.

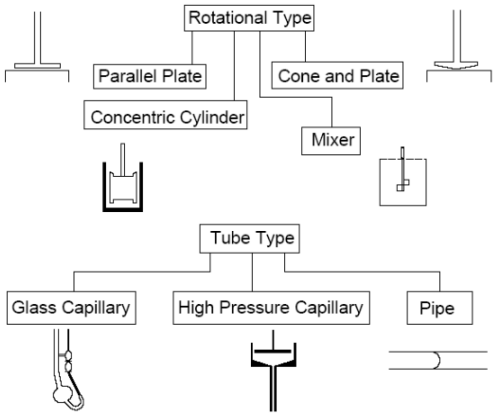

Fig. A.2.: Classification of rheological instruments

To measure the viscosity of the samples, we have used a cone and plate viscometer with a cup that contains the sample and serves as the plate and also a spindle with specific dimensions as the cone. The main advantage of this type of viscometers to the other instruments is that it requires small volumes of the fluid. Consequently, temperature adjustment and sample replacement become easier. After pouring the appropriate amount of fluid into the cup, the spindle will rotate by a shaft and the viscous drag of the fluid against the spindle is transferred through the shaft to a calibrated spring. Recording the spring deflection with a rotary transducer, the

machine is able to measure the shear stress corresponding to each specified shear rate. An appropriate selection of shear rate will result in measurements made between 10 to 100 on the instrument % torque scale. If the chosen rotation speed results in a torque reading above 100%, then either the rotation speed should decrease or a spindle with a smaller diameter must be employed. To accurately calculate the viscosity, at least seven to eight different shear stress–shear rate data points are required. Using the least square method, the best line should be fitted to the data points and the viscosity can be calculated accordingly. As the heavy petroleum samples and the irradiated hydrocarbons exhibited Newtonian fluid behavior, we can fit a straight line to the shear stress vs shear rate graph and read the slope of the line as the viscosity (Fig. A.3). If the shear stress is measured in dyne/cm^2 and the shear rate in 1/s, the slope of the line represents the viscosity in poise.

Before measuring the viscosities, the viscometers should be calibrated to assure the integrity of the measurements. To do so, we have used two calibration fluids with viscosities of 706.7 and 5313 cp and the viscosity is measured at different shear rates. The points were then plugged into special graphs provided by the manufacturer (Fig. A.4 and A.5). According to the graphs, it is apparent that the viscometer provides quite reliable measurements.

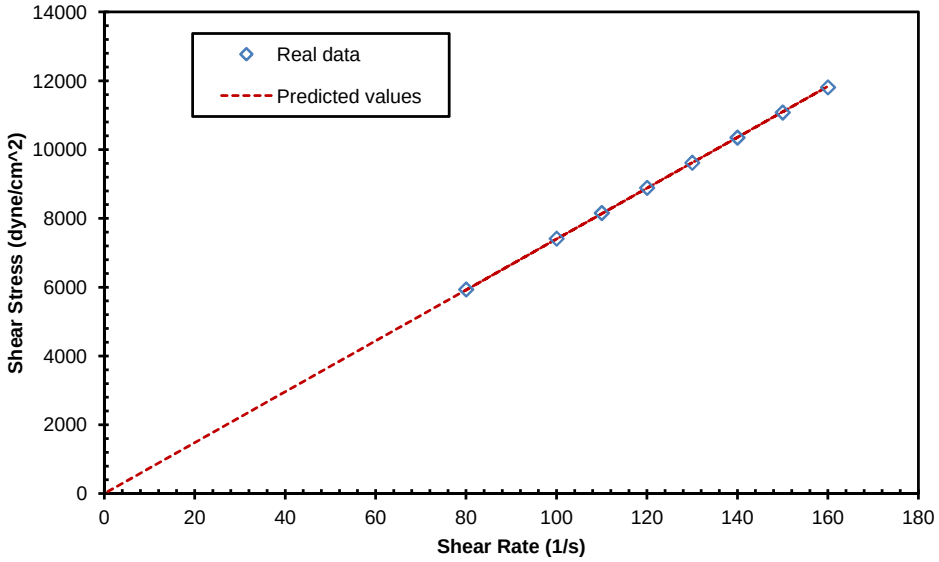

Fig. A.3.: Viscosity calculation example

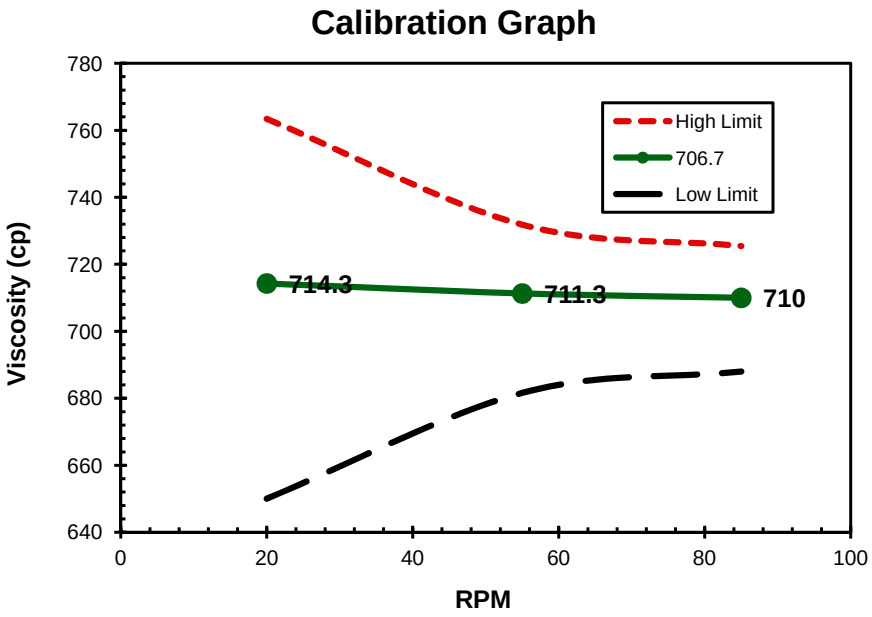

Fig. A.4.: Viscometer calibration graphs show that the viscometer provides promising measurements for low viscosity fluids

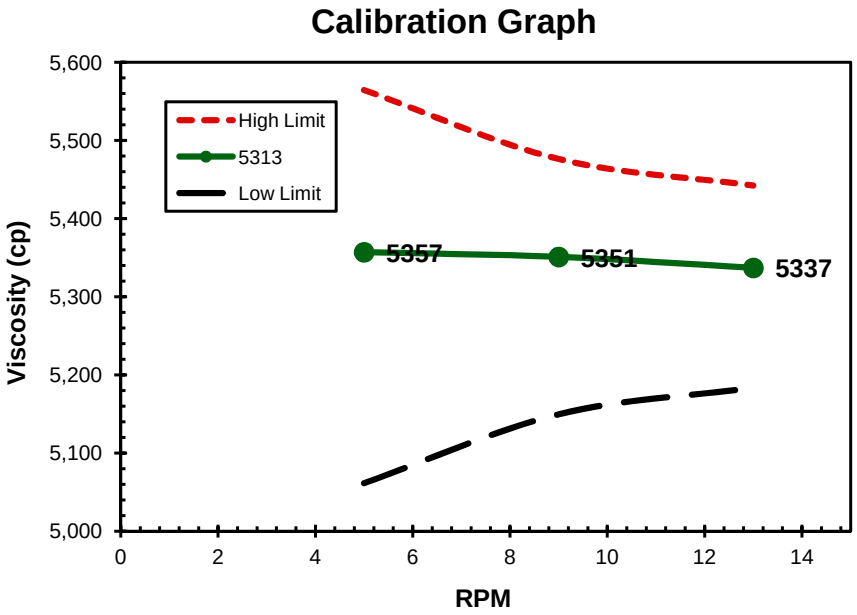

Fig. A.5.: Viscometer calibration graphs show that the viscometer provides promising measurements for high viscosity fluids

APPENDIX B

GAS CHROMATOGRAPHY INSTRUMENTS

By classical definition, chromatography is a separation process that is achieved by distributing the substances to be separated between a moving phase and a stationary phase. Those substances distributed preferentially in the moving phase pass through the chromatographic system faster than those that distributed preferentially in the stationary phase. Thus, the substances are eluted from the column in the inverse order of the magnitude of their distribution coefficients with respect to the stationary phase [136]. The international union of pure and applied chemistry (IUPAC) defines chromatography as "a physical method of separation in which the components to be separated are distributed between two phases, one of which is stationary (stationary phase) while the other (the mobile phase) moves in a definite direction" [137]. The chromatographic process in which gas components serve as the mobile phase is called gas chromatography. Note that the solute molecules move through the chromatographic system only if they are in the mobile phase and they will stay static while they are distributed in the stationary phase. The development technique that is employed during the GC process is called elution development which is best described as a series of absorption–extraction processes which are continuous from the time the sample is injected into the chromatographic system until the time it exits from

the column. Consider the progress of a solute down a chromatographic column in the manner depicted in Fig. B.1.

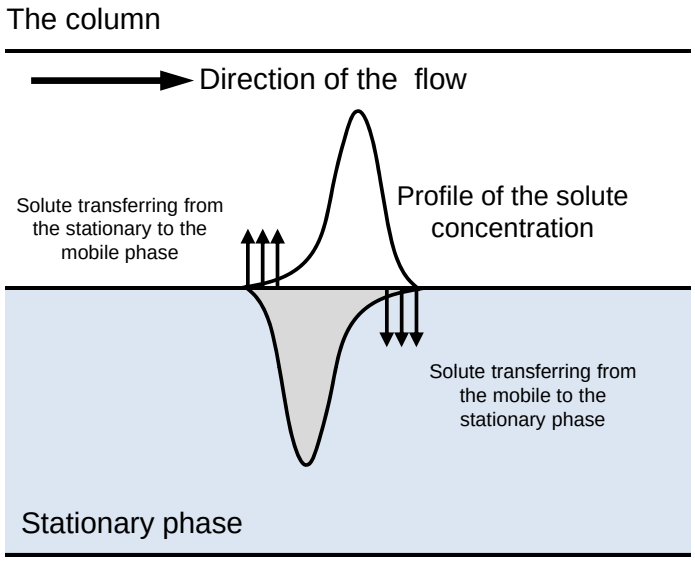

Fig. B.1.: The elution of the solute through a GC column (regenerated after Scott [136])

Equilibrium occurs between the gas and the stationary phase when the probability of a solute molecule striking the surface and entering the stationary phase is the same as the probability of a solute molecule randomly acquiring sufficient kinetic energy to leave the stationary phase and enter the gas phase. At all times, the distribution system is thermodynamically driven toward equilibrium. However, as the mobile phase, by definition, is moving, it will continuously displace the concentration profile of the solute in the mobile phase forward, relative to that in the stationary phase and

this displacement, in a grossly exaggerated form, is depicted in Fig. B.1. It is seen that, as a result of this displacement, the concentration of solute in the mobile phase at the front of the peak exceeds the equilibrium concentration with respect to that in the stationary phase. Consequently, the solute from the mobile phase in the front part of the peak will continually enter the stationary phase to reestablish equilibrium as the peak progresses along the column. At the rear of the peak, the converse occurs. As the concentration profile moves forward, the concentration of solute in the stationary phase at the rear of the peak is now in excess of the equilibrium concentration. Thus, solute leaves the stationary phase and enters the mobile phase in an attempt to reestablish equilibrium. In this manner, the solute band moves through the chromatographic system as a result of the solute entering the mobile phase at the rear of the peak and returning to the stationary phase at the front of the peak. It should be emphasized that at all times the solute is shifting between the two phases throughout the whole of the peak in an attempt to attain or maintain thermodynamic equilibrium.

The gas components, evolved during the experiment, were quantitatively analyzed by a refinery gas analyzer machine (Agilent 7890A). The machine is able to analyze light liquid and gas samples and has two different detectors working at the temperature of 200°C. Thermal conductivity detector (TCD) analyzes permanent gases such as H_2 and N_2 while flame ionization detector (FID) evaluates hydrocarbon molecules. A capillary column of 60 m length and 0.32 mm ID, which contains

silica as the stationary phase, was used to separate hydrocarbon molecules in the mixture (the column is well suited for cases of hydrocarbon and sulfur gases). Helium with a flow rate of 1.5 ml/min was employed as the carrier gas. The separation process started at temperature of 40°C and the oven was held at this temperature for 10 min. Afterwards, the temperature increased to 100°C with a ramp of 3°C/min and was kept at 100°C for 40 min. The RGA machine provides us very promising information regarding the gas samples with a solid resolution. The results from the RGA machine were qualitatively confirmed using the GC–MSD machine.

VITA

Name	Masoud Alfi
Address	3116 TAMU–711 Richardson Building, College Station, TX 77843-3116
Email Address	masoud.alfi@pe.tamu.edu
Education	B.S., Petroleum Engineering, Amirkabir University of Technology (Tehran Polytechnic), 2009 M.S., Petroleum Engineering, Texas A&M University, 2012